4

Results and Discussion

The results of the present work entitled "**Corrosion Inhibition and Adsorption Potential of Biomass Extracts-Leaves and Flowers of *Heliconia rostrata and Canna indica* on Corrosion of Mild Steel/Aluminium 1100 in 1 M HCl"** are discussed under the following headings in the light of the objectives set forth.

Phase I : Characterization of selected Biomass extracts

Phase II : Methods adopted-Electrochemical & Mass loss measurements

Phase III : Surface Analytical Techniques

Phase IV : Theoretical calculation using Mopac software.

Phase I:

4.1 Characterization of selected Biomass extracts

The following techniques were carried out to characterise the selected biomass extracts-*Heliconia rostrata* leaves (HRL), *Heliconia rostrata* flowers (HRF), *Canna indica* leaves (CIL) and *Canna indica* flowers (CIF)

4.1.1 Phytochemical screening

4.1.2 HPTLC

4.1.3 GC-MS

4.1.4 FT-IR

4.1.5 UV

Phase II:

Methods adopted - Electrochemical & Mass loss measurements

4.2 Electrochemical measurements

4.2.1 Potentiodynamic polarisation studies of Mild steel in 1 M HCl with and without HRL, HRF, CIF, CIL extracts.

4.2.2 Electrochemical impedance measurements of Mild steel in 1 M HCl with and without HRL, HRF, CIF, CIL extracts.

4.2.3 Potentiodynamic polarisation studies of AA1100 in 1 M HCl with and without HRL, HRF, CIF, CIL extracts

4.2.4 Electrochemical impedance measurements of AA1100 in 1 M HCl with and without HRL, HRF, CIF, CIL extracts.

4.3 Mass loss Measurements

4.3.1 Effect of concentration of HRL, HRF, CIL, CIF extracts and period of immersion on corrosion of mild steel in 1 M HCl.

4.3.2 Influence of temperature on the corrosion of mild steel in the presence of HRL, HRF, CIL and CIF extracts.

4.3.3 Effect of concentration of HRL, HRF, CIL,CIF extracts and period of immersion on corrosion of AA1100 in 1 M HCl.

4.3.4 Influence of temperature on the corrosion of AA1100 in the presence of HRL, HRF, CIL and CIF extracts.

4.3.5 **Adsorption isotherm**

Statistical Analysis was carried out to investigate whether the inhibitor system is statistically significant or not by doing F- tests by using the Analysis of Variance ANOVA

4.3.6 **Activation Parameters for inhibition process**

Activation energy, Enthalpy and Entropy of activation

4.3.7 **Thermodynamic adsorption parameters**

Free energy, Enthalpy and Entropy of adsorption

Phase III :

4.4 Surface Analytical Techniques

The following surface analytical techniques were used to study the surface of mild steel and aluminium in the absence and presence of selected biomass extracts.

4.4.1 UV Visible spectral Analysis

4.4.2 FT-IR Spectral studies

4.4.3 X-ray diffraction Analysis

4.4.3 Scanning Electron Microscopic studies

4.4.4 Energy dispersive X-ray analysis

4.4.5 Study of roughness by 3D optical profilometry

Phase IV:

4.5 Theoretical calculation using Mopac software

Quantum chemical calculations are carried out to interpret the experimental results with theoretical calculations.

4.1 Characterization of *Heliconia rostrata* (HR) and *Canna indica* (CI) extracts

4.1.1 Phytochemical screening of selected biomass extracts

The preliminary phytochemical screening tests may be useful in the detection and identification of chemical constituents present in the biomass extracts. Further, the presence of different phytoconstituents in the extracts may be responsible for corrosion inhibition. Phytochemical screening tests were carried out in the selected biomass extracts using the standard procedures as described by **Harborne, 1973**. The investigated plant extracts were screened for the presence of flavonoids, alkaloids, terpenoids, saponins, tannins, reducing sugar, polyphenols and anthraquinones.

Table : 4.1 Preliminary phytochemical screening of the crude extracts of HR/CI

Phytochemical constituents	HR		CI	
	Leaves	Flowers	Leaves	Flowers
Alkaloids	-	-	+	++
Carbohydrates	+	++	+	+
Flavonoids	+	++	+	++
Glycosides	-	-	+	+
Phlobatinins	-	-	+	+
Proteins	+	++	+	+
Anthroquinone	-	-	-	-
Saponins	-	+	+	++
Steroids	-	-	+	++
Terpenoids	+	++	+	++
Tannin	+	-	+	+
Coumarine	+	+	-	-
Phenolic compounds	+	+	+	+

(+) = indicate presence ++ =moderate amount (-) = indicate absence

The results indicated the presence of terpenoids, coumarin and phenolic compounds in HRL and HRF extracts. Similarly for CIL and CIF extracts presence of alkaloids, flavonoids, saponins, steroids and terpenoids are detected. These results reflect the presence of a broard spectrum of secondary metabolites containing 'N' and 'O' rich centres in them.

4.1.2 HPTLC

HPTLC is an analytical tool to identify the presence of terpenoid, flavonoid and coumarin present in the plant extracts. A detailed report of the phytochemical constituents

present in *Canna indica* has already been reported in the literature (**Bachhet *et al*, 2013**) and in the present study HPTLC analysis is carried for ethanol extracts of leaves and flowers of ***Heliconia rostrata*** (HRL, HRF) only.

4.1.2.1 HPTLC analysis of ethanol extracts of HRL and HRF

To find out the presence of terpenoid, flavonoid and coumarin present in the ethanol extract of HRLE and HRFE, different compositions of the mobile phase of HPTLC analysis are tested to obtain high resolutions and reproducible peaks. The desired solvent system for terpenoid has been achieved using n-Hexane-Ethyl acetate (7.2:2.9), for the flavonoid it is Ethyl acetate-Butanone-Formic acid-Water (5:3:1:1) and for Coumarins it is found to be toluene-Diethylether (1:1) saturated with 10% Glacial acetic acid.

a) Terpenoid profile of *ethanol extracts of* HRL and HRF

The ethanolic extract of the plant HRL and HRF reflects the presence of nineteen different type of terpenoids with Rf values *0.*07,0.12,0.23,0.25,0.30,0.43,0.47,0.61,0.64, 0.72,0.76,0.82,0.89,*0.97,*0.822,0.74,0.07,0.12,0.86,0.94 and 0.97 (Table 4.2). Blue, Violet coloured zone observed from the chromatogram after derivatization, confirms the **presence of Terpenoid.**

Table: 4.2 Terpenoid profile of HRL and HRF

Track	Peak	Rf	Height	Area	Assigned substance
Sample HRL	1	0.07	11.4	110.7	Unknown
Sample HRL	2	0.12	19.1	366.6	Unknown
Sample HRL	3	0.23	10.4	198.6	Unknown
Sample HRL	4	0.25	15.2	243.0	Unknown
Sample HRL	5	0.30	15.6	289.7	Unknown
Sample HRL	6	0.43	24.1	545.1	Unknown
Sample HRL	7	0.47	38.2	903.7	Unknown
Sample HRL	8	0.61	26.6	393.7	Terpenoid 1
Sample HRL	9	0.64	40.7	1193.7	Terpenoid 2
Sample HRL	10	0.72	83.2	2634.4	Terpenoid 3
Sample HRL	11	0.76	156.1	5843.2	Terpenoid 4
Sample HRL	12	0.82	185.0	6499.4	Terpenoid 5
Sample HRL	13	0.89	162.2	6434.8	Terpenoid 6
Sample HRL	14	0.97	339.2	9065.0	Terpenoid 7
STD	1	0.87	390.8	14648.5	Terpenoid standard
Sample HRF	1	0.22	10.7	292.9	Unknown
Sample HRF	2	0.74	142.8	5604.6	Terpenoid 1
Sample HRF	3	0.86	103.9	4609.0	Terpenoid 2
Sample HRF	4	0.94	58.5	1449.9	Terpenoid 3
Sample HRF	5	0.97	145.7	2730.7	Terpenoid 4

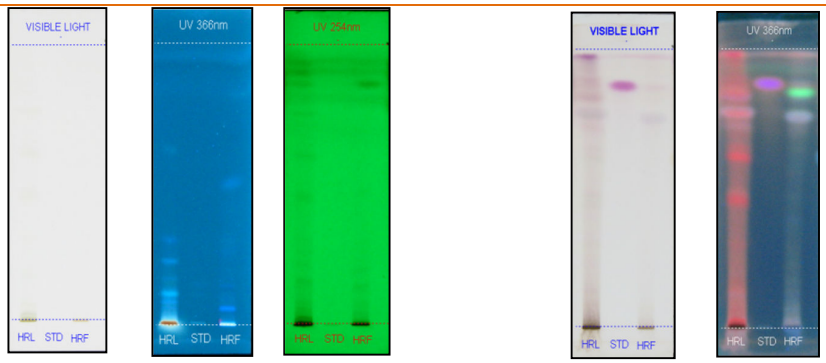

Before derivatization **After derivatization**

Figure 4.1: Terpenoid chromatogram of ethanol extracts of HRL and HRF before and after derivatization.

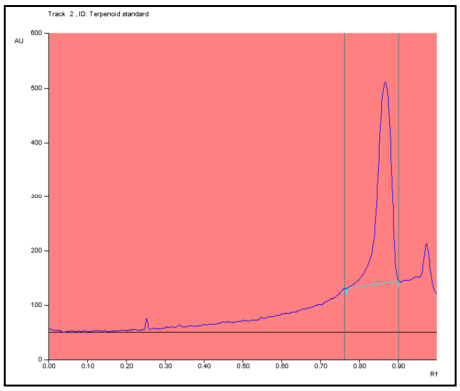

Terpenoid standard- Baseline display (Scanned at 500 nm)

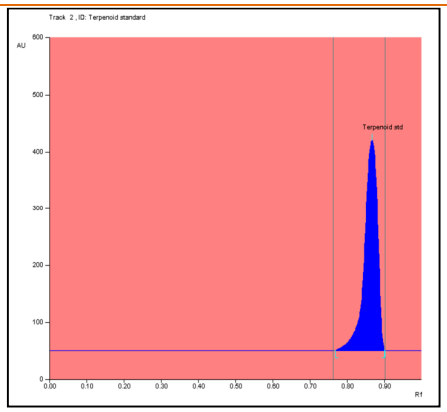

Terpenoid standard- Peak densitogram display (Scanned at 500 nm)

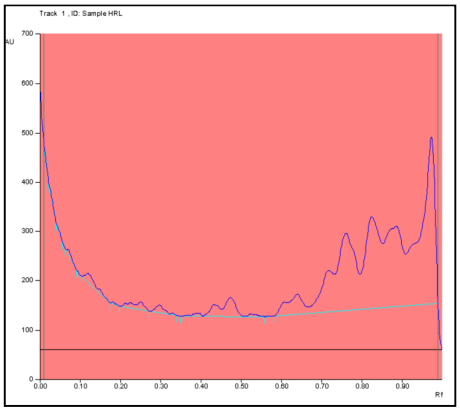

HRL extract - Baseline display (Scanned at 500 nm)

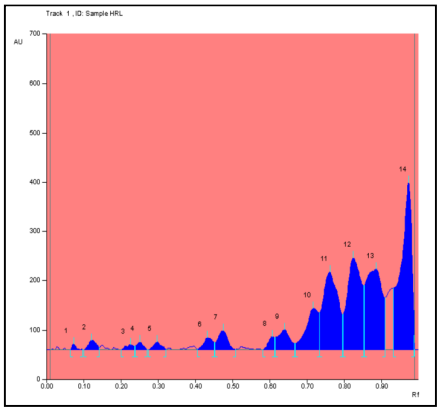

HRL extract - Peak densitogram display (Scanned at 500 nm)

Figure 4.2 : Baseline and peak densitogram display of HRL extract with standard for Terpenoid profile.

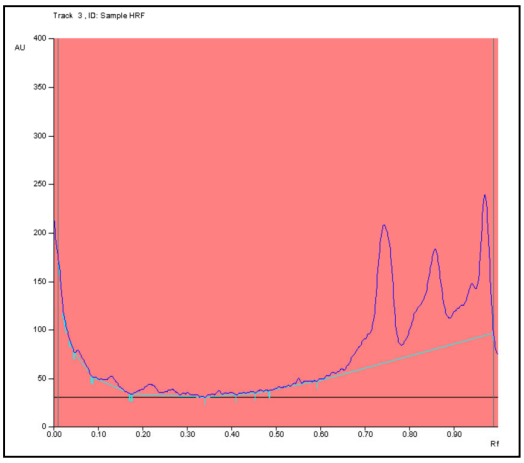

HRF extract-Baseline display
(Scanned at 500 nm)

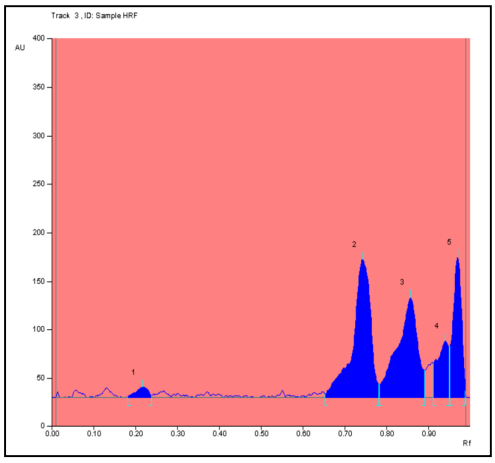

HRF extract-Peak densitogram display
(Scanned at 500 nm)

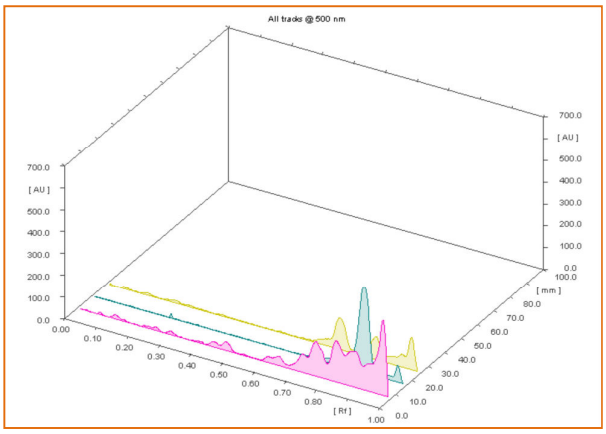

3D display of all Tracks

Figure 4.3 : Baseline and peak densitogram display of HRF extract and 3D display of all Tracks for terpenoid profile.

b) Flavonoid profile of HRL and HRF extracts

The ethanolic extract of HRL,HRF showed the presence of eleven different type of flavonoid with Rf values 0.17,0.22,0.30,0.49,0.57,0.65,0.81,0.97,0.07,0.35 and 0.96 (Table 4.3). Yellow, Yellowish blue coloured fluorescent zone after derivatization confirms the **presence of Flavonoid.**

Table : 4.3 Flavonoid profile of HRL and HRF extracts

Track	Peak	Rf	Height	Area	Assigned substance
Sample HRL	1	0.17	17.0	318.8	Unknown
Sample HRL	2	0.22	97.8	2375.3	Flavonoid 1
Sample HRL	3	0.30	14.5	420.9	Unknown
Sample HRL	4	0.49	48.9	2364.6	Flavonoid 2
Sample HRL	5	0.57	238.0	9191.3	Flavonoid 3
Sample HRL	6	0.65	147.1	5104.0	Flavonoid 4
Sample HRL	7	0.81	23.3	525.6	Flavonoid 5
Sample HRL	8	0.97	187.5	4743.6	Unknown
STD	1	0.49	590.3	22669.0	Flavonoid Standard
Sample HRF	1	0.07	13.9	188.6	Unknown
Sample HRF	2	0.35	19.5	600.6	Flavonoid 1
Sample HRF	3	0.96	126.9	3561.3	Flavonoid 2

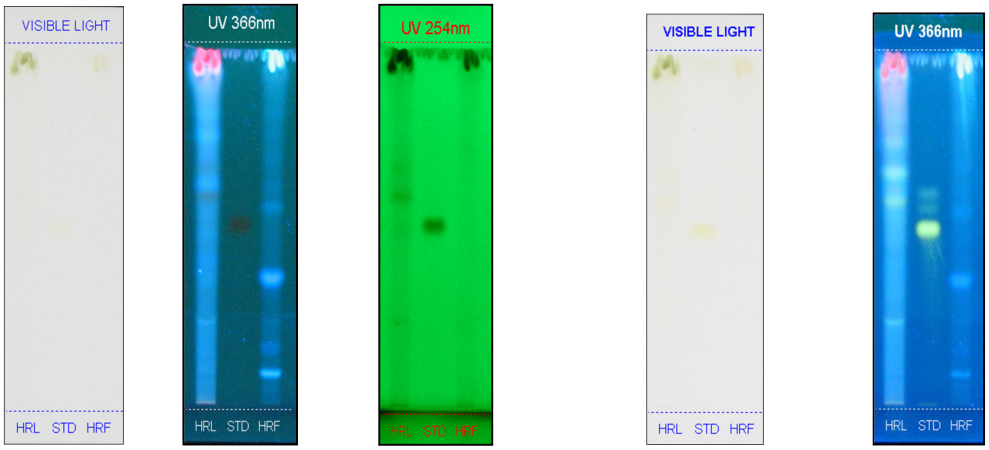

Before derivatization **After derivatization**

Figure 4.4: Flavonoid chromatogram of ethanol extracts of HRL and HRF before and after derivatization

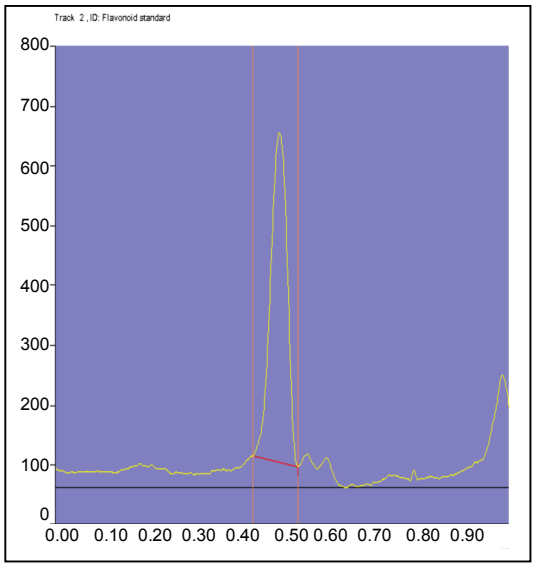

Flavonoid standard Baseline display (Scanned at 366 nm)

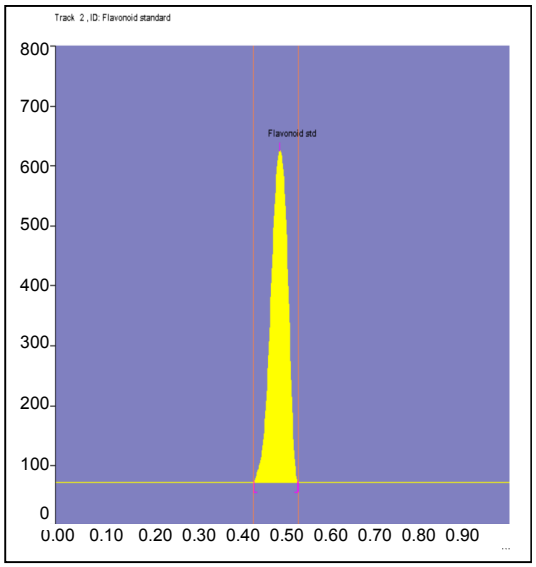

Flavonoid standard Peak densitogram display (Scanned at 366 nm)

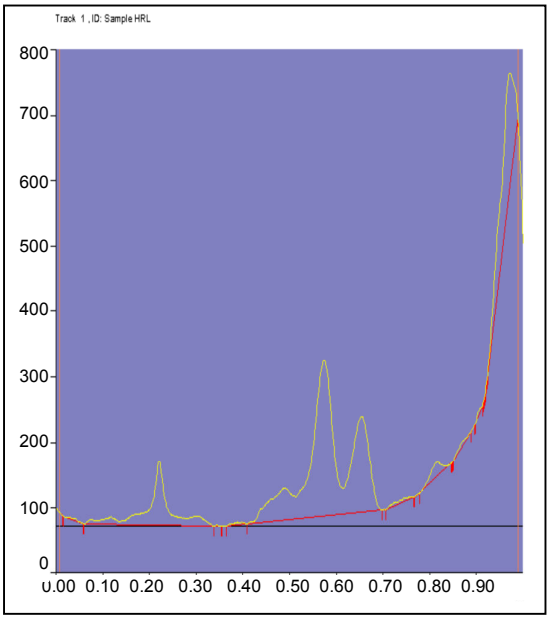

HRL extract - Baseline display (Scanned at 366 nm)

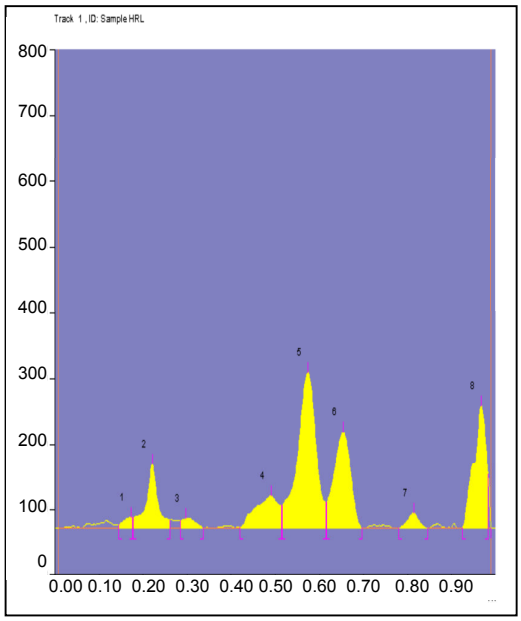

HRL extract - Peak densitogram display (Scanned at 366 nm)

Figure 4.5: Baseline and peak densitogram display of HRL extract with standard for Flavonoid profile.

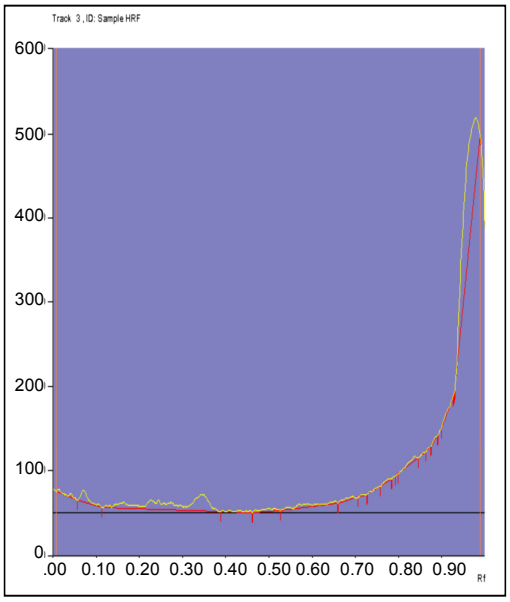

HRF extract -Baseline display
(Scanned at 366 nm)

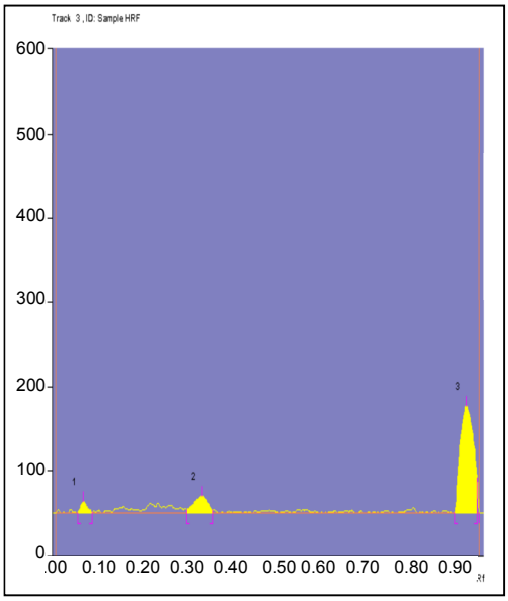

HRF extract - Peak densitogram
display(Scanned at 366 nm)

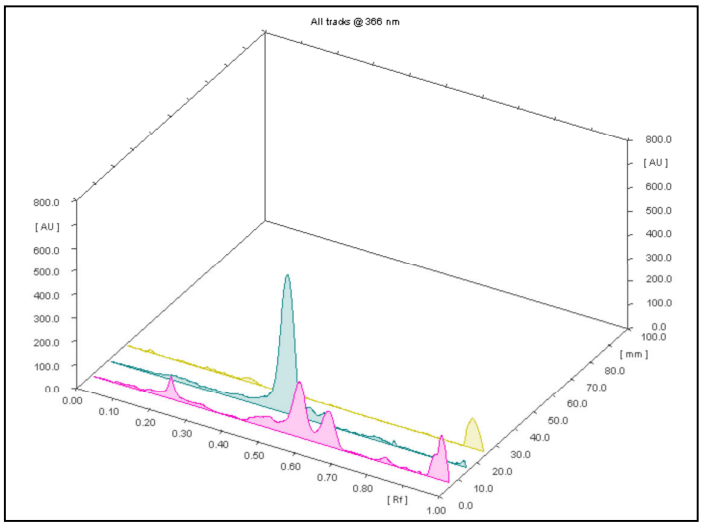

3D display of all Tracks

Figure 4.6: Baseline and peak densitogram display of HRF extract, 3D display of all Tracks for Flavonoid profile.

c) Coumarin profile of ethanol extract of HRL and HRF

The ethanolic extract of HRL,HRF indicates the presence of twenty six different type of coumarins with Rf values 0.01,0.03,0.060.15,0.23,0.26,0.42,0.48,0.60,0.66,0.77,0.86,0.91,0.94,0.98,0.06,0.14,0.21,0.25,0.36,0.53,0.57,0.60,0.71,0.83 and 0.96 (Table 4.4). Blue, Yellowish blue coloured fluorescent zone at UV 366nm after derivatization confirms the **presence of Coumarin.**

Table: 4.4 Coumarin profile of HRL and HRF extract

Track	Peak	Rf	Height	Area	Assigned substance
Sample HRL	1	0.01	43.7	194.1	Unknown
Sample HRL	2	0.03	60.8	406.0	Unknown
Sample HRL	3	0.06	26.8	293.8	Unknown
Sample HRL	4	0.15	11.1	188.0	Unknown
Sample HRL	5	0.23	55.3	1333.4	Unknown
Sample HRL	6	0.26	43.3	900.6	Unknown
Sample HRL	7	0.42	12.0	252.6	Unknown
Sample HRL	8	0.48	85.2	2035.5	Unknown
Sample HRL	9	0.60	19.9	521.7	Unknown
Sample HRL	10	0.66	85.8	4202.6	Unknown
Sample HRL	11	0.77	61.6	2285.1	Unknown
Sample HRL	12	0.86	14.5	409.8	Unknown
Sample HRL	13	0.91	26.4	800.2	Unknown
Sample HRL	14	0.94	14.4	261.5	Unknown
Sample HRL	15	0.98	15.5	141.9	Unknown
STD	1	0.70	88.3	5227.2	Coumarin standard
Sample HRF	1	0.06	39.0	535.3	Unknown
Sample HRF	2	0.14	20.3	369.5	Unknown
Sample HRF	3	0.21	39.0	955.4	Unknown
Sample HRF	4	0.25	47.5	1098.6	Unknown
Sample HRF	5	0.36	18.2	525.8	Unknown
Sample HRF	6	0.53	16.8	292.0	Unknown
Sample HRF	7	0.57	65.9	2016.9	Coumarin 1
Sample HRF	8	0.60	41.7	1749.3	Unknown
Sample HRF	9	0.71	41.4	1814.9	Coumarin 2
Sample HRF	10	0.83	36.0	1509.9	Coumarin 3
Sample HRF	11	0.96	14.8	212.0	Unknown

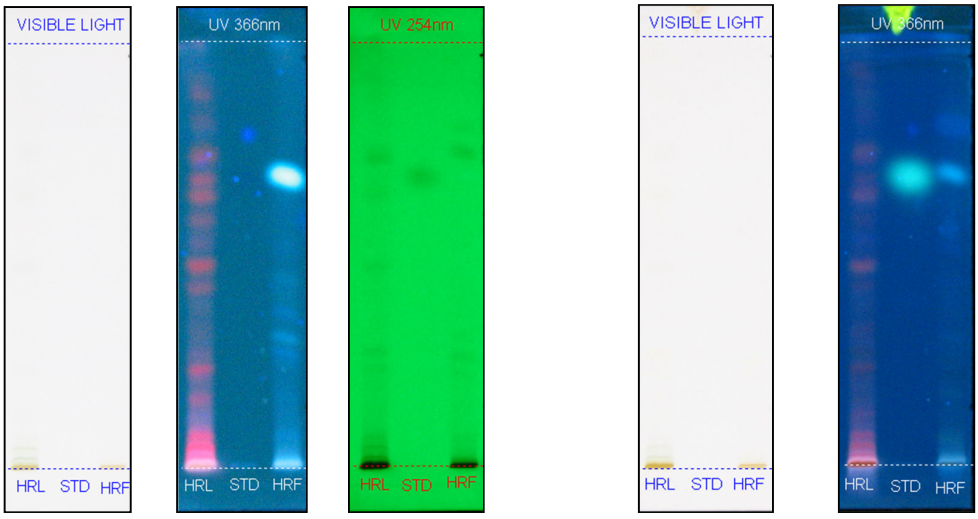

Figure 4.7. Coumarin chromatogram of ethanol extracts of HRL and HRF before and after derivatization.

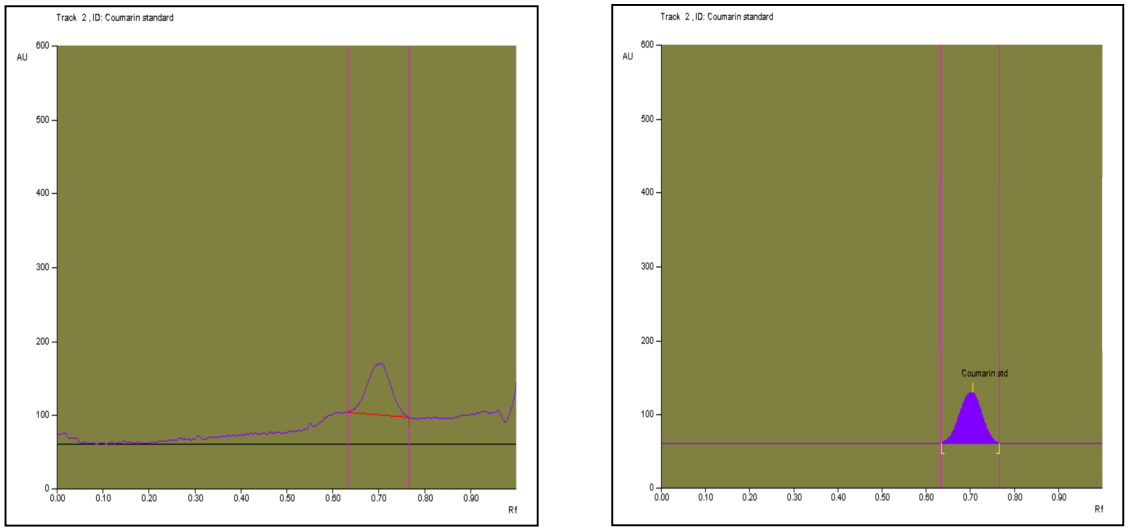

Coumarin standard -Baseline display (Scanned at 366 nm)

Coumarin standard-Peak densitogram display (Scanned at 366 nm)

Figure 4.8: Coumarin standard **-**Baseline and peak densitogram display

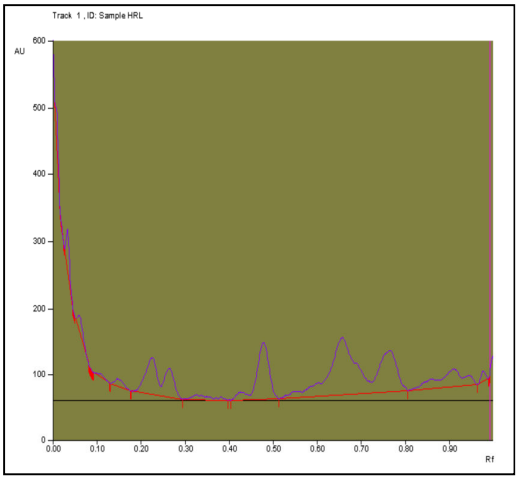

HRL extract - Baseline display
(Scanned at 366 nm)

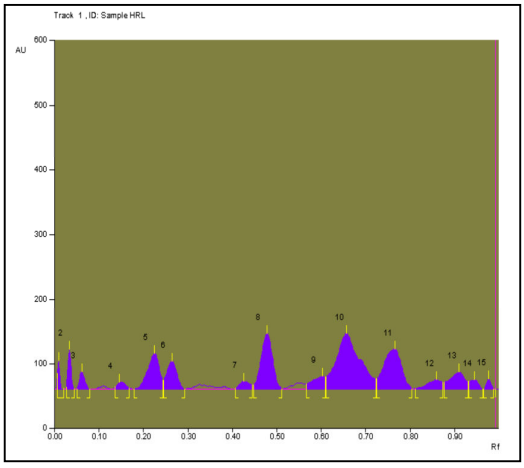

HRL extract - Peak densitogram display
(Scanned at 366 nm)

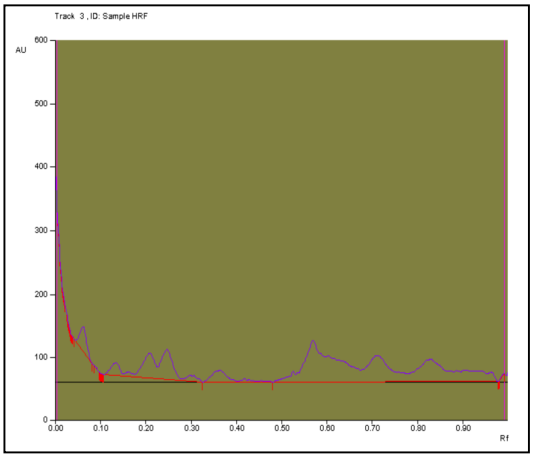

HRF extract - Baseline display
(Scanned at 366 nm)

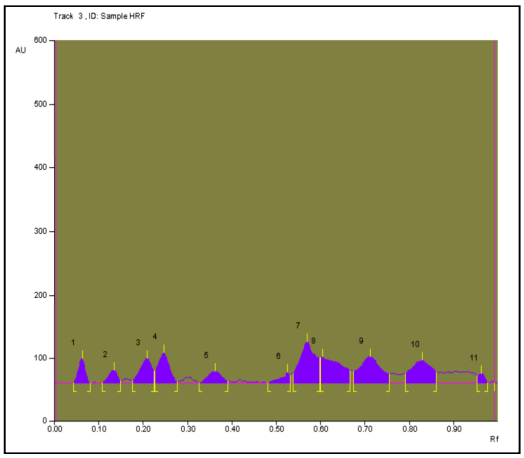

HRF extract -Peak densitogram display
(Scanned at 366 nm)

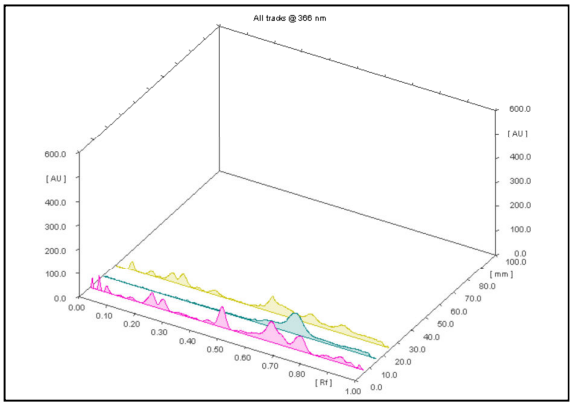

Figure 4.9: Baseline and peak densitogram display of HRL, HRF extracts and 3D display of all Tracks for coumarine pro

The HPTLC analysis of ethanol extracts of HRL, HRF reveals the presence of terpeniods, coumarines and Flavonoids. These results are supported by the phytochemical screening test.

4.1.3 GC-MS Analysis

4.1.3.1 GC-MS analysis of HRL extract

The GC spectrum of HRL extract shown in Figure 4.10 exhibits peaks at retention time 14.14, 14.55, 14.88, 15.22, 15.62 and 15.71. The mass spectra of GC peaks at retention times 14.14 and 14.55 are presented in Figure 4.10.

The mass spectrum of GC peak of HRL extract at retention time 14.14 shows molecular ion peak at m/z 429 and base peak at m/z 229. The spectrum shows various characteristic peaks at m/z 359, 299, 151 corresponds to M^+ -42, M^+ -46, indicating the presence of oxygen functionality. Also M^+ - 18 peak is noticed at m/z 211 and M^+ -61 peaks are noted at m/z 75 confirming the presence of –OH and -CH_2COOH moieties present in the extract constituents. Hence the phytochemical compound may contain hydroxyl and acid functional groups. Similar trend is also seen for the mass fragmentation patterns of other compounds present in HRL extract at retention time 14.55, 14.88, 15.22, 15.62 and 15.71. **The mass fragmentation pattern present in the extract indicates that the extract may contain the phytochemical compounds with hydroxyl and acid groups.**

4.1.3.2 GC-MS Analysis of HRF extract

The GC spectrum of HRF extract (Figure 4.11) exhibits peaks at retention time 14.33, 14.70, 15.42, 15.75 along with the MS pattern of the GC peaks noted at 14.33 and 15.42. The mass spectrum of GC peak of 14.33 retention time reflects molecular ion peak at m/z 429 and base peak at m/z 229. The spectrum shows a characteristic M^+- 49 peak at m/z 429, indicating the loss of –HO_3 group. M^+- 48 and M^+- 46 peaks are found at m/z 151 and m/z 105 which relates the presence of oxygen functionality. M^+- 30 peak observed at m/z 269, may be due to the loss of CH_2O. Hence the compound may contain oxygen containing functional groups. Similar trend is also observed for the mass fragmentation patterns for the other compounds present in HRF extract at retention time 14.70, 15.42 and 15.75. **Hence the extract may contain oxygen containing groups.**

4.1.3.3 GC-MS Analysis of CIL extract

The GC spectrum of CIL extract exhibits 12 peaks at retention time 3.80, 11.28, 16.92, 23.61, 25.43, 33.08, 33.89, 36.11, 36.77 & 37.88 (Figure 4.12). The mass spectrum

of GC- peak of CIL extract at retention time 11.28, displays molecular ion peak at m/z 359 and base peak at m/z 63. The characteristic M^+- 60 peak at m/z 299 reveals loss of $–CH_2COOH$ group. Hence the compound may contain carboxylic functional group. Also M^+- 75 peak at m/z 94 of retention time 16.92 is observed due to the loss of $-COOC_2H_5$ indicating that the extract contains ester. The mass spectrum of GC- peak of CIL extract at retention time 36.11 shows M-30 and M-40 peaks evidencing the presence of nitrogen containing compounds. The M- 18 peak which was seen at m/z 73 is due of presence of –OH group. **Hence the compound may contain nitrogen and hydroxyl groups respectively.**

Similar spectrum is noticed for the MS of other compounds present in CIL extract at retention times 3.80, 16.92, 23.61, 25.43, 33.08, 33.89, 36.77 and 37.88. **This confirms the presence of nitrogen containing compounds probably alkaloids, esters and acids in CIL extract.**

4.1.3.4 GC-MS Analysis of CIF extract

The GC-MS spectrum of CIF extract (presented in Figure 4.13) exhibits peaks at retention time 12.32, 14.24, 15.02, 15.62, 15.71 and 16.62. The mass spectrum of GC-peak of CIF extract at retention time 12.32 shows molecular ion peak at m/z 419 and base peak at m/z 229. The M^+- 60 peak at m/z 299 indicates the loss of $–CH_2COOH$ group. Hence the compound may contain an acidic functional group. The M-30 peak observed at m/z 269 of retention time 14.24 indicates the presence of $–CH_2NH_2$ group. Hence the compound may be a nitrogen containing compound. The M^+- 19 peak observed at m/z 299 of retention time 15.71, may be due to the loss of H_3O^+, confirming the **presence hydroxyl groups.**

Similar M^+- 60, M-30, M^+- 19 peaks are present in the fragmentation patterns for the of other compounds present in CIF extract at retention times 15.02, 15.62, 15.71 and 16.62. **This confirms the presence of nitrogen containing compounds probably alkaloids and acids in CIF extract.**

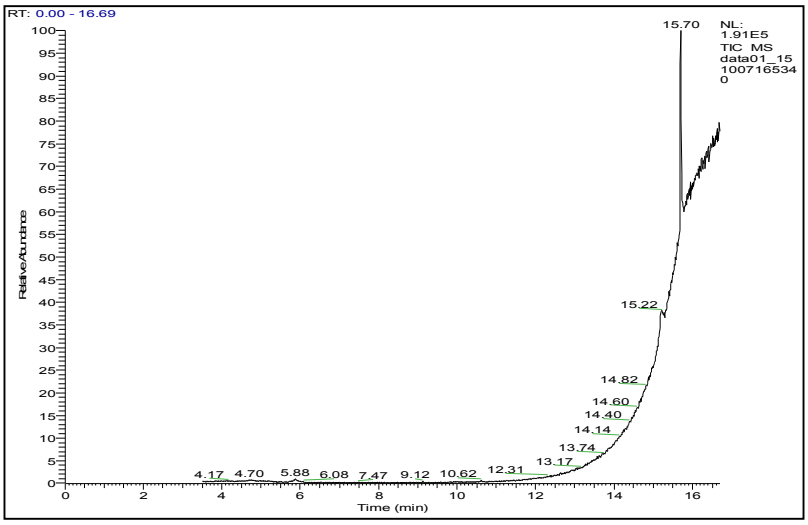

GC-MS

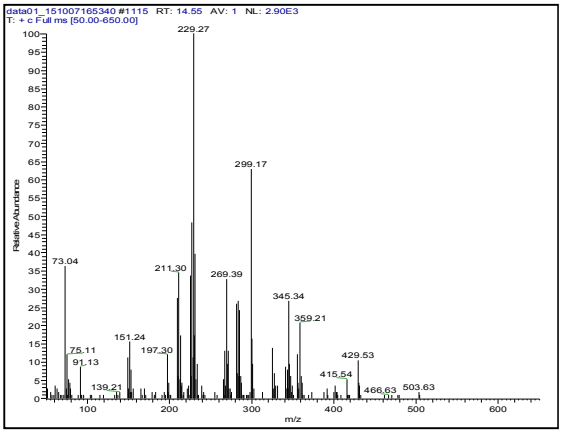

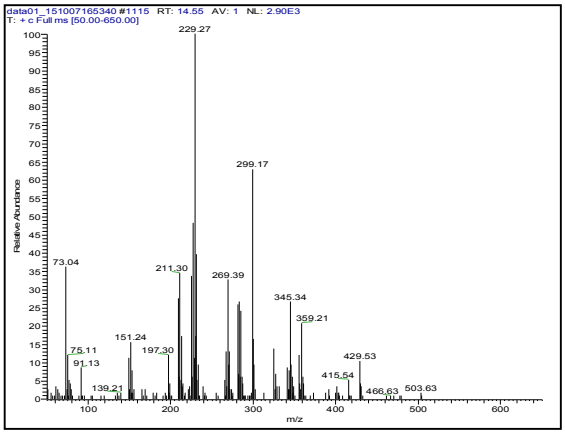

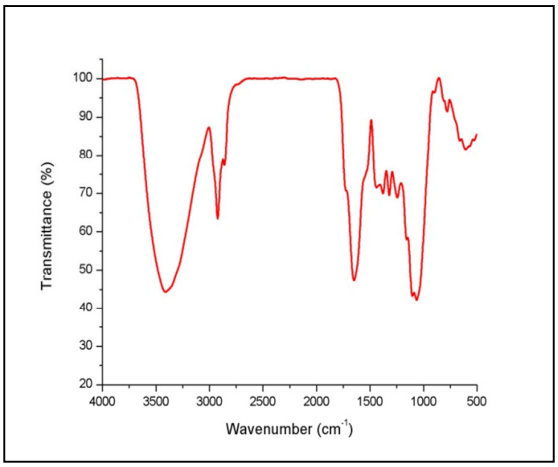

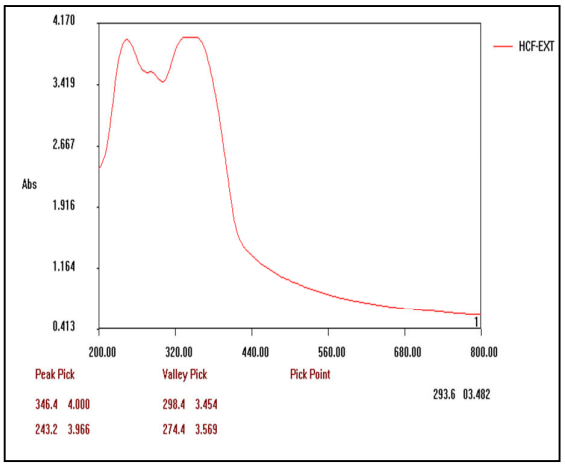

FTIR **UV**

Figure 4.10 : Characterization of HRL extract

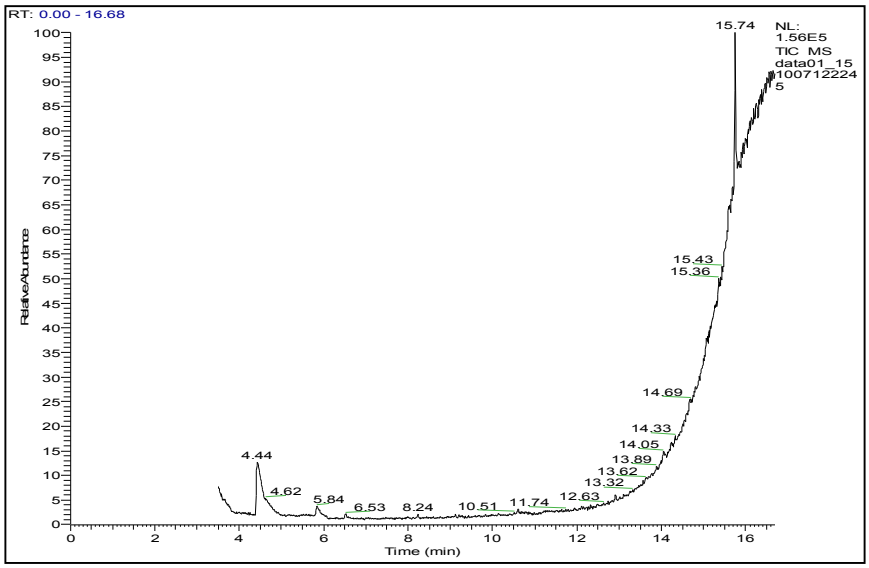

GC-MS

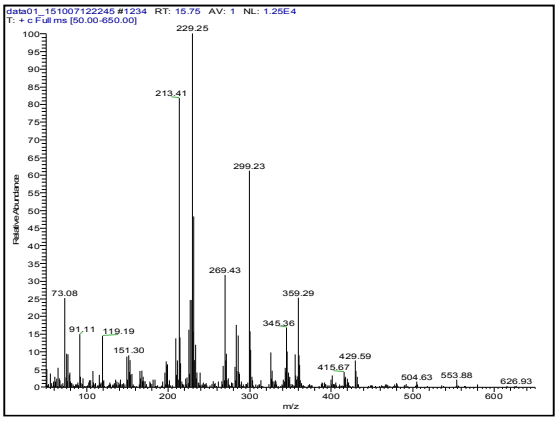

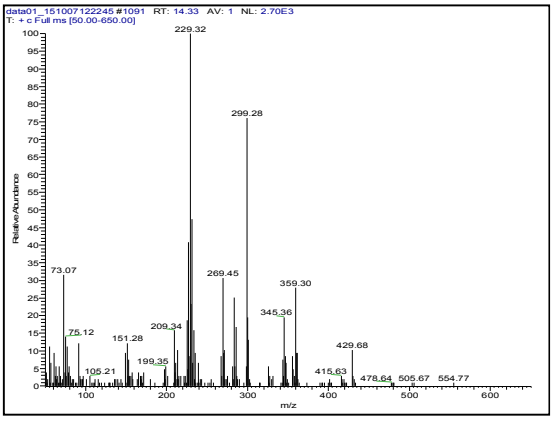

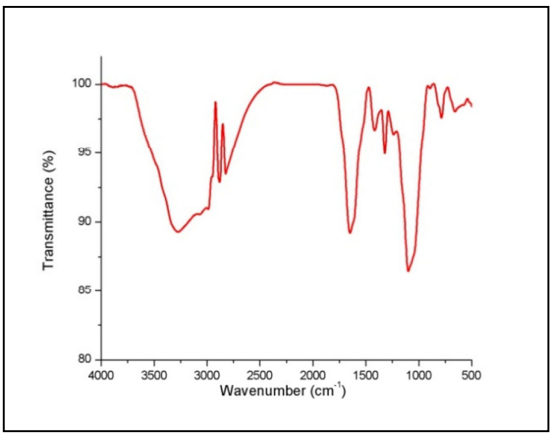

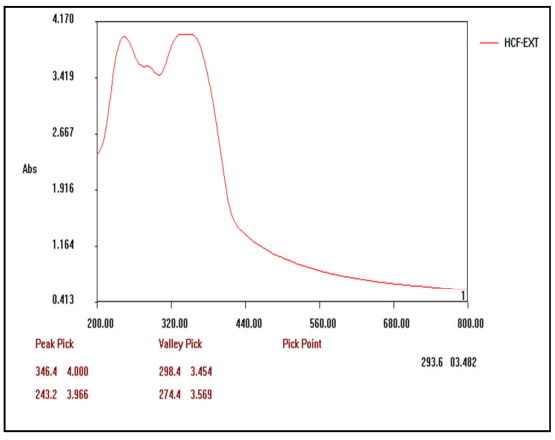

FTIR **UV**

Figure 4.11: Characterization of HRF extract

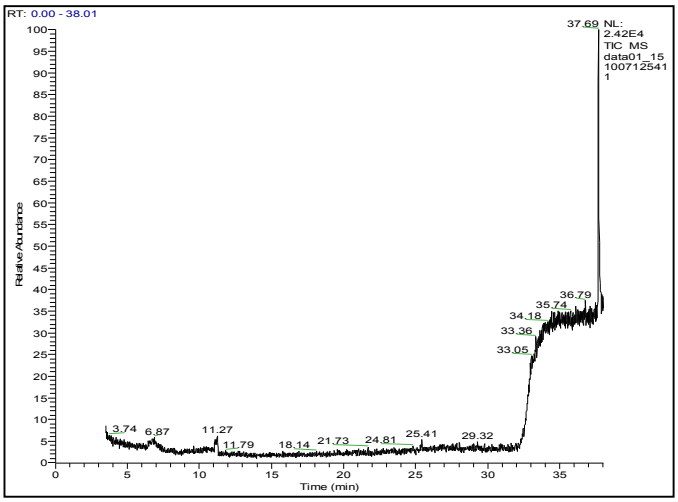

GC-MS

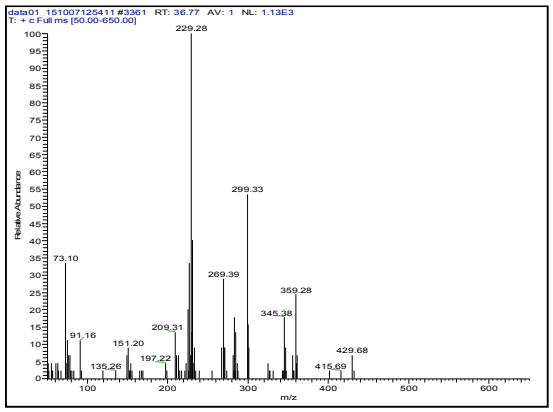

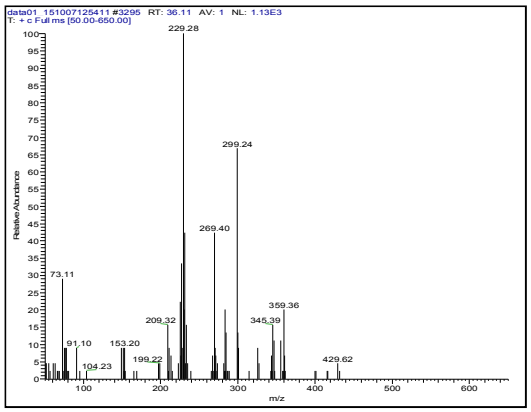

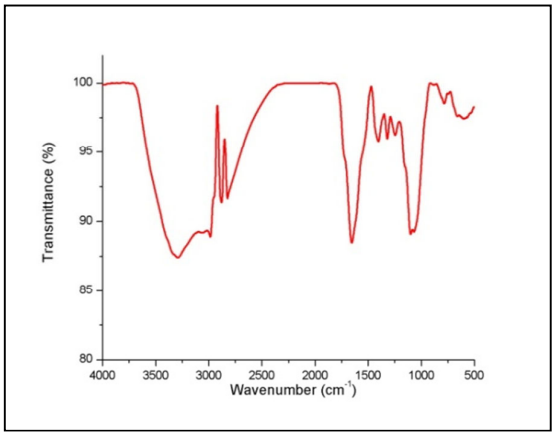

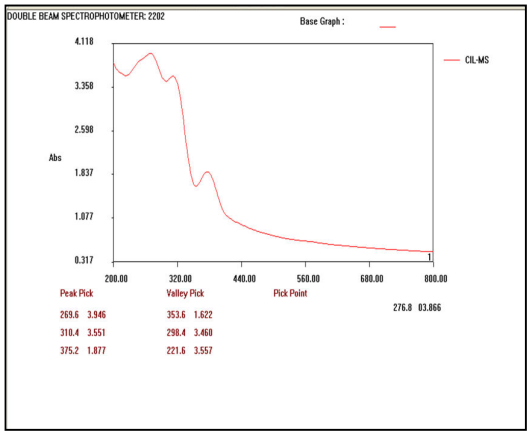

FTIR **UV**

Figure 4.12: Characterization of CIL extract

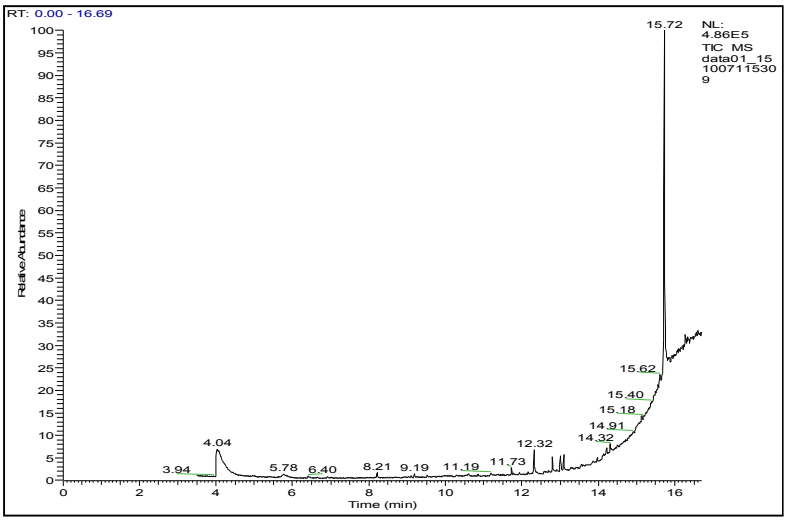

GC-MS

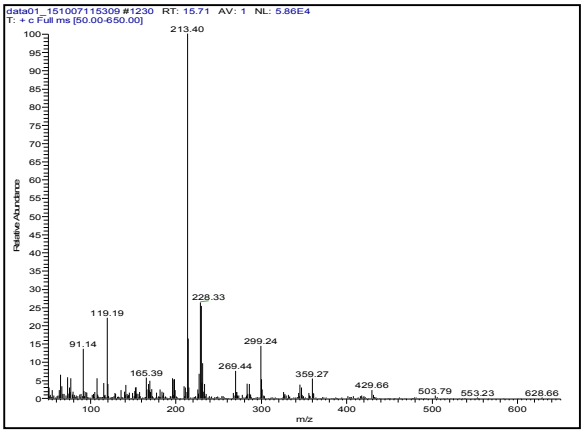

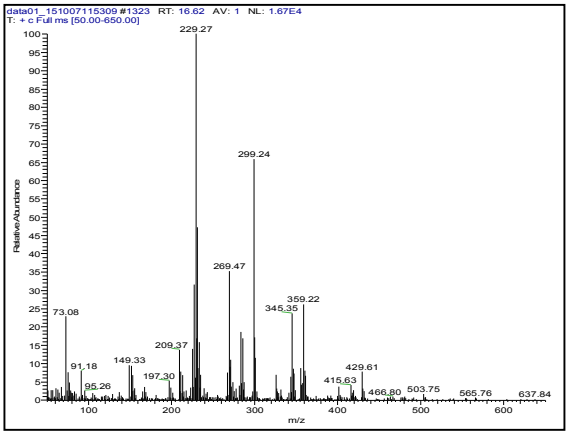

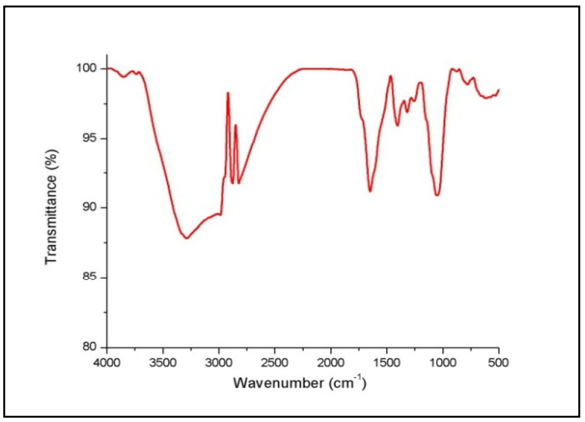

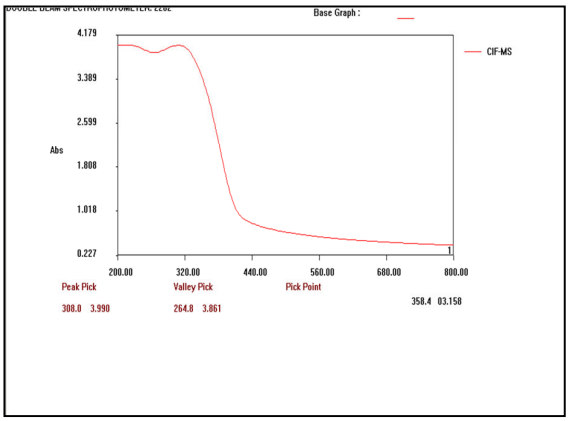

FTIR **UV**

Fig 4.13 : Characterization of CIF extract

4.1.4 FT-IR Analysis

The frequencies of the FTIR bands of the studied extracts HRL, HRF, CIL and CIF are tabulated in Table 4.5.

4.1.4.1 FT-IR spectroscopic study of HRL extract

The FT-IR spectrum of HRL extract (Figure 4.10) indicates a strong band at 3411 cm^{-1} and 3395 cm^{-1} that is attributed to N-H/O-H stretching. An absorption band related to – CH_2 stretching is noticed at 2924 cm^{-1}. A strong band at 1632 cm^{-1} corresponds to C=O stretching. Peaks observed at 1379 cm^{-1} and 1072 cm^{-1} indicates C-O-C stretching and C-O stretching. A peak at 633 cm^{-1} denotes C=C bending vibration of the aromatic ring system. This shows that this plant extract contained a mixture of compounds, terpenoids and organic acids **(Satapathy *et al*, 2009)**.

4.1.4.2 FT-IR spectroscopic study of HRF extract

The FT-IR spectrum of HRF extract reflects a strong band at 3950 cm^{-1} and 3395 cm^{-1} that is attributed to N-H /OH stretching. An absorption band related to – CH_2 stretching is noticed at 2376 cm^{-1}. A strong band at 1628 cm^{-1} is assigned to C=O stretching (**Bahrami *et al,* 2010**). Peaks obtained at 1427cm^{-1},1381 cm^{-1} , 1265 cm^{-1} reveals C=C stretching, C-O-C stretching and C-O stretching evidencing the presence of O and N containing compounds in the HRF extract.

4.1.4.3 FT-IR spectroscopic study of CIL extract

The FT-IR spectrum of CIL extract shows a strong band at 3290 cm^{-1} that is attributed to N-H /OH stretching. An absorption band assigned to – CH_2 stretching is noticed at 2985 cm^{-1}. A strong band at 1654 cm^{-1} corresponds to C=O stretching. Peaks observed at 1320 cm^{-1}, 1072 cm^{-1} indicate C-O-C stretching and C-O stretching. This shows that CIL extract contains a mixture of compounds, i.e., alkaloids, flavonoids and organic acids **(Satapathy *et al*, 2009)**.

4.1.4.4 FT-IR spectroscopic study of CIF extract

The FT-IR spectrum of CIF extract indicates a strong band at 3850 cm^{-1} and 3735 cm^{-1} that is attributed to N-H /OH stretching. An absorption band pertaining to – CH_2 stretching is noticed at 2879 cm^{-1}. A strong band at 1651 cm^{-1} corresponds to C=O stretching. Peaks observed at 1406 cm^{-1}, 1319 cm^{-1} , 1058 cm^{-1} indicates C=C stretching C-O-C stretching and C-O stretching. A peak at 622 cm^{-1} reflects C=C bending vibration of the aromatic ring system. Thus the FT IR spectrum implies the presence of O and N atom containing functional groups (**Li *et al*, 2012).**

Table: 4.5. FTIR -observed frequencies and the peak assignments of HR/ CI plant extracts

HR		CI		Frequency Assignment	Reference
HCL	HCF	CIL	CIF		
3411	3450	-	3850	O-H stretch	**Odiongenyi *et al*, 2009**
3395	3395	3290	3735	N-H/ O-H stretch	
2924	-	2924	2879	C-H stretch	**Bahrami *et al*, 2010**
-	2376	-	-	C≡ N	**Ibrahim *et al*,2012**
1632	1628	1654	1651	C=O stretch	**Li *et al*,2012**
-	1427	-	1406	C-H bend	**Eddy *et al*, 2009**
1379	1381	1302	-	C-O-C stretch	**Li *et al*,2009**
-	1265	1072	1260	C-O stretch	**Eddy *et al*, 2009**
1065	1065	-	1058	Aromatics	**Eddy *et al*, 2009**
633	772	784	779	OH bend	**Eddy *et al*, 2009**

4.1.5 UV-Vis analysis

UV-Vis absorption spectra of crude extract of HRL, HRF, CIL and CIF are given in Figures 4.10-4.13 and values of absorption bands are presented in Table 4.6

Table : 4.6 UV-Vis spectral data of crude HRL/HRF/CIL/CIF extracts

Inhibitor	Absorption bands (nm)	Transitions
HRL	246,349	$n \rightarrow \pi^*$
HRF	243,274,298,346,	$\pi \rightarrow \pi^*$
CIL	344,239	$n \rightarrow \sigma^*$
CIF	260,375,318,291,344,224	

4.1.5.1 UV-Vis spectrophotometric study of HRL extract

The UV-visible spectrum of HRL crude extract is shown in Figure 4.10. Major peaks appear at 246 nm and 349 nm. This is due to the presence of flavonoid type of compounds and other phytochemical constituents like terpenoids **(Gupta and Singh, 1991).**

4.1.5.2 UV-Vis spectrophotometric study of HRF extract

Figure 4.11 shows UV absorption spectrum of HRL extract. The profile shows the peaks at 243 nm, 274 nm, 298 and 346 nm .The might be due to the presence of terpenoids and coumarins and other compounds containing N and O atoms.

4.1.5.3 UV-Vis spectrophotometric study of CIL extract

UV absorption spectra of crude extract of CIL and values of absorption bands are represented in Table 4.6. Generally, UV spectra of flavonoids have two characteristic absorption peaks at 300–400nm and 240–280nm (**Li *et al,* 2012**). In the spectrum of CIL the absorption peaks appear at 344 and 239 nm which confirm the presence of flavonoid based compounds in the plant extracts and literature studies are also supporting the results of spectral studies. **(Vankar *et al*, 2008***)***

4.1.5.4 UV-Vis spectrophotometric study of CIF extract

Figure-4.13 and Table-4.6 represents the UV-Vis absorption spectra of crude CIF extract. Figure 4.13 reveals major peaks at 260 nm and 318 nm. The indicates the presence of flavonoids and other compounds containing N or O atoms.The other bands could be connected with the transitions π-π* transition. The results suggest the presence of carbonyl functions in conjugation with aromatic ring system. This is supported by IR absorption bands and mass spectral results.

Characterization of the biomass extracts by **HPTLC, GC-MS, FT-IR and UV-Vis** spectral studies confirms the presence of **Flavonoids, terpenoids, coumarines** and other phytochemical compounds in the investigated biomass extracts.

4.2 ELECTROCHEMICAL MEASUREMENTS

4.2.1 Potentiodynamic polarization studies of Mild steel/Biomass extracts/1 M HCl and AA1100/Biomass extracts/ 1 M HCl

Potentiodynamic polarization experiments were carried out to understand the influence of leaves and flower extracts of *Heliconia rostrata* and C*anna indica* on the kinetics of the anodic and cathodic reactions. It is well established that polarization curves can help to understand how a certain corrosion inhibitor works. The changes observed in the polarization curves after the addition of the inhibitor are usually used as the criteria to classify inhibitors as cathodic, anodic, or mixed. The data obtained from polarization curves by Tafel extrapolations for all the studied biomass extracts are presented in Tables 4.7-4.10 and discussed below. The results of the experiments in the presence and absence of different concentration of investigated biomass extracts are depicted in Figure 4.14

❖ **Mild steel as working Electrode**

4.2.1.1 Potentiodynamic polarization studies of Mild steel (MS) in the presence of HRL extract in 1 M HCl

The electrochemical polarization parameters such as corrosion potential (E_{corr}), corrosion current density (I_{corr}), anodic and cathodic Tafel slopes (b_a and b_c), polarization resistance (R_p), and inhibition efficiency (IE %) for mild steel in the absence and presence of various concentrations of HRL extract is given in Table 4.7

Table: 4.7 Potentiodynamic polarization parameters for the corrosion of MS in the absence and presence of HRL/HRF extracts in 1 M HCl

S.No.	Conc. (%)	Tafel polarisation parameters					Linear polarisation resistance parameters	
		$-E_{corr}$ mV/ SCE	I_{corr} µA/cm^2	b_a mV/ decade	b_c mV/ decade	IE (%)	R_p Ohm/cm^2	IE (%)
HRL								
1.	Blank	494	1846	91	142	-	13.5	-
2.	0.1	425	899	85	136	51.3	23.0	41.3
3.	0.2	434	770	79	127	58.3	31.2	56.7
4.	0.3	431	606	91	118	67.2	32.9	59.0
5.	0.4	430	515	90	131	72.1	35.7	62.2
6.	0.5	438	458	92	117	75.2	38.8	65.2
7.	0.6	448	346	80	128	81.3	60.6	77.7
8.	0.7	458	221	69	121	**88.0**	83.3	83.8
HRF								
1.	Blank	494	1846	91	142	-	13.5	-
2.	0.1	428	692	79	128	62.5	27.8	51.4
3.	0.2	444	406	88	131	78.0	35.3	61.8
4.	0.3	438	391	64	129	78.8	41.6	67.6
5.	0.4	456	390	83	134	78.9	48.2	72.0
6.	0.5	429	309	92	125	83.3	54.6	75.3
7.	0.6	449	257	73	139	86.1	71.5	81.1
8.	0.7	441	237	70	133	**87.2**	75.2	82.1

Figures 4.14 (a) shows the potentiodynamic polarization curve for the MS specimen in 1 M HCl without and with HRL extracts. Close examination of Figure 4.14(a) reveals that the addition of inhibitor to 1 M HCl affects both the anodic and cathodic parts of the curve. This indicates that the addition of extract to acid solution reduces the anodic dissolution of metal and also impedes the cathodic hydrogen evolution reaction (**Lebrini *et al,* 2011**).

The anodic (b_a) and cathodic (b_c) slope values of inhibited solution have changed with respect to uninhibited solution which also indicates that, the extract behaves like mixed type inhibitor. The values given in the Table 4.7 show that corrosion current (I_{corr}) decreases remarkably from 1846 μA/cm^2 to 221 μA/cm^2 in the presence of HRL extract .This confirms the inhibitive action of the biomass extract in HCl medium. The calculated values of inhibition efficiency indicate that, IE increases with increasing extract concentration**,** due to increase in the blocked fraction of the electrode surface by adsorption. The inhibition efficiency reaches up to a maximum of 88%, which indicates that HRL extract is a good inhibitor. It can be seen that the addition of the inhibitor shifts the E_{corr} values towards the positive direction. A compound can be classified as an anodic or cathodic type inhibitor when the change in E_{corr} value is larger than 85mv. Since the E_{corr} values exhibited by HRL extract is less than 85mv it may be concluded that this extract behaves as a mixed inhibitor ie, the addition of the inhibitor reduces both the anodic dissolution of MS and also retards the cathodic hydrogen evolution.

The increasing linear polarization (R_p) values also confirm the corrosion inhibitive nature of the plant extract. R_p values varied from 13.5 ohm/cm^2 to 83.3 ohm/cm^2 in the presence of HRL extract. The increase in the polarization resistance is possibly due to the formation of the film of active substance covering the surface of the electrode (**Lebrini *et al*, 2010**) Maximum efficiency of 83.8% is obtained by LPR method.

4.2.1.2 Potentiodynamic polarization studies of Mild steel (MS) in the presence of HRF extract in1 M HCl

The effects of HRF on the corrosion reaction of MS has been studied and the changes observed in the polarization curves after the addition of the inhibitor is depicted in Figure 4.14(b).The corrosion parameters namely corrosion potential (E_{corr}), Tafel slopes (b_a, b_c), linear polarization resistance (R_p) and corrosion current (I_{corr}) are listed in Table 4.7.It can be seen from table that the corrosion current (I_{corr}) decrease tremendously from 1846 μA/cm^2 to 237 μA/cm^2 as the inhibitor concentrations increases. This suggests that a protective film is formed on the metal surface (**Sangeetha *et al*, 2011**). The inhibition efficiency at optimum concentration of 0.7 % concentration of HRF is found to be 87.2%.

The values of Tafel slopes b_a and b_c are found to change with inhibitor concentration which clearly indicated that the inhibitor controlled both anodic and cathodic reactions (**Benali *et al*, 2013**). The corrosion potential, E_{corr}, becomes less negative as the concentration of the inhibitor increases. It can also be observed that the R_p value increases considerably from 13.5 Ohm/cm^2 (blank) to 75.2 Ohm/cm^2 (0.7% conc) with increasing concentration of extract and maximum inhibition effiency of 82.1% is obtained. From the values of inhibition efficiency, it is clear that the corrosion inhibition may be due to the increase in the adsorption of the inhibitor on the metal surface by blocking the active sites on the metal surface **(Abdel-Gaber, *et al,* 2006).**

4.2.1.3 Potentiodynamic polarization studies of CIL extract / MS/ 1 M HCl

Polarisation behaviour of mild steel in 1 M HCl in the absence and presence of various concentrations of the plant extract CIL is shown in the Figures 4.14 (c). The corresponding electrochemical parameters derived from the polarization curves are presented in Table 4.8.

Table 4.8 : Potentiodynamic polarisation parameters for the corrosion of MS in the absence and presence of different concentrations of CIL, CIF extracts in 1 M HCl

S.No.	Conc. of inhibitor in (%)	Tafel polarisation parameters					Linear polarisation resistance arameters	
		$-E_{corr}$ mV/ SCE	I_{corr} µA/cm^2	b_a mV/ decade	b_c mV/ decade	IE (%)	R_p Ohm/cm^2	IE (%)
CIL								
1.	Blank	416	1007	90	171	-	17.3	-
2.	0.1	435	749	108	134	25.6	24.7	30.0
3.	0.2	438	657	96	149	34.8	25.3	31.6
4.	0.3	434	592	104	121	41.2	26.7	35.2
5.	0.4	410	515	90	145	48.8	32.6	46.9
6.	0.5	424	382	86	131	62.1	37.6	54.0
7.	0.6	408	356	86	141	64.6	48.1	64.0
8.	0.7	409	290	71	114	71.2	79.3	**78.2**
CIF								
1.	Blank	416	1007	90	171	-	17.3	-
2.	0.1	432	743	104	135	26.2	20.4	15.2
3.	0.2	424	652	111	88	35.2	22.9	24.5
4.	0.3	493	414	100	188	58.9	30.1	42.5
5.	0.4	431	400	79	89	60.3	52.5	67.1
6.	0.5	462	369	128	138	63.4	62.6	72.4
7.	0.6	471	223	73	209	77.8	68.6	74.8
8.	0.7	431	166	70	89	**83.5**	100	82.7

The values of both anodic and cathodic Tafel constants b_a and b_c respectively are markedly changed in the presence of the extract. The non-constancy of Tafel slopes for different concentration of the inhibitor reveals that the inhibitor action is due to the interference in the mechanism of the corrosion processes at cathode as well as anode **(Samide *et al,* 2005).**This confirms the mixed mode of inhibition of the extract. It could be observed from the table that the corrosion current density I_{corr} decreases noticeably from1007 μA/cm^2 to 290 μA/cm^2 with increase in concentration of CIL extract. Analysis of the Table 4.8 reveals that with increase in plant extract concentration, the corrosion potential (E_{corr}) does not vary much. This confirms the inhibitive action of the extract in HCl medium. A maximum of 78.2 IE is noticed at 0.7% concentration of CIL extract.

The results in Table 4.8 show that the increase in extract concentration leads to increase in R_p value from17.3 Ohm/cm^2 to 79.3 Ohm/cm^2. The increase of Rp offers a high level of protection of the interface against hydrogen reduction and iron dissolution. The increase in the polarization resistance is possibly due to the formation of the film of active substances of the inhibitor covering the surface of the electrode.

4.2.1.4 Potentiodynamic polarization studies of CIF extract/ MS/ 1 M HCl

The anodic and cathodic polarization curves were recorded in the absence and presence of various concentrations of CIF extract and their polarization curves are shown in Figure 4.14 (d). The corrosion kinetic parameters derived from these curves are presented in Table 4.8.As can be seen from Figure 4.14 (d) and Table 4.8, the values of b_a and b_c exhibited no significant changes suggesting that CIF extract acts as mixed type inhibitor and inhibit corrosion by blocking active sites of the metal **(Quraishi,1996)**.It can be seen from the table that the corrosion potential (E_{corr}) was not shifted significantly in presence of the extract suggesting that CIF extract controls both anodic and cathodic reaction.On the other hand, the corrosion current (I_{corr}) density markedly declines from 1007 μA/cm^2 to 166 μA/cm^2 by the addition of the CIF. This decrease may be due to the adsorption of the inhibitor onto the metal surface **(Hussin and Kassim,2011)**. This suggests that the extract has an efficient inhibitory effect on mild steel corrosion in acid solution. The maximum inhibition efficiency calculated from the values of corrosion current density is 83.5% at optimum concentration of 0.7%. Linear polarisation resistance (R_p) of mild steel in the absence and presence of CIF in 1 M HCl is listed in Table 4.8.From R_p values, it can be seen that as the concentration of CIF increases, the Rp values also increase. Maximum increase in R_p value at 0.7% infers that the CIF inhibits corrosion of mild steel by adsorption process**.**Maximum inhibition efficiency is found to be 82.7 %.

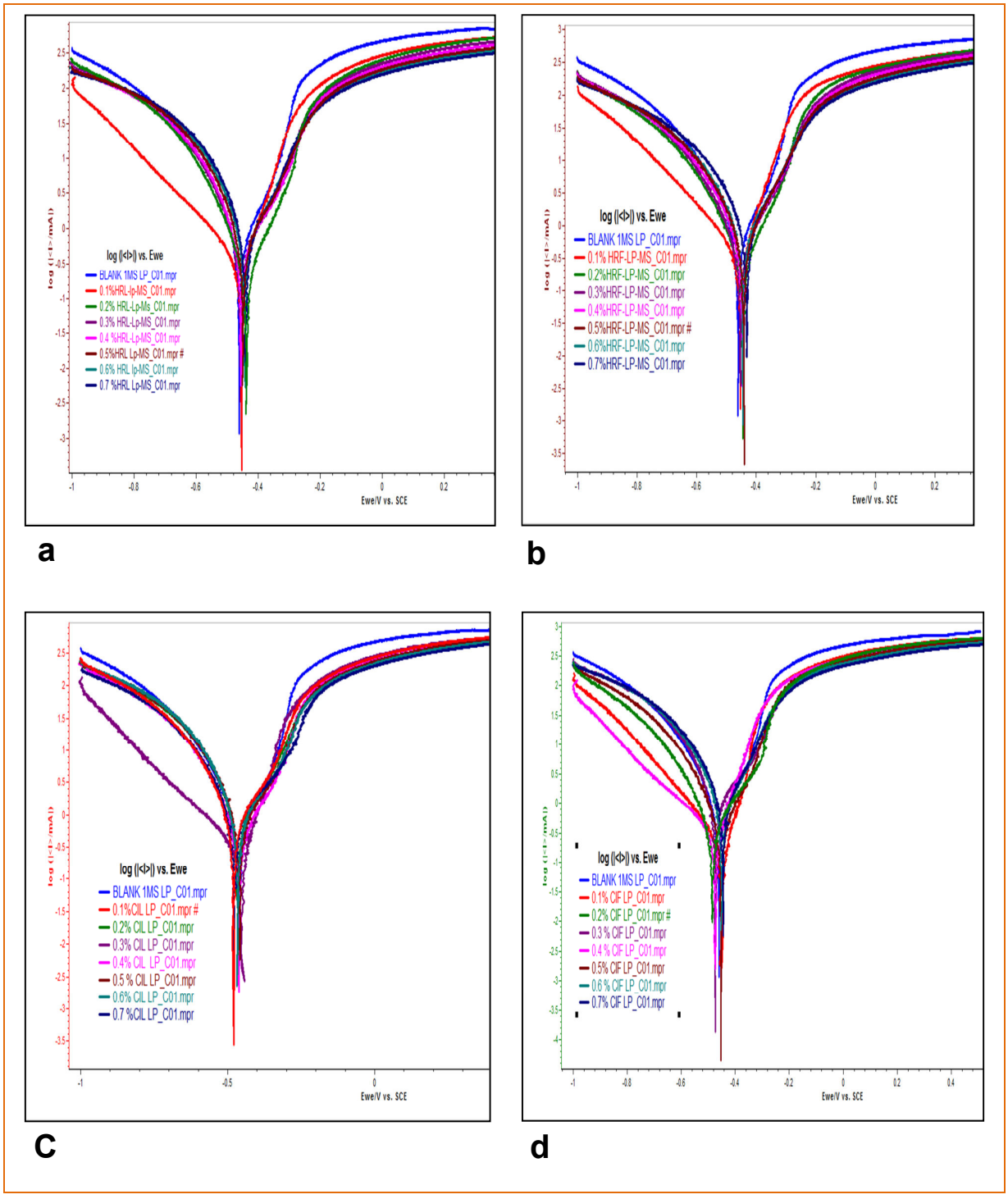

Figure 4.14 Potentiodynamic polarization curves for MS in 1 M HCl in the absence and presence of (a) HRL (b) HRF (c) CIL (d) CIF extracts.

4.2.2 ELECTROCHEMICAL IMPEDANCE MEASUREMENTS

Electrochemical impedance spectroscopy (EIS) has been widely used in investigating corrosion inhibition processes since it provides more information on both the resistive and capacitive behavior at metal/solution interface. Impedance measurements provide an insight into the kinetics of interfacial mass transfer processs **(Bentiss *et al,*1999)**. In the present investigation, the electrochemical measurements were carried out to obtain information about the kinetics of iron acid corrosion taking place at the metal/solution interface in presence of of leaves and flower extracts of ***Heliconia rostrata*** and ***Canna indica*** (HRL, HRF, CIL and CIF). The results are tabulated below and discussed.

4.2.2.1 Electrochemical Impedance spectroscopy Studies of MS in the presence of different concentration of HRL & HRF in1 M HCl

i) HRL extract/ MS/ 1 M HCl

The Nyquist plot of mild steel in uninhibited and inhibited HCl solution with various concentration of the inhibitor at ½ hr immersion period is shown in Figure. 4.15 (a).The parameters such as charge transfer resistance (R_{ct}), the interfacial double layer capacitance (C_{dl}), and solution resistance (R_s) deduced from the Nyquist diagram is given in Table 4.9. The impedance diagram contains a depressed semicircle with the centre under the real axis, which often corresponds to surface heterogeneity which may be the result of surface roughness, dislocations, distribution of the active sites, or adsorption of the inhibitor molecules **(Shukla and Quraishi, 2009).** The diameter of the semicircle gives the charge transfer resistance R_{ct} and this diameter increases on increasing the plant extract concentration which implies an increase in corrosion resistance of the material **(Ghareba and Omanovic , 2010)** The data given in Table 4.9 infers that R_{ct} values increase from 4.6 Ωcm^2 to 22.4 Ωcm^2 with increase in inhibitor concentration which suggests the formation of a protective layer on the mild steel surface **(Murlidharan *et al*, 1995)**.The maximum corrosion inhibition efficiency calculated using these value is 79.3%.The corresponding Bode plots show only one maximum phase reflecting one time constant. This is indicative of one step mechanism **(Khamis *et al*, 2007).**The C_{dl} values shown in the Table 4.9 is found to decrease with increase in the inhibitor concentration. This decrease in C_{dl} value results from a decrease in the local dielectric constant and/or an increase in th thickness of the electrical double layer at acid/metal interface **(Hosseini *et al,* 2007).**

ii) HRF extract/ MS/ 1 M HCl

Figure 4.15(b) shows the electrochemical impedance spectra of Nyquist and Bode plot for mild steel in 1 M HCl in the absence and presence of different concentrations of

HRL extract.The data derived from these Figures are given in Table 4.10. It is evident from Figure 4.15 (b) that the impedance spectra exhibits a single capacitive semicircle in the high frequency region corresponding to one time constant in the Bode plots **(Oguzie *et al*, 2010).** Nyquist plot in Figure 4.15 (b) shows only one capacitive loop for uninhibited solution (1 M HCl) and the same trend is also noticed for mild steel immersed in 1 M HCl containing different concentration of the plant extract. The increasing value of charge transfer resistance R_{ct} (from 3.5 Ωcm^2 to 13.4 Ωcm^2) implies that corrosion rate is reduced in presence of the plant extract and maximum inhibition efficiency of 74.1% is obtained. The C_{dl} values shown in Table 4.10 are found to decrease with increase in inhibitor concentration. The decrease in C_{dl} is because of adsorption of this compound on the metal surface leading to the formation of a surface film in the acidic solution **(Bentiss *et al*, 1999)**

4.2.2.2 Electrochemical Impedance response of MS electrode in the presence of different concentrations of CIL and CIF extracts in 1 M HCl

i) CIL extract / MS/ 1 M HCl

The impedance spectra of CIL extract in 1 M HCl is given in Figure 4.16 (a) and the parameters deduced from the analysis are summarized in Table 4.11. The deviation of perfect circular shape is interpreted by in homogeneity of the electrode surface arising from surface roughness or interfacial phenomena **(Shih and Mansfeld, 1989)**.

It is evident from the figure that the radii of the capacitive circles increase by increasing the concentration of the extract which implies the impedance of the inhibited system increases with inhibitor concentration. The shape is maintained throughout the concentration range, indicating that almost no change in the corrosion mechanism occurred because of addition of inhibitor **(Lahhit *et al*, 2011).**

The results in the Table 4.11 shows that R_{ct} value increases from 3.3 Ωcm^2 to 8.7 Ωcm^2 with increase of CIL extract concentration. The increase in R_{ct} value is attributed to the formation of protective film on the metal/solution interface. This layer makes a barrier for mass and charge-transfer and led to an increase in the inhibition efficiency of 61.6%.The values of C_{dl} gradually decreased from 4125 to 953 $\mu F/ cm^2$ with an increase in the concentration of the extract. This considerable change in C_{dl} values is caused by the gradual displacement of water molecules by the adsorption of the organic molecules on the metal surface, decreasing the extent of the metal dissolution **(McCafferty and Hackerman, 1972).**

ii) CIF extract / MS/ 1 M HCl

Nyquist representation of the impedance behaviour of mild steel in 1 M HCl with and without the inhibitor is shown in Figure 4.16 (b). The impedance data derived from the spectra is given in Table 4.12. The existence of the single semicircle indicates the presence of single charge transfer process during which corrosion was unaffected by the presence of inhibitor molecules **(Ashassi-Sorkhabi *et al*, 2005).**

Inspection of data in Table 4.12 clearly shows that R_{ct} and C_{dl} values have opposite trend at the whole concentration range (R_{ct} increases and C_{dl} decreases with extract concentration).R_{ct} values increase from 3.3 Ωcm^2 to 14.8 Ωcm^2 for the maximum concentration of the (0.7%) in 1 M HCl .

This shows that the plant constituents are adsorbed on the metal surface forming a protective layer on the electrode surface **(Lebrini *et al*,2007)**. Maximum inhibition efficiency of 77.8% is obtained at optimum concentration of 0.7% CIF extract. The thickness of the protective layer formed increases with increasing concentration of the inhibitor resulting lower C_{dl} values. The increase of absolute impedance at low frequencies in the Bode plot confirms the higher protection with increasing concentration of the inhibitor, which is related to adsorption of the inhibitor on the MS surface**. ((Bentiss *et al*, 1999)**

Table: 4.9 Electrochemical Impedance parameters for corrosion of MS in absence and presence of different concentrations of HRL extract in 1 M HCl

Conc (%)	HRL								
	R_S (Ωcm^2)	Y_0 ($\mu F/cm^2$)	n	R_{ct} (Ωcm^2)	IE (%)	f_{max} (Hz)	C_{dl} ($\mu F/cm^2$)	θ	τ (S^n)
Blank	2.055	34333	0.57	4.6	-	5	6910	-	0.032
0.1	1.814	31034	0.6	5.1	9.6	5	6198	0.1	0.032
0.2	1.894	28288	0.62	5.6	17.6	7.3	3884	0.44	0.022
0.3	2.014	23938	0.67	6.7	30.3	7.2	3328	0.52	0.022
0.4	2.313	22706	0.68	7.0	33.9	7.6	2997	0.57	0.021
0.5	1.412	17310	0.75	9.2	49.6	7.5	2300	0.67	0.021
0.6	1.05	9890	0.88	16.1	71.2	5.5	1804	0.74	0.029
0.7	1.326	7106	0.95	22.4	**79.3**	4.3	1662	0.76	0.037

Table: 4.10 Electrochemical Impedance parameters for corrosion of MS in absence and presence of different concentrations of HRF extract in 1 M HCl

Conc (%)	HRF								
	R_S (Ωcm^2)	Y_0 ($\mu F/cm^2$)	n	R_{ct} (Ωcm^2)	IE (%)	f_{max} (Hz)	C_{dl} ($\mu F/cm^2$)	θ	τ (S^n)
Blank	1.305	46075	0.47	3.5	-	15.6	2951	-	0.010
0.1	1.199	35536	0.54	4.5	22.9	21.4	1664	0.44	0.008
0.2	1.414	32014	0.57	5.0	30.5	25.2	1270	0.57	0.006
0.3	1.565	26762	0.62	6.0	41.9	24.6	1089	0.63	0.007
0.4	1.421	23594	0.65	6.7	48.8	22.9	1031	0.65	0.007
0.5	1.324	23034	0.65	6.9	50.0	24.4	944	0.68	0.007
0.6	1.657	16192	0.74	9.8	64.9	20.8	779	0.74	0.008
0.7	1.159	11928	0.8	13.4	**74.1**	19.6	608	0.79	0.008

Table: 4.11 Electrochemical Impedance parameters for corrosion of MS in absence and presence of different concentrations of CIL extract in 1 M HCl

CIL									
Conc (%)	R_S (Ωcm^2)	Y_0 ($\mu F/cm^2$)	n	R_{ct} (Ωcm^2)	IE (%)	f_{max} (Hz)	C_{dl} ($\mu F/cm^2$)	θ	τ (S^n)
Blank	1.405	47804	0.46	3.331	-	11.6	4125	-	0.014
0.1	1.481	40652	0.50	3.917	14.96	23.3	1743	0.58	0.007
0.2	1.761	36413	0.53	4.373	23.83	24.6	1481	0.64	0.006
0.3	1.37	29887	0.59	5.328	37.48	21.6	1382	0.66	0.007
0.4	2.625	26057	0.63	6.111	45.49	19.9	1309	0.68	0.008
0.5	2.182	20955	0.69	7.599	56.17	16.6	1266	0.69	0.010
0.6	1.684	20793	0.69	7.658	56.50	18.6	1118	0.73	0.009
0.7	1.376	18347	0.71	8.679	**61.62**	19.3	953	0.77	0.008

Table: 4.12 Electrochemical Impedance parameters for corrosion of MS in absence and presence of different concentrations of CIF extract in 1 M HCl

Conc (%)	CIF								
	R_S (Ωcm^2)	Y_0 ($\mu F/cm^2$)	n	R_{ct} (Ωcm^2)	IE (%)	f_{max} (Hz)	C_{dl} ($\mu F/cm^2$)	θ	τ (S^n)
Blank	1.593	48533	0.45	3.3	-	20.6	2360	-	0.008
0.1	1.292	44629	0.47	3.6	8.0	19.7	2271	0.04	0.008
0.2	1.581	42565	0.49	3.7	12.3	21	2024	0.14	0.008
0.3	1.354	35528	0.54	4.5	26.8	18.1	1968	0.17	0.009
0.4	1.574	30354	0.59	5.2	37.5	18.1	1679	0.29	0.009
0.5	1.508	27897	0.61	5.7	42.5	17	1638	0.31	0.009
0.6	1.438	24226	0.64	6.6	50.1	28.4	852.6	0.64	0.006
0.7	1.339	10781	0.82	14.8	**77.8**	18.5	583.4	0.75	0.009

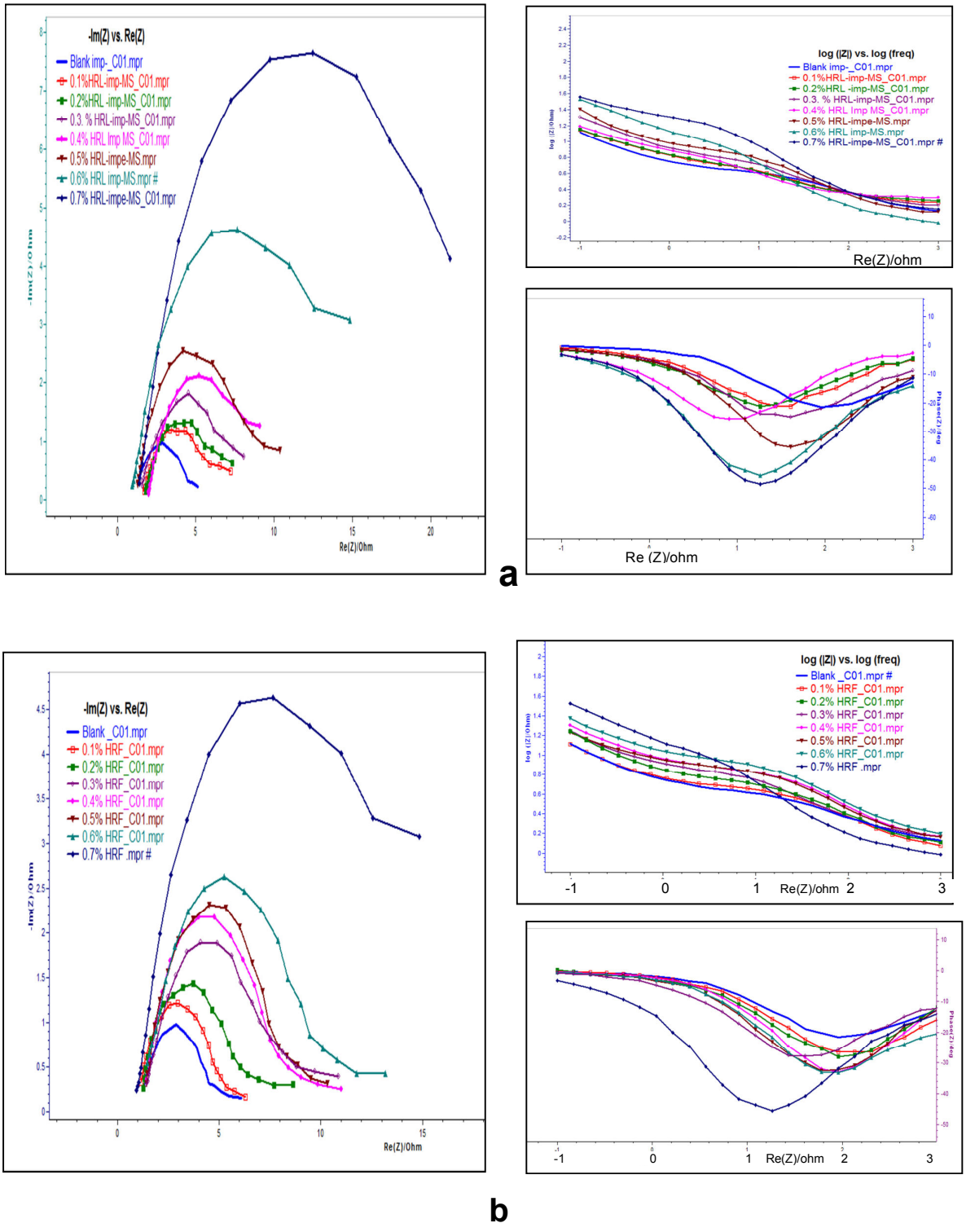

Figure 4.15 Nyquist and Bode diagrams for MS Electrode in 1 M HCl in the absence and presence of (a) HRL (b) HRF extracts

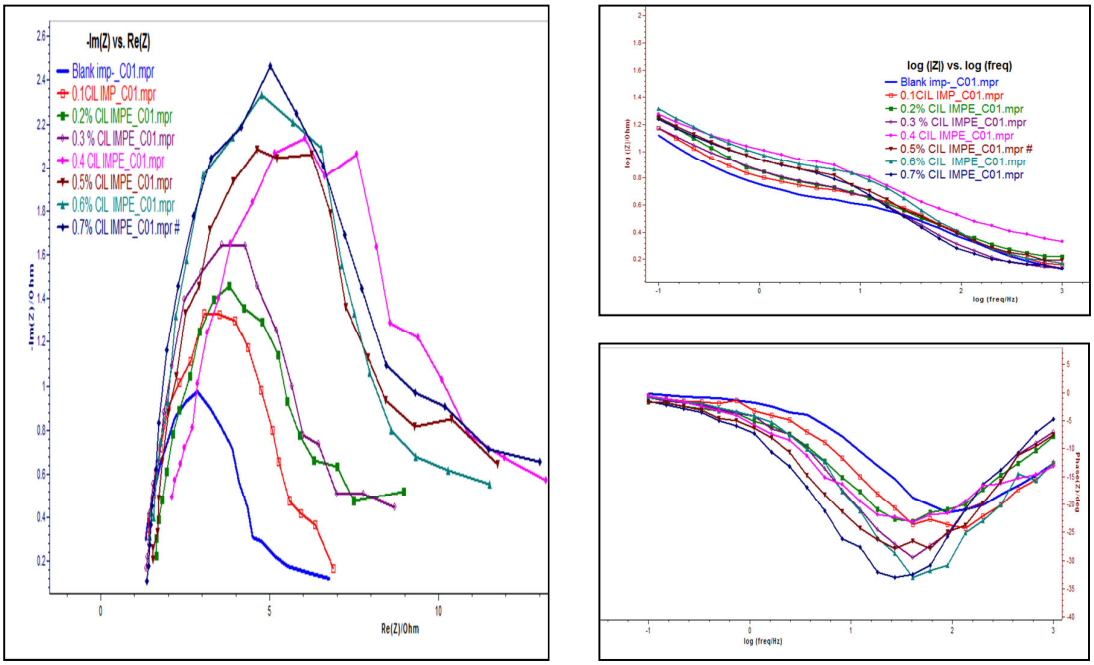

c

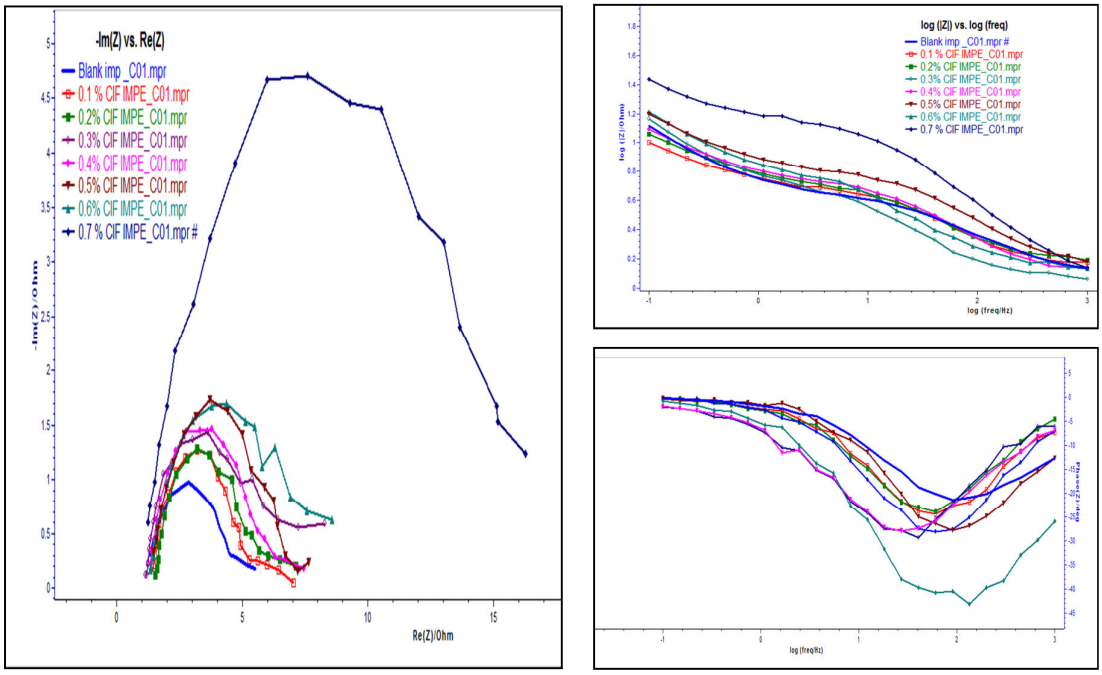

d

Figure 4.16 Nyquist and Bode diagrams for MS Electrode in 1 M HCl in the absence and presence of (a) CIL (b) CIF extracts

Analysis of Impedance spectral data

The impedance diagrams for mild steel in the absence and presence of leaves and flowers of HR/CI extracts in 1 M HCl contain depressed semicircles with the center under the real axis. Such behaviour characteristic for solid electrodes are often referred to frequency dispersion could be attributed to different physical phenomena such as roughness and inhomogeneities of the solid surfaces, impurities, grain boundaries and distribution of the surface active sites. For corrosion reactions which are strictly charge transfer controlled, impedance behaviour can be explained with the help of a simple and commonly used equivalent circuit composed of a double layer capacitance, charge transfer resistance (R_{ct}) and solution resistance (R_s). The resistor R_s is in series to the double layer capacitance and R_{ct}, while double layer capacitance is parallel to R_{ct}. The double layer capacitance is in parallel with the impedance due to the charge transfer reaction. This type of circuit is used to model the iron/acid interface (**Li et *al,* 2007**). The constant phase element (CPE) is introduced in the circuit instead of a pure double layer capacitance to give more accurate fit as shown in the Figure 4.17 (**Macdonald *et al,* 1987**).

The impedance function of a CPE is defined by the mathematical expression given below:

$$Z_{CPE} = Y_o^{-1} (i\omega)^{-n} \qquad \textbf{(4.1)}$$

where Y_o is the CPE constant (in Ω^{-1} s^n cm^{-2}), ω is the sine wave modulation angular frequency (in rad s^{-1}), i^2 =-1 is the imaginary number, n=α/ (π/2) in which α is the phase angle of CPE and n is the CPE exponent (0 ≤ n≤ 1) which measures the deviation from the ideal capacitive behaviour and it represents the surface irregularity. The constant phase element (CPE) is used in the place of capacitor to compensate the non-homogeneity of the surface that causes a greater depression in Nyquist semicircle diagram. (**Havriliak *et al,* 1997; Cruz *et al*, 2008; Lopez *et al,* 2005**).

The CPE is considered to be a surface irregularity of the electrode causing a depression in the Nyquist semicircle diagram (**Garcia-Ochoa and Genesca , 2004**); thus, we could not draw a conclusion that the metal solution interface performs as a capacitor. If the electrode surface is considered as homogeneous and plane, the exponential value (n) becomes equal to 1.0 and the metal-solution interface acts as a capacitor with regular surface. The impedance parameters, namely charge-transfer resistance (R_{ct}), solution resistance (R_s), the constant phase element (Y_o) related to the capacity of the double layer and the exponent (n), relevant to the capacitive semicircle of the mild steel/ 1 M HCl /

HR/CI extracts are listed in Table 4.9 - 4.12. These parameters are calculated from the non-linear least square fit of the equivalent circuit as depicted in Figure 4.17. Simulation of Nyquist plots with above model shows an excellent agreement with experimental data. It means that the suggested equivalent circuit model, presented in Figure 4.17, could reasonably represent the charge-transfer and metal/solution interface features related to the corrosion process of mild steel in acidic solution containing investigated inhibitors.

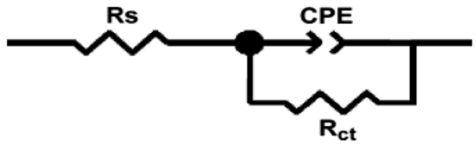

Fig. 4.17 Equivalent Circuit model for MS/1 MHCl

The impedance data are analysed with the equivalent circuit as shown in the Figure 4.17 where R_{ct} is the charge transfer resistance, R_s is the solution resistance and CPE is the constant phase element of double layer capacitance (C_{dl}). In Table 4.9-4.12, the double layer capacitance (C_{dl}) derived from the CPE are also presented, using the following equation (4.2)

$$C_{dl} = Y_o (2\pi f_{max})^{n-1} \qquad \textbf{(4.2)}$$

The CPE is attributed to the non-homogeneity of the electrode surface as well as due to the mass transport process. If the electrode surface is homogeneous and plane, the exponential value (n) is equal to 1 and the electrode surface can be treated as an ideal capacitance. The interface time constant (τ) and the double layer capacitance value (C_{dl}) of the CPE can be calculated by the following equations (4.3 and 4.4) (**Guo Gao and Cheng Hao Liang, 2007).**

$$C_{dl} = Y_o (2\pi f_{max})^{n-1} \qquad \textbf{(4.3)}$$

$$Y_o = \tau^n / R_{ct} \qquad \textbf{(4.4)}$$

The relaxation time (τ) of the surface, that is, the time required for attaining the charge distribution to equilibrium (**Toshima and Uchida, 1970**) is given by:

$$\tau = C_{dl} \times R_{ct} \qquad \textbf{(4.5)}$$

The adsorption of inhibitor needs some time to attain equilibrium. This time is very short, as shown in Table 4.9-4.12. In 1 M HCl containing different inhibitor concentration,

τ remains unchanged irrespective of inhibitor concentration which means fast adsorption process (**Nasibi *et al,* 2013**).

After analyzing the impedance results (Table 4.9 -4.12), it is obvious that the charge-transfer resistance value, R_{ct}, increases with the concentration of HR/Cl and reaches a maximum value at 0.7% in the case of studied inhibitors. A large charge-transfer resistance is associated with a slower corroding system, due to a decrease in the active surface necessary for the corrosion reaction. The increase of the n value after addition of inhibitors in the corrosive solution can corroborate this conclusion. Indeed, the lower n value for uninhibited solution (n = 0.45) indicates a surface inhomogeneity resulting from surface metal roughening and/or formation on the surface of corrosion products. The values of n lies between 0.5 and 0.9 in the case of inhibited solutions. Addition of inhibitors increases n value indicating reduction of surface inhomogeneity due to the adsorption of investigated inhibitors on the most active adsorption sites at the mild steel surface. Experimentally determined values of n for the corroding metal electrode lies around 0.9 (**Hosseini *et al,* 2003**); as can also been seen from Tables 4.9-4.12 in the present cases. Also, the addition of investigated inhibitors to the corrosive solution decreases the double layer capacitance (C_{dl}) and it reflects the time constant (τ) value (Table 4.9-4.12**)**. For example, when the plant extract concentration is increased to 0.7% in the corrosive medium (1 M HCl) the interface (τ) parameter remains constant while the capacitance (C_{dl}) value decreases signifying that the charge and discharge rates to the metal–solution interface is greatly decreased.

This shows that there is agreement between the amount of charge that can be stored (i.e. capacitance) and the discharge velocity in the interface (τ).The double layer between the charged metal surface and the solution is considered as an electrical capacitor. The adsorption of investigated inhibitors on the mild steel surface decreases its electrical capacity because they displace the water molecules and other ions originally adsorbed on the surface. The decrease in this capacity with increase in investigated inhibitors concentration may be attributed to the formation of a protective layer on the electrode surface. The thickness of this protective layer increases with increase in inhibitor concentration, since more investigated inhibitors will electrostatically adsorb on the electrode surface, resulting in a noticeable decrease in C_{dl}. i.e., the inhibitor molecules may reduce the capacitance by increasing the double layer thickness according to the Helmholtz model (**Oguzie *et al,* 2007**) given by the following equation

$$C_{dl} = \varepsilon \varepsilon_o / d \quad \textbf{(4.6)}$$

where d is the thickness of the protective layer, ε is the dielectric constant of the protective layer and ε_o is the permittivity of free space (8.854×10^{-14} Fcm^{-1}).

The AC impedance investigations show that all investigated extracts exhibit excellent inhibitor properties, the best being the HRL extract /mild steel/1 M HCl.

Discussion on Bode Plots

Phase angle at higher frequencies provide a general idea of anti corrosion performance. As the phase angle tends to become more negative, the electrochemical behaviour is found to be more capacitive **(Mahdavian and Attar, 2006)**. Charge transfer increment could raise current tendency to pass through the capacitor in the circuit. According to the appearance of θ vs phase diagrams; increasing concentration of the plant extracts results in more negative values of phase angles at higher frequencies indicating superior inhibitive behaviour at higher concentrations. Also depression of phase angle at relaxation frequency occurs with decreasing the concentration of the plant extracts which indicates the decrease of capacitive response with the decrease of inhibitor concentration. Such a phenomenon could be attributed to higher corrosion activity at lower concentration of the inhibitors. The increase of absolute impedance at low frequencies in Bode plot (Figures 4.15 and 4.16) confirms the higher protection with increasing concentration of the inhibitors, which is related to adsorption of inhibitors on MS surface.

The results drawn from Impedance and Polarisation measurements are quite comparable.

4.2.3 Potentiodynamic polarization studies of AA1100

❖ **Aluminium alloy 1100 (AA1100) as Working Electrode:**

4.2.3.1 Potentiodynamic polarization parameters for the corrosion of AA 1100 in the absence and presence HRL extract/ 1 M HCl

Potentiodynamic polarization plots for AA1100 in 1 M HCl in the absence and presence of different concentrations of HRL extract is shown in Figure 4.18 (a).The respective kinetic parameters including corrosion current density (I_{corr}), corrosion potential (E_{corr}), anodic and cathodic Tafel slope (b_a and b_c) and inhibition efficiency (IE%) are given in Table 4.13.

Table 4.13 points out that the addition of HRL extract affects the cathodic and anodic reactions thereby leading to a noticeable shift in the b_a and b_c values in comparison

to the potential of inhibitor for solution. Such findings in potential support mixed type inhibitor behaviour of HRL in 1 M HCl.

Table 4.13: Potentiodynamic polarization parameters for the corrosion of AA 1100 in the absence and presence of different concentrations of HRL/HRF extract

S.No.	Conc. (%)	Tafel polarisation parameters					Linear polarisation resistance parameters	
		$-E_{corr}$ mV/ SCE	I_{corr} µA/cm^2	b_a mV/ decade	b_c mV/ decade	IE (%)	R_p Ohm/cm^2	IE (%)
HRL								
1.	Blank	817	34377	308	295	-	1.1	-
2.	0.1	882	23048	393	285	33.0	2.5	54.8
3.	0.2	824	20839	319	291	39.4	3.1	63.0
4.	0.3	807	19946	312	312	42.0	3.2	64.4
5.	0.4	797	18079	314	333	47.4	3.6	68.5
6.	0.5	784	16222	312	353	52.8	4.3	73.4
7.	0.6	762	1837	207	293	68.5	4.7	76.1
8.	0.7	827	2734	206	218	92.0	17.9	**93.7**
HRF								
1.	Blank	817	34377	308	295	-	1.1	-
2.	0.1	881	22566	319	198	34.4	1.8	36.5
3.	0.2	848	18811	254	235	45.3	2.1	46.2
4.	0.3	787	18423	175	233	46.4	2.3	49.8
5.	0.4	778	16993	161	235	50.6	2.5	54.6
6.	0.5	774	15080	155	185	56.1	2.7	58.6
7.	0.6	764	12296	135	184	64.2	2.9	61.6
8.	0.7	832	2466	188	226	92.8	20.2	**94.4**

The corrosion current (I_{corr}) is a function of the reactivity of a metal and higher the values of I_{corr}, greater the dissolution of the metal. But in the present study it is seen that addition of HRL extract decreases I_{corr} value from 34377 µA/cm^2 to 2734 µA/cm^2 and this decrease in I_{corr} is due to the formation of an insoluble films formed by the oxidation of aluminium which assist in the process of retardation or dissolution processes **(Fayomi and Popoola,2014).**

A maximum of 92.8% of inhibition efficiency is obtained with 0.7% HRL extract. It is also noted that addition of inhibitor does not remarkably shift the corrosion potential (E_{corr}).Therefore HRL extract is classified as mixed-type inhibitor.

Values of R_p increase appreciably with increasing concentration of HRL extract indicating the effectiveness of the inhibitor in minimising the corrosion of the metal under investigation **(Morad, 2008).**The results in Table 4.13, show that the increase in extract concentration leads to increase in R_p value from 1.1 ohm/cm^2 to 17.9 ohm/cm^2. A maximum of 93.7% of inhibition efficiency is obtained with 0.7% HRL extract.

4.2.3.2 Potentiodynamic polarization parameters for the corrosion of AA 1100 in the absence and presence HRF extract /1 M HCl

Figure 4.18 (b) show Potentiodynamic polarization curves for AA1100 in 1 M HCl without and with various concentrations of HRF extract**.** The evaluated parameters obtained from the extrapolation of the Tafel region are listed in Table 4.13. Table 4.13 reflects that there is no significant variation in b_a and b_c values, it is suggested that HRF extract behaves as mixed type inhibitor **(Amar *et al*, 2007)**.

Inspection of data reveals that I_{corr} decreases considerably in the presence of HRF extract. The current density in uninhibited 1 M HCl solution (blank) is 34377 μA/cm^2 and this value considerably decreases to 2466 μA/cm^2 by the increase of the inhibitor concentration. A maximum inhibition efficiency of 92.8% is obtained with 0.7% HRF extract. This shows the inhibiting action of the inhibitor in the aggressive solution **(Obot *et al*, 2010).**

It can be seen that the presence of HRF extract causes a minor change in E_{corr} value in the absence of an inhibitor. This implies that the inhibitor acts as a mixed type inhibitor affecting both anodic and cathodic reactions.

The estimated R_p values are tabulated in Table 4.13. The R_p values increased from 1.1 ohm/cm^2 to 20.2 Ohm/cm^2 with increase in concentration of inhibitor up to 0.7%.This indicates HRF extract is a better corrosion inhibitor. A maximum of 94.4% of inhibition efficiency is obtained with 0.7% HRF extract.

4.2.3.3 Potentiodynamic polarization studies of CIL extract on AA 1100/1 M HCl

Polarization curves obtained for AA1100 in 1 M HCl solution without and with various concentrations of CIL extract is shown in Fig.4.18 (c). The corrosion kinetic parameters obtained from these curves are depicted in Table 4.14

Table 4.14: Potentiodynamic polarisation parameters for the corrosion of AA 1100 in the absence and presence of different concentrations of CIL/CIF extracts

S.No.	Conc. (%)	Tafel polarisation parameters					Linear polarisation resistance parameters	
		$-E_{corr}$ mV/ SCE	I_{corr} µA/cm^2	b_a mV/ decade	b_c mV/ decade	IE (%)	R_p Ohm/cm^2	IE (%)
CIL								
1.	Blank	817	34377	308	295	-	1.1	-
2.	0.1	819	29141	313	292	15.2	1.5	26.6
3.	0.2	875	17044	308	210	50.4	2.0	42.1
4.	0.3	851	16491	319	255	52.0	2.2	48.6
5.	0.4	879	14448	311	216	58.0	2.3	50.0
6.	0.5	848	1758	315	253	60.0	2.4	53.7
7.	0.6	836	12590	308	263	63.4	2.9	60.4
8.	0.7	875	6197	221	187	82.0	6.3	**82.1**
CIF								
1.	Blank	817	34377	308	295	-	1.1	-
2.	0.1	890	26853	428	211	21.9	1.8	37.2
3.	0.2	851	22085	339	261	35.8	2.7	58.1
4.	0.3	824	21016	311	290	38.9	2.9	61.2
5.	0.4	812	19656	302	316	42.8	3.6	68.8
6.	0.5	818	17082	312	297	50.3	3.7	69.8
7.	0.6	777	13582	225	287	60.5	4.0	71.8
8.	0.7	859	2786	223	203	91.9	21.0	**94.6**

It can be also observed from the table that no sharp changes are observed in b_a and b_c values. This feature indicates that inhibitor does not affect the mechanism of the corrosion reaction **(Negm *et al*, 2010)**.

It is clear from the results that the addition of inhibitor causes a decrease in current density. The I_{corr} value decrease from 34377 µA/cm^2 to 6197 µA/cm^2 during the addition of the CIL extract inhibitor. This is due to adsorption of inhibitor on metal surface which retards the rate of corrosion current density and increases inhibition efficiency **(Ahamad *et al*, 2010).** The inhibitor affords maximum of 82% efficiency at 0.7% CIL extract.

The polarization resistance (R_p) increases noticeably with the increase in CIL concentration and the IE is found to be 82.1% at 0.7% concentration.

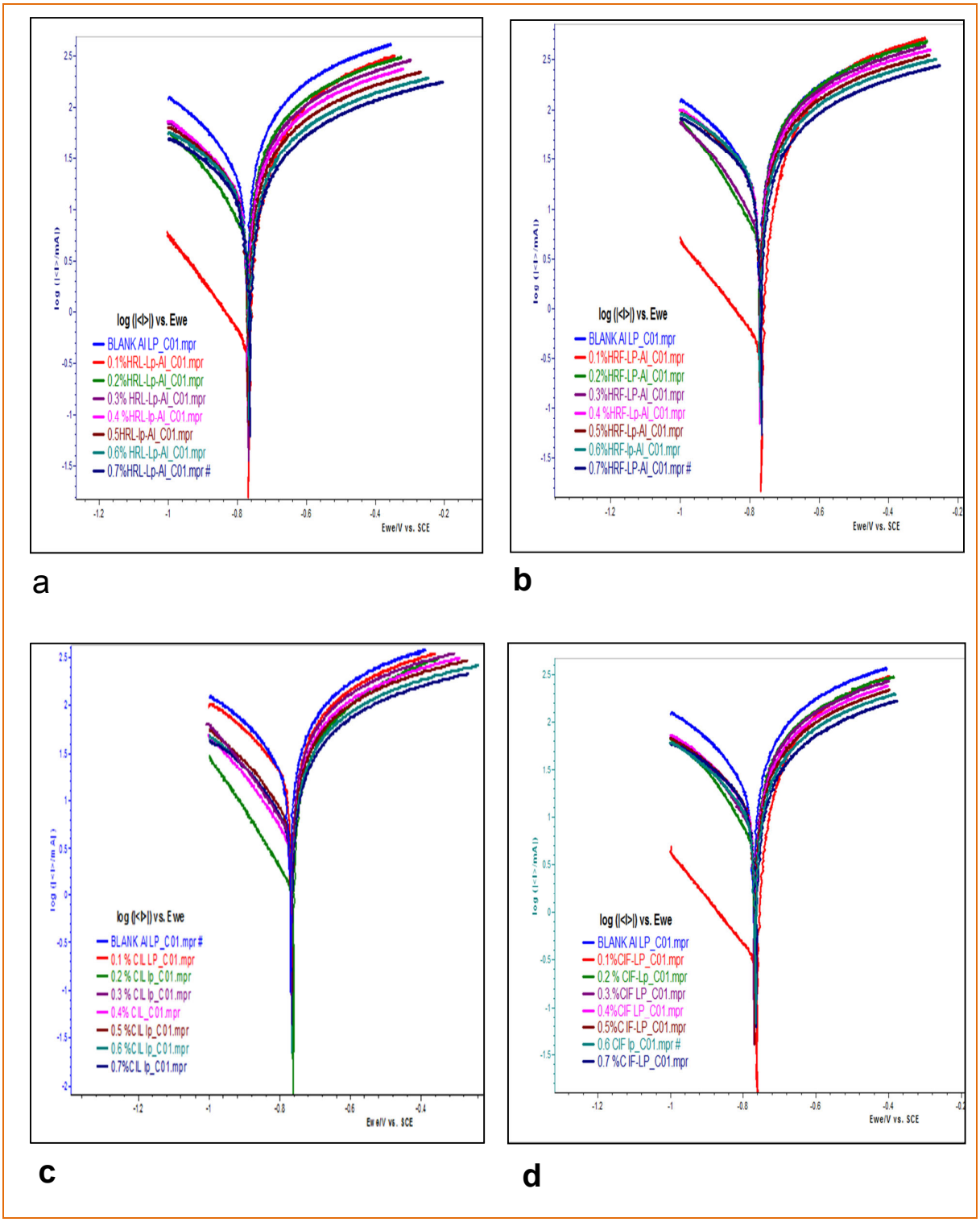

Figure 4.18 Potentiodynamic polarization plots of AA 1100 in 1 M HCl in absence and presence of (a) HRL (b) HRF (c) CIL (d) CIF extracts

4.2.3.4 Potentiodynamic polarization studies of AA 1100/CIF extract /1 M HCl

Potentiodynamic polarization curves of mild steel in 1 M HCl in the absence and presence of CIF extract are presented in Fig 4.18 (d). The corrosion kinetic parameters obtained from these curves are tabulated in Table 4.14.

It is apparent from the figure that, both the anodic and cathodic branches of the polarization curves shifted towards lower current density at all investigated concentrations.This indicates that both the anodic and cathodic reactions of AA1100 corrosion are inhibited by CIF extract in 1 M HCl and there is no significant variation in ba and bc values. This suggests that CIF extract behaves as mixed type inhibitor **(Amar *et al*, 2007).**

It can be seen from the table that the current density decreases noticeably with the increase in inhibitor concentration which brings increase in inhibition efficiency. At higher inhibitor concentration more inhibitor molecules are adsorbed on the metal surface providing wider surface coverage. The lowest I_{corr} value obtained for AA1100 is 2786 $\mu A/cm^2$ at 0.7% concentration of CIF. The decrease of I_{corr} indicates the tendency of the inhibitor to retard the dissolution reaction of the AA1100.

The (Rp) value increases noticeably from 1.1 Ohm/cm^2 to 21 Ohm/cm^2 with the increase in CIF concentration and the IE is found to be 94.6% at 0.7% concentration.

4.2.4 Electrochemical Impedance spectroscopy of AA1100

4.2.4.1 Electrochemical Impedance spectroscopy Studies in the presence of different concentration of HRL/HRF on AA1100/ 1 M HCl

i) AA1100/HRL extract/1 M HCl

The corrosion behaviour of AA1100 sample in 1 M HCl in the absence and presence of HRL extracts is investigated by EIS method. The impedance parameters derived from these investigations are given in Table 4.15.

Figure 4.19(a) shows Nyquist and Bode plots. It is noticed that the obtained impedance diagram is almost a semi-circular in appearance and exhibits one single capacitive loop, which indicates that the corrosion of AA1100 is mainly controlled by a charge transfer process **(Behpour *et al,* 2010).** The imperfect semicircles represented in Figure 4.19(a) are related to the frequency dispersion due to the roughness and inhomogeneous of the electrode surface**(Lebrini *et al,*2007).** Further, it is seen that the diameter of the capacitive loop in the presence of inhibitor is larger than that in blank solution, and enlarges with increased inhibitor concentration. This confirms the impedance

of AA1100 increases due to increase in surface coverage of inhibitor molecules on the electrode surface which results an increase in inhibition efficiency **(Deng *et al,* 2010).**

It can also be seen from the table that the presence of HRL extract enhances the R_{ct} values and reduces the C_{dl} values.The R_{ct} value increases from 1.1 Ωcm^2 to 12.5 Ωcm^2. The increase in R_{ct} values is attributed to increase in resistance and adsorption of inhibitor molecules on A1100 ssurface **(Banerjee *et al*, 2012).** The C_{dl} value decreases from 71.7 $\mu F/cm^2$ to 19 $\mu F/cm^2$. This decrease of C_{dl} values is due to increase in the thickness of the electrical double layer and suggests that molecules present in HRL extracts blocking the metal surface by their adsorption at the metal/solution interface **(Singh *et al*,2011).**

ii) AA1100/HRF extract/1 M HCl

Nyquist and Bode plots for AA 1100 sample immersed in 1 M HCl solution in the presence and absence of various concentrations of HRF extracts are given in Figure.4.19 (b) and the corresponding parameters are tabulated in Table 4.16 . The semi-circular appearance in the figure, indicates corrosion of aluminum is controlled mainly by a charge transfer process. The inhibiting effect of HRF extract is characterized by increase in diameter of capacitive loop, indicating the continuous formation of passive film on the sample surface.

The R_{ct} values increase from 1.1 Ωcm^2 to 11.3 Ωcm^2. This increase in R_{ct} value is generally associated with slower corroding system **(Bessone *et al*, 1983).**Values of double layer capacitance (C_{dl}) are also brought down in the presence of inhibitor. The decrease in C_{dl} comparing with blank solution (without inhibitor), is due to formation of a complex at the metal surface **(Quraishi *et al*, 1999).**

4.2.4.2 Electrochemical Impedance response of AA1100 electrode in the presence of different concentrations of CIL & CIF extracts

i) AA1100/CIL extract/1 M HCl

The obtained Nyquist diagrams for AA1100 in 1 M HCl solution without and in the presence of various concentrations of CIL extract are given in Figure 4.20 (a). It is observed that after adding CIL extract the diameter of the capacitance loop increases with increasing concentration of inhibitor and, the shape is not changed throughout a series of inhibitor concentrations. This shows there is almost no change in the corrosion mechanism due to the addition of the inhibitor. As the inhibitor concentration is raised the Rct values increase from 1.3 Ωcm^2 to 8.6 Ωcm^2. This indicates the resistance toward charge transfer reactions responsible for corrosion process. These observations clearly prove the dependence of inhibitor concentration on corrosion control. Values of double layer

capacitance is decreased from 75.2 μF/cm^2 to 19.8 μF/cm^2 in the presence of inhibitor. This confirms the increased level of adsorption of the inhibitor on the metal surface **(Shanbhag *et al,* 2008).**

ii) AA1100/CIF extract/1 M HCl

Corrosion behaviour of AA1100 in 1 M HCl solution in the absence and presence of the CIF extract is shown in Figure 4.20(a). The inhibiting effect of CIF is characterized by the increase in diameter of capacitive loop, indicating the continuous formation of CIF extract containing passive film on the sample surface. The capacitive and inductive loops showed in the Nyquist plots reveal the formation of metal inhibitor complex at metal/solution interface.

Due to the formation and thickening of corrosion products of the alloy, the contact area between substrate and electrolyte was reduced and caused the change of the capacitance loop, resulting in the lower corrosion rate. Obtained results also confirmed that compact and coherent protective film of inhibitors molecule is formed on aluminium surface, acting as a physical barrier to prevent the corrosion attack of the hydrochloric acid solution.

The R_{ct} value increased from 1.3 Ωcm^2 to 13.4 Ωcm^2. The increase in R_{ct} values as shown in Table 4.18 is attributed due to increase in resistance and adsorption of inhibitor molecules on aluminium surface **(Raja *et al,* 2011) .**

The decrease in C_{dl} indicates the gradual replacement of water molecules by the adsorption of the inhibitor molecules on the metal surface, decreasing the extent of dissolution reaction **(Hmamou *et al*, 2013).**

Table 4.15: Electrochemical Impedance parameters for corrosion of AA1100 in the absence and presence of different concentrations of HRL extract in 1 M HCl

Conc (%)	R_S (Ωcm^2)	Y_0 (μF/cm^2)	n	R_{ct} (Ωcm^2)	IE (%)	f_{max} (Hz)	C_{dl} (μF/cm^2)	θ	τ (S^n)	L
Blank	6.582	141292	0.05	1.1	-	1970	71.7	-	0.0001	1.472
0.1	3.457	135751	0.07	1.2	3.9	2520	53.9	0.25	0.0001	3.868
0.2	3.715	63365	0.32	2.5	55.2	1415	44.8	0.38	0.0001	4.328
0.3	3.514	42215	0.42	3.8	70.1	1194	35.4	0.51	0.0001	3.9
0.4	3.887	40725	0.42	3.9	71.2	1356	30.0	0.58	0.0001	4.669
0.5	4.108	36673	0.44	4.3	74.0	1400	26.2	0.63	0.0001	4.055
0.6	4.643	22113	0.52	7.2	84.3	1087	20.3	0.72	0.0001	4.626
0.7	5.479	12759	0.59	12.5	**91.0**	672	19.0	0.74	0.0002	3.765

Table 4.16: Electrochemical Impedance parameters for corrosion of AA1100 in the absence and presence of different concentrations of HRF extract in 1 M HCl

Conc (%)	R_S (Ωcm^2)	Y_0 ($\mu F/cm^2$)	n	R_{ct} (Ωcm^2)	IE (%)	f_{max} (Hz)	C_{dl} ($\mu F/cm^2$)	θ	τ (S^n)	L
Blank	2.483	141292	0.05	1.127	-	1970.3	71.71	-	0.0001	1.472
0.1	3.537	69932	0.30	2.277	50.5	1384.0	50.53	0.30	0.0001	1.262
0.2	4.355	62765	0.32	2.537	55.6	1443.2	43.49	0.39	0.0001	1.299
0.3	3.123	46669	0.40	3.412	67.0	1284.6	36.33	0.49	0.0001	2.849
0.4	2.591	39503	0.43	4.031	72.0	1187.3	33.27	0.54	0.0001	1.769
0.5	2.806	31670	0.48	5.028	77.6	991.5	31.94	0.55	0.0002	1.454
0.6	2.806	15385	0.60	10.35	89.1	531.3	28.96	0.60	0.0003	1.145
0.7	3.144	14054	0.60	11.33	**90.1**	543.3	25.87	0.64	0.0003	3.666

Table 4.17 Electrochemical Impedance parameters for corrosion of AA1100 in the absence and presence of different concentrations of CIL extract in 1 M HCl

Conc (%)	R_S (Ωcm^2)	Y_0 ($\mu F/cm^2$)	n	R_{ct} (Ωcm^2)	IE (%)	f_{max} (Hz)	C_{dl} ($\mu F/cm^2$)	θ	τ (S^n)	L
Blank	2.513	121647	0.11	1.309	-	1619	75.15	-	0.0001	1.542
0.1	3.272	83195	0.23	1.914	31.6	1695	49.09	0.35	0.0001	5.915
0.2	3.427	53905	0.33	2.954	55.7	1302	41.39	0.45	0.0001	1.934
0.3	4.442	51835	0.33	3.072	57.4	1517	34.17	0.55	0.0001	5.897
0.4	4.679	43329	0.34	3.675	64.4	1577	27.48	0.63	0.0001	13.54
0.5	4.329	39969	0.33	3.984	67.1	1809	22.1	0.71	0.0001	10.6
0.6	5.05	26655	0.32	5.974	78.1	1296	20.57	0.73	0.0001	12.57
0.7	5.148	18449	0.26	8.631	**84.8**	934	19.75	0.74	0.0002	9.685

Table 4.18 Electrochemical Impedance parameters for corrosion of AA1100 in the absence and presence of different concentrations of CIF extract in 1 M HCl

Conc (%)	R_S (Ωcm^2)	Y_0 ($\mu F/cm^2$)	n	R_{ct} (Ωcm^2)	IE (%)	f_{max} (Hz)	C_{dl} ($\mu F/cm^2$)	θ	τ (S^n)	L
Blank	2.513	121647	0.11	1.309	-	1619	75.15	-	0.0001	1.542
0.1	3.245	61244	0.33	2.6	49.7	1474	41.54	0.45	0.0001	3.942
0.2	3.63	54254	0.36	2.935	55.4	1688	32.15	0.57	0.0001	1.164
0.3	4.17	44220	0.40	3.601	63.7	1796	24.62	0.67	0.0001	20.69
0.4	4.235	24734	0.51	6.438	79.7	1023	24.17	0.68	0.0002	9.999
0.5	4.721	18339	0.55	8.683	84.9	814	22.52	0.70	0.0002	5.487
0.6	4.434	14609	0.58	10.9	88.0	683	21.38	0.72	0.0002	8.02
0.7	4.936	11883	0.60	13.4	**90.2**	600	19.8	0.74	0.0003	12.58

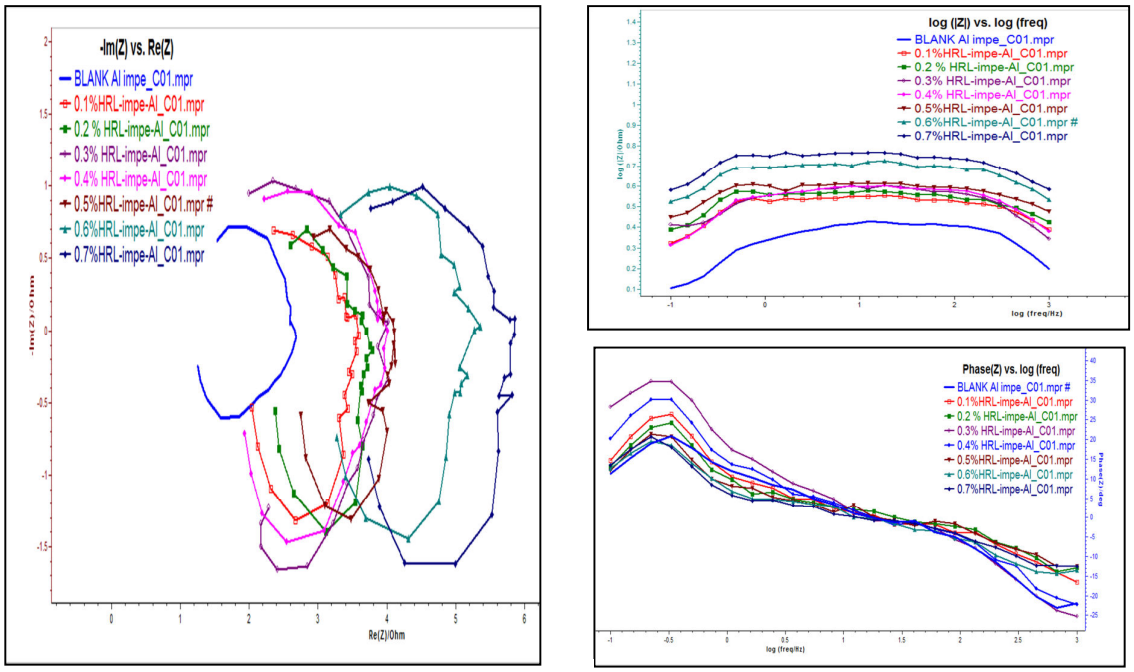

a

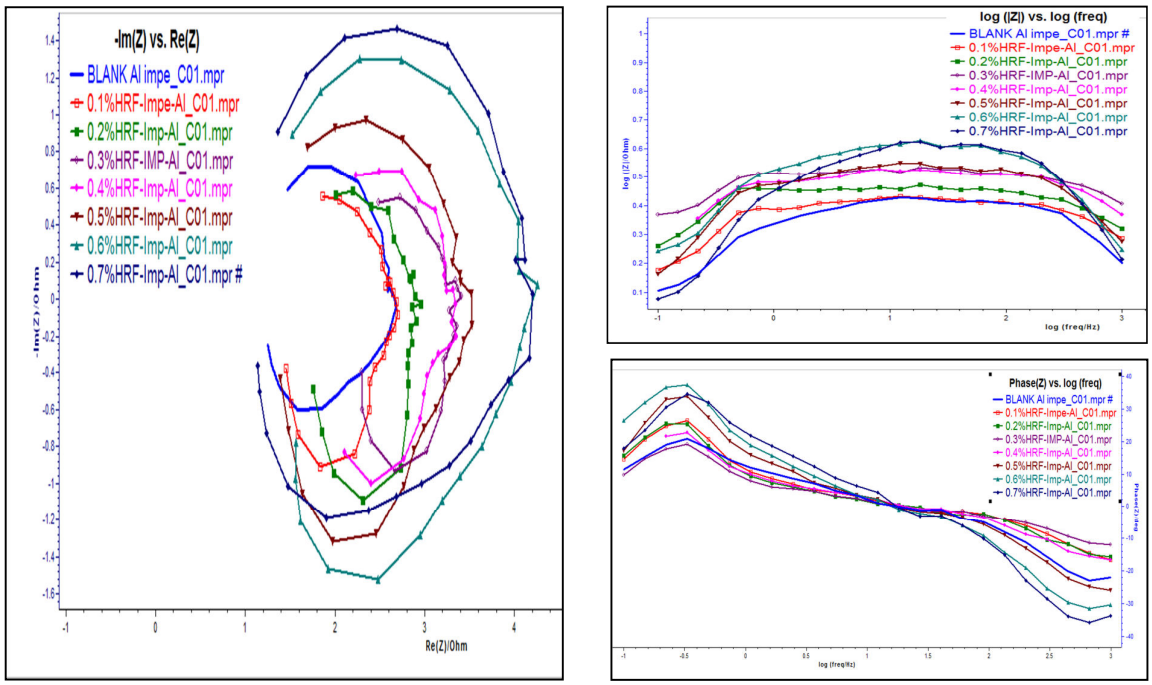

b

Figure 4.19 Impedance response of AA 1100 electrode in the absence and presence of (a) HRL (b) HRF extracts in Nyquist and Bode format

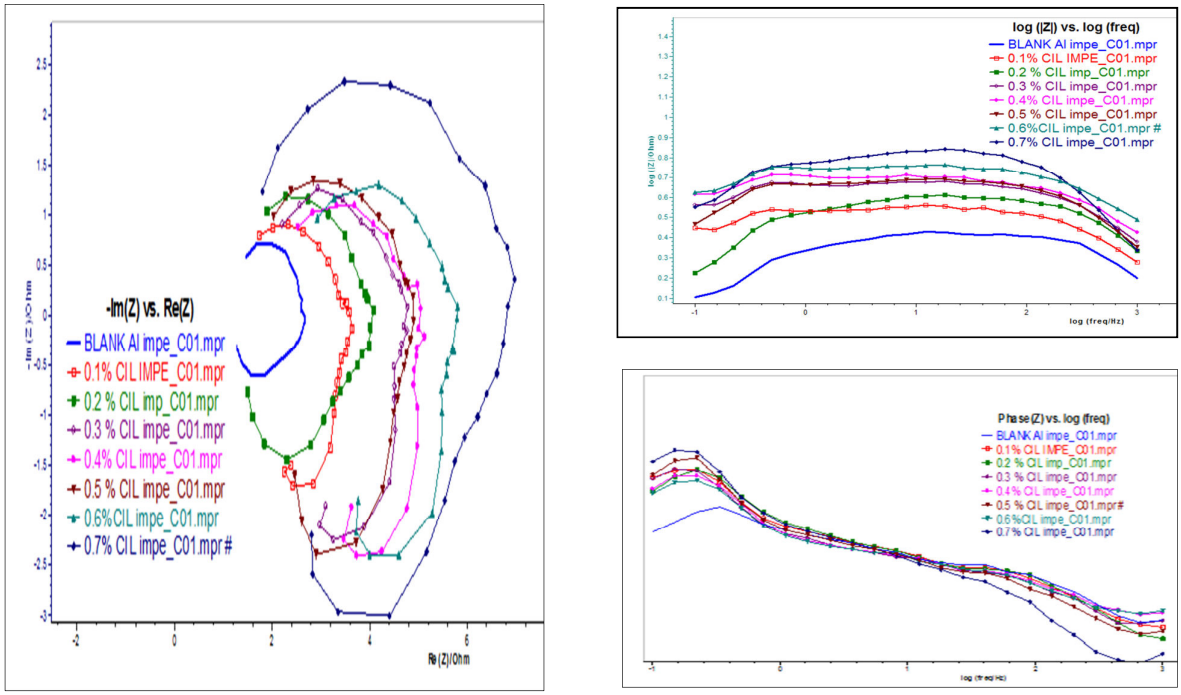

c

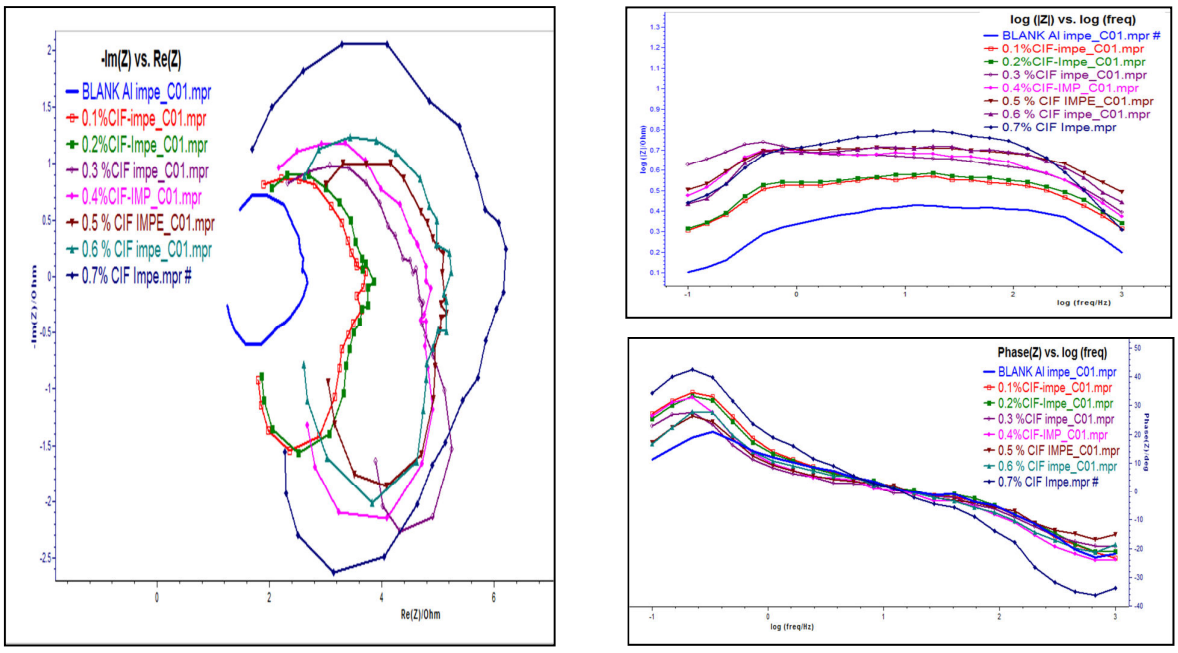

d

Figure 4.20 Nyquist and Bode plots of AA 1100 Electrode in the absence and presence of (c) CIL (d) CIF extracts

Analysis of Impedance Spectral data for AA1100 / HRL/HRF / CIF/ CIL extracts

The capacitive loop at HF could be assigned to the formation of oxide layer on Al. According to **Mansfeld *et al* , 1987; Bessone *et al* ,1983; De Wit and Lenderink ,1996** and **Brett 1992** , an oxide free Al surface is very difficult to produce. Even if producing such a surface, it repassivates very fast by O_2 to form the oxide layer **(Burstein and Cinderey, 1991).** The capacitive loop at HF corresponded to the interfacial reactions, particularly, the reaction of aluminium oxidation at the metal/ oxide / electrolyte interface **(Bret, 1992).** In the present system, formation of Al^+ ions at the metal/oxide interface occurs due to the dissolution of the oxide layer in the presence of 1.0 M HCl.Migration of Al^+ occurs through the oxide/solution interface wherein they are further oxidized to $Al^{3+.}$ The complex of [metal-oxide-hydroxide-inhibitor]$_{ads}$ could also be formed in the presence of inhibitor (MetlkošHukovic´ ,1998). All the above said processes are represented by only one loop that could be attributed either to the overlapping of the loops of processes, or to the assumption that one process dominates and, therefore, excludes the other processes **(De Wit and Lenderink, 1996).**

The presence of the large inductive loop at low frequency might be due to the relaxation of adsorbed charged intermediates **(Amin et al, 2009)**. This is found to be more pronounced when the intermediates such as H^+_{ads} **(De Wit, 1993),** Cl^-, O^{2-} ion or inhibitor species **(Quraishi *et al,* 2010)** are strongly adsorbed onto the electrode surface. It might be also attributed to the re-dissolution of the oxide layer surface or Al-dissolution at low frequencies **(Bessone *et al*, 1992).**

Impedance analysis is a powerful tool for the mechanistic analysis of interfacial processes **(Girija *et al*, 2006).**The impedance spectra obtained from Nyquist plots are analysed by fitting into the equivalent circuit model in Figure 4.21 that is used elsewhere to describe aluminium / acid interface**.(Li *et al*, 2013).** R_s, R_{ct} and RL reflect the solution resistance, charge transfer resistance and inductive resistance, respectively connected with the capacitive loop. L is the inductance that is correlated with the inductive loop. Inductive elements are commonly observed for aluminium impedance behaviour in acid solution **(Yurt *et al* ,2006 ; Metikos *et al*, 2002)** . The impedance values of CPE can be calculated by

$$Z_{CPE} = 1/Y_0 (j\omega)^n \qquad \textbf{(4.7)}$$

where Y_0 is the CPE constant (in Ω^{-1} s^n cm^{-2}), ω is the angular frequency (in rad s^{-1}), j is the imaginary root and n the exponential term.

In general, the impedance loops measured are often depressed semi circles with centres below the real axis. This kind of phenomena is known as dispersing effect. Considering that the impedance of a double layer does not behave as an ideal capacitor in the presence of a dispersing effect, a CPE is used as a substituent for a capacitor to fit more accurately the impedance behaviour of the electrical double layer. **(Li *et al,* 1999)** The impedance parameters, namely charge-transfer resistance (R_{ct}),inductive resistance RL, the constant phase element (Y_0) related to the capacity of the double layer and the exponent (n), relevant to the capacitive and inductive loops of the AA1100/ 1 M HCl/ inhibitor system are given in Tables 4.14 - 4.17. These parameters are calculated from the non-linear least square fit combined with randomisation at 5000 iterations of the equivalent circuit shown in Figure 4.21.

It means that the suggested equivalent circuit model, presented in Figure 4.21 , could reasonably represent the charge-transfer and metal / solution interface features related to the corrosion process of in acidic solution containing HRL / HRF / CIL / CIF extracts.

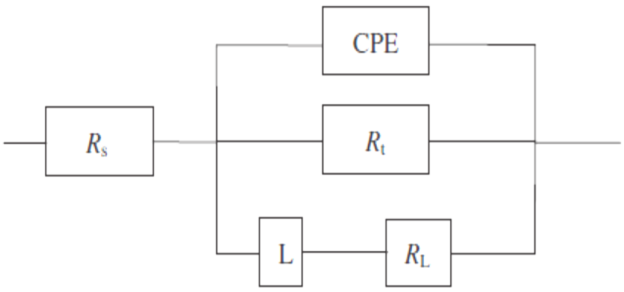

Figure 4.21

Proposed equivalent circuit model for AA1100 / Inhibitors / 1 M HCl (Li *et al*, 2012)

With the help of the equivalent circuit, the polarisation resistance (Rp) can be calculated as follows

$$Rp = \frac{R_{ct} \times RL}{R_{ct} + RL} \qquad (4.8)$$

The interface time constant (τ) and the double layer capacitance value (C_{dl}) of the CPE can be calculated by the following equations **(Guo Gao *et al,* 2007).**

$$C_{dl} = Y_o (2\pi f_{max})^{n-1} \qquad (4.9)$$
$$Y_o = \tau^n / R_{ct}$$

After analyzing the impedance results (Tables 4.14-4.17), it is obvious that the charge-transfer resistance value, R_{ct}, increases with the concentration of HRL / HRF / CIL / CIF and reaches a maximum value at 0.7%. A large charge-transfer resistance is associated with a slower corroding system, due to a decrease in the active surface necessary for the corrosion reaction. The increase of the n value after addition of inhibitor in the corrosive solution can corroborate this conclusion. Indeed, the lower n value for uninhibited solution (n = 0.11) indicates a surface inhomogeneity resulting from surface metal roughening and / or formation on the surface of corrosion products. The values of n lies between 0.3-0.6 in the case of inhibited solutions. Addition of HRL / HRF / CIL / CIF increases n value indicating reduction of surface inhomogeneity due to the adsorption of molecules on the most active adsorption sites at the AA1100 surface. Also, the addition of the inhibitors to the corrosive solution decreases the double layer capacitance (C_{dl}) and it increases the time constant (τ) value (Tables 4.14-4.17). For example, when the concentration increases to 0.7% in the corrosive medium (1 M HCl), the interface (τ) parameter increases while the capacitance (C_{dl}) value decreases signifying that the charge and discharge rates to the metal–solution interface greatly decreases. This shows that there is agreement between the amount of charge that can be stored (i.e. capacitance) and the discharge velocity in the interface (τ).

The double layer between the charged metal surface and the solution is considered as an electrical capacitor. The adsorption of the inhibitor molecules on the AA1100 surface decreases its electrical capacity because they displace the water molecules and other ions originally adsorbed on the surface. The decrease in this capacity with increase in concentration may be attributed to the formation of a protective layer on the electrode surface. The thickness of this protective layer increases with increase in inhibitor concentration, since more of the inhibitor species will electrostatically adsorb on the electrode surface, resulting in a noticeable decrease in C_{dl}. This trend is in accordance with Helmholtz model, given by the following equation

$$C_{dl} = \varepsilon \varepsilon_o / d \qquad \textbf{(4.10)}$$

where d is the thickness of the protective layer, ε is the dielectric constant of the protective layer and εois the permittivity of free space (8.854×10^{-14} Fcm^{-1}).

The shape of the Bode plots is related to the thickness and the dielectric properties of the film formed on the AA1100 electrode. In the high-frequency region the phase angle

approaches 0° while in the middle frequency region the capacitive behavior of the system is evident for all concentrations, determined by the dielectric properties of the formed film. Also, depression of phase angle at relaxation frequency occurs at lower concentration of HRL / HRF / CIL / CIF resulting in decrease of capacitive response with the decrease of inhibitor concentration. Such a phenomenon could be attributed to higher corrosion activity at low concentrations of inhibitors. The increase of absolute impedance at low frequencies in Bode plot confirms the higher protection with increasing the concentration of inhibitors, which is related to adsorption of inhibitors on the AA1100 surface. **(Mahdavian and Attar, 2006).**

4.3 MASS LOSS METHOD

The simplest and the longest established technique for estimating the corrosion process in boiler plants and industrial equipments is the mass loss method. This method of monitoring corrosion rate is useful because of its simple application and reliability. Although there are many experimental techniques which can be used to evaluate the percentage inhibition efficiency of studied inhibitors, mass loss is probably the most widely and frequently used method **(Ekpe *et al*, 1995).** In the present study experiments were conducted by varying the concentration of the inhibitor for different immersion period and at different temperatures.

4.3.1 Effect of concentration and immersion time for MS/ 1 M HCl / HRL/HRF/CIL/ CIF extratcs

Concentration of the inhibitor plays an important role on the mild steel corrosion in 1 M HCl. Mass loss measurements are carried out to study the inhibition performance of the selected plant extracts(HRL,HRF,CIL and CIF) for its different concentrations on the corrosion of mild steel in 1 M HCl. The results are discussed below.

4.3.1.1 Effect of concentration and immersion time of HRL extract on MS/1 M HCl

The calculated corrosion rate and inhibition efficiency values are provided in Table 4.19. The variation of corrosion rate and inhibition efficiency with the concentration of HRL extract is depicted in Figure 4.22. The corrosion rate of the mild steel in 1 M HCl is 1032 mpy for 0.5 h of exposure and it is decreases to 219 mpy on the successive addition of the extract. Similarly for the other immersion periods the corrosion rate decreases with increase in concentration the inhibitor.

Table 4.19. Inhibition efficiency as a function of immersion time and concentration of HRL/HRF/ MS/1 M HCl systems

Conc. %	1/2 h		1h		3h		6h		12h		24h	
	CR (mpy)	IE (%)	CR (mpy)	IE (%)	CR (mpy)	IE (%)	CR (mpy)	IE (%)	CR (mpy)	IE (%)	CR (mpy)	IE (%)
HRL												
Blank	1032	-	1273	-	1482	-	1734	-	1762	-	1232	-
0.1	364	64.7	247	80.6	511	65.5	207	88.1	475	73.0	349	71.7
0.2	321	68.9	212	83.4	431	70.9	206	88.1	292	83.4	206	83.3
0.3	316	69.4	189	85.2	267	82.0	195	88.8	272	84.6	186	84.9
0.4	284	72.5	162	87.2	233	84.3	171	90.1	169	90.4	141	88.6
0.5	250	75.8	160	87.4	190	87.2	154	91.1	142	92.0	112	90.9
0.6	247	76.0	125	90.2	177	88.1	123	92.9	114	93.5	80	93.5
0.7	219	78.8	125	90.2	166	88.8	107	93.9	100	94.4	45	**96.3**
HRF												
Blank	1032	-	1273	-	1482	-	1734	-	1762	-	1232	-
0.1	345	66.6	372	70.8	442	70.2	573	66.9	562	68.1	389	68.5
0.2	329	68.1	351	72.4	363	75.5	384	77.9	266	84.9	256	79.2
0.3	310	70.0	297	76.7	157	89.4	205	88.2	239	86.4	249	79.8
0.4	284	72.5	240	81.1	157	89.4	185	89.3	185	89.5	153	87.6
0.5	249	75.9	205	83.9	151	89.8	158	90.9	157	91.1	148	88.0
0.6	227	78.0	193	84.8	94	93.7	129	92.6	139	92.1	145	88.3
0.7	224	78.3	190	85.1	83	94.4	97	**94.4**	123	93.0	123	90.0

The inhibition efficiency of HRL extract increases with increase in concentration of the extract. The inhibition efficiency increases from 64.7 to 78.8 % as the concentration increases from 0.1 to 0.7 % for 0.5 h immersion. The increase in inhibition efficiency is due to the adsorption of the organic compounds present in the extract (**Akalezi *et al,* 2013**). With further increase in concentration of the extract there is not much difference in the inhibition efficiency. Above 0.7%, the corrosion rate approximately remained constant.The constant rate obtained could be attributed to the competitive adsorption effect between inhibitor molecules and the metal surface which is already covered with initial layers of molecules **(Shivakumar *et al*, 2013).**Thus the concentration of 0.7 % is selected as an optimum concentration for the HRL extracts.This indicates the attainment of a saturation value in surface coverage. Similar trend is observed for the various studied immersion periods.

The corrosion rate and inhibition efficiency is found to vary with the exposure time for HRL extracts and is presented in Figure 4.22. IE increases from 78.8% to 96.3% as the immersion time increases from ½ to 24 h for 0.7 concentration. On prolonged immersion, the time permits the adsorption of large number of molecules on the metal surface. Maximum inhibition efficiency observed for HRL extract is 96.3%.

4.3.1.2 Effect of concentration and immersion time of HRF extract on MS/1 M HCL

The values of corrosion rates and inhibition efficiencies calculated for the HRF extract is summarized in Table 4.19 and picturised in Figure 4.22. It has been observed that the inhibition efficiencies increase with increase in concentration of HRF extract and a maximum inhibition efficiency of 94.4 % (3 h) is obtained with 0.7 % concentration of the extract at 3 h of exposure. The increase in inhibition efficiency is due to the increase in the number of constituent molecules of HRF extract adsorbed on the metal surface at 0.7% concentrations **(Zhang and Hua, 2009)**. With further increase in exposure time the inhibition efficiency decreased. This may be due to the permeable nature of the formed protective layer. The variation of the corrosion rate and inhibition efficiency with concentration and immersion time for mild steel corrosion in the absence and presence of HRL extract is depicted in Figures 4.22. It is clear from the graph that inhibition efficiency of the extract increases with concentration of the extract. This is because of the availability of large number of molecules in the extract for adsorption which in turn results in better surface coverage and hence high protection.

4.3.1.3 Effect of concentration and immersion time of CIL extract on MS/1 M HCl

The material loss expressed as the corrosion rate (mpy) for the mild steel coupons in 1 M HCl solutions containing different concentrations of CIL extract as a function of inhibitor concentration is enlisted in Table 4.20 and are pictorially presented in Figure 4.22**.**

It has been observed that the corrosion rate decreases with the increase in concentration of CIL extract, indicating that the extent of corrosion mitigation is dependent on the concentration of the extract present in the stagnant solution.

The examination of results obtained indicates that the plant extract CIL show a significant inhibitive effect on mild steel in 1 M HCl solutions at various time intervals. From the Table 4.20 and Figure 4.22, it is clear that the corrosion process of the mild steel is brought down in presence of the extract. The corrosion rate decreases considerably and the inhibition efficiency increases with increase in concentration. This indicates that the number of molecules adsorbed increases as the extract content increases from 0.1% to 0.7% concentration.

A maximum inhibition efficiency of 95.9 % is observed for 0.7 % of CIL extract at 12 h of immersion. The inhibition efficiency is increased with increase in the extent of

exposure up to 12h and thereafter a slight decline is observed and the efficiency stabilises to 92.9% at 24 h of exposure.

Table 4.20. Inhibition efficiency as a function of immersion time and concentration of CIL/CIF extracts/ MS/1 M HCl

Conc. %	1/2 h		1h		3h		6h		12h		24h	
	CR (mpy)	IE (%)	CR (mpy)	IE (%)	CR (mpy)	IE (%)	CR (mpy)	IE (%)	CR (mpy)	IE (%)	CR (mpy)	IE (%)
CIL												
Blank	1032	-	1273	-	1482	-	1734	-	1762	-	1232	-
0.1	156	84.9	397	68.8	235	84.1	370	78.6	257	85.4	410	66.7
0.2	139	86.5	348	72.7	171	88.5	156	91.0	147	91.7	206	83.3
0.3	128	87.6	332	73.9	134	91.0	97	94.4	130	92.6	160	87.0
0.4	108	89.5	321	74.8	116	92.2	96	94.5	129	92.7	137	88.9
0.5	108	89.5	316	75.2	101	93.2	85	95.1	96	94.6	124	89.9
0.6	108	89.5	310	75.6	99	93.3	84	95.2	75	95.7	108	91.2
0.7	103	90.1	310	75.6	97	93.4	80	95.4	72	**95.9**	88	92.9
CIF												
Blank	1032	-	1273	-	1482	-	1734	-	1762	-	1232	-
0.1	189	81.7	663	47.9	394	73.4	295	83.0	280	84.1	312	74.6
0.2	154	85.1	643	49.5	362	75.6	155	91.1	143	91.9	204	83.5
0.3	141	86.3	643	49.5	350	76.4	139	92.0	131	92.6	168	86.4
0.4	121	88.3	583	54.2	342	76.9	93	94.7	107	93.9	161	87.0
0.5	99	90.4	530	58.3	318	78.6	84	95.1	106	94.0	146	88.1
0.6	99	90.4	488	61.7	315	78.7	82	95.3	86	95.1	129	89.5
0.7	94	90.9	458	64.1	283	80.9	79	**95.5**	84	95.2	116	90.6

4.3.1.4 Effect of concentration and immersion time of CIF extract on MS/1 M HCl

The values of corrosion rates and inhibition efficiencies calculated for the CIF extract is summarized in Table 4.20 and picturised in Figure 4.22. In presence of CIF extract the same trend is followed with concentration. As the concentration of the extract increases the number of molecules available for the adsorption, in the solution increases and it leads to the greater adsorption. This results in increased surface coverage and in turn inhibition efficiency of the extract.

The corrosion rate decreases with increasing concentration of the extract for all studied immersion period. Maximum of 95.5% inhibition efficiency is obtained at 6 h of immersion. For all the studied extracts the inhibition efficiency is increased with increase in immersion time and a slight declination is observed followed by a stabilisation **(Zakvi and Mehta, 1987).** This behaviour is either due to the increase in hydrogen evolution process or due to the exposure of more cathodic sites to the aggressive environment.

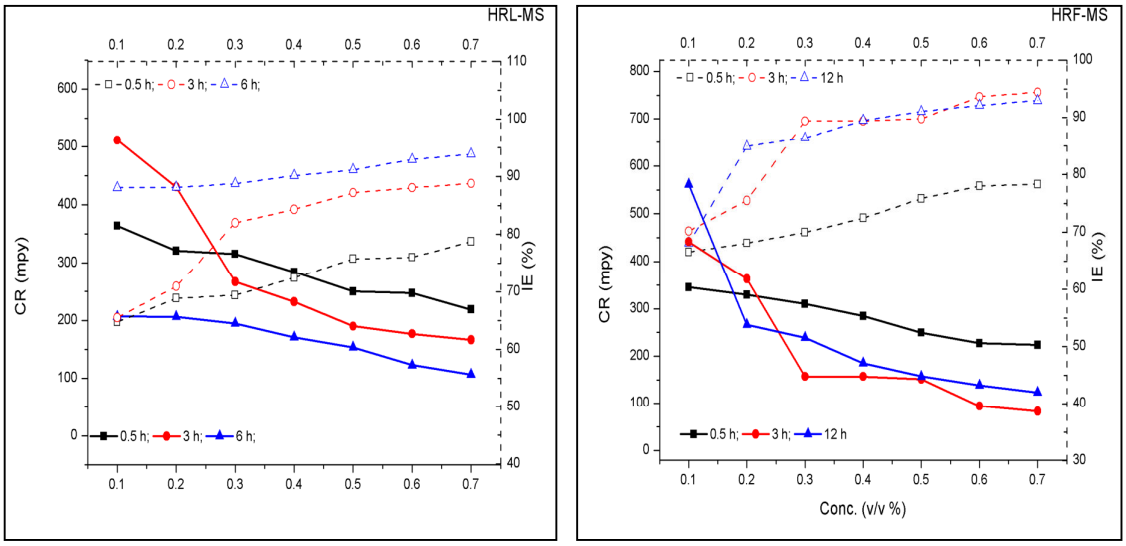

MS/HRL/1 M HCl **MS/HRF/1 M HCl**

MS/CIL/1 M HCl **MS/CIF/1 M HCl**

Figure 4.22. Inhibition efficiency as a function of time and concentration of HRL/HRF/CIL/CIF extracts on MS in 1 M HCl

4.3.2 Effect of temperature:

Temperature plays an important role in understanding the inhibitive mechanism of the corrosion process. As like in a normal chemical reaction it has practical and theoretical importance. Like most chemical reactions, the rate of corrosion of Mild steel increases with temperature especially in media in which evolution of hydrogen occurs, e.g. during

corrosion of mild steel in acids. Acid pickling of steel is usually carried out at elevated temperature – up to 60°C in hydrochloric acid solution. Accordingly, pickling inhibitors are expected to be chemically stable to provide high protective efficiency under the above mentioned conditions. To assess the temperature effect, experiments are performed in the range of 303-353 K in the uninhibited and inhibited solutions containing various concentrations of extracts.

4.3.2.1 Role of Temperature on IE of HRL and HRF extracts

The calculated corrosion rate and inhibition efficiencies of the extracts HRL and HRF are summarized in Table 4.21. It can be noted from the table 4.21 that the maximum inhibition efficiency obtained is 91.3 % for HRL and 86.6 % for HRF extracts. The table values reflect that the IE increases upto 323 K for HRL and 333 K for HRF extracts. It also evidenced the slight decrease in IE after the mentioned temperatures. Thus the HRL shows IE of 84.5 % at 343 and 78.6 % at 353 K whereas HRF shows a IE of 75.9% at 343 K and 70.9% at 353 K.

Table 4.21: Relationship between Inhibition efficiency and concentration for HRL/HRF extracts / MS/1 M HCl/ systems at various temperatures

Conc. %	TEMPERATURE (K)											
	303		313		323		333		343		353	
	CR (mpy)	IE (%)	CR (mpy)	IE (%)	CR (mpy)	IE (%)	CR (mpy)	IE (%)	CR (mpy)	IE (%)	CR (mpy)	IE (%)
HRL												
Blank	1032	-	2791	-	6613	-	8342	-	17090	-	19362	-
0.1	364	65	626	77.6	1794	72.9	2891	65.4	8104	52.6	9149	52.8
0.2	321	69	506	81.9	1049	84.1	1959	76.5	4620	73.0	7257	62.5
0.3	316	69	407	85.4	866	86.9	1530	81.7	4514	73.6	6428	66.8
0.4	284	72	381	86.4	737	88.9	1475	82.3	4356	74.5	5493	71.6
0.5	250	76	352	87.4	648	90.2	1412	83.1	3023	82.3	4411	77.2
0.6	247	76	352	87.4	624	90.6	1346	83.9	2919	82.9	4233	78.1
0.7	219	79	339	87.9	574	**91.3**	1296	84.5	2693	84.2	4145	78.6
HRF												
Blank	1032	-	2791	-	6613	-	8342	-	17090	-	19362	-
0.1	345	66.6	1247	55.3	2166	67.3	3670	56.0	10847	36.5	11147	42.4
0.2	329	68.1	1049	62.4	1843	72.1	3537	57.6	7509	56.1	10512	45.7
0.3	310	70.0	846	69.7	1670	74.7	2659	68.1	7157	58.1	8924	53.9
0.4	284	72.5	786	71.9	1323	80.0	2297	72.5	5606	67.2	7967	58.9
0.5	249	75.9	736	73.6	1237	81.3	1794	78.5	4963	71.0	7061	63.5
0.6	227	78.0	692	75.2	1184	82.1	1439	82.8	4498	73.7	5764	70.2
0.7	224	78.3	637	77.2	1117	83.1	1120	**86.6**	4124	75.9	5638	70.9

This trend is due to the increased effect of temperature on the dissolution process of MS and partial desorption of the inhibitor molecules from the metal surface, **(Ashish Kumar Singh *et al,* 2009)**. This is also favoured by the vigorous hydrogen evolution resulting in the deformation of the formed protective layer.

The impact of temperature on the corrosion rate and inhibition efficiencies in the absence and presence of HRL and HRF extracts are depicted in Figure 4.23. The decrease in inhibition efficiency at higher temperature may be due to the existence of adsorption desorption equilibrium, (**Putilova, 1960).** The adsorption desorption equilibrium is shifted in such a way that the desorption process is favored at higher temperatures. Thus higher desorption rate at the equilibrium at high temperature results lower inhibition efficiencies.

4.3.2.2 Role of Temperature on IE of CIL and CIF extracts

The results obtained for the experiments conducted for MS corrosion in presence of CIL and CIF extracts at various temperatures from 303 to 353 K is summarized in Table 4.22.

Table 4.22: Relationship between Inhibition efficiency and concentration for MS/1 M HCl/ CIL/CIF extracts at various temperatures

Conc. %	TEMPERATURE (K)											
	303		313		323		333		343		353	
	CR (mpy)	IE (%)	CR (mpy)	IE (%)	CR (mpy)	IE (%)	CR (mpy)	IE (%)	CR (mpy)	IE (%)	CR (mpy)	IE (%)
CIL												
Blank	1032	-	2791	-	6613	-	8342	-	17090	-	19362	-
0.1	156	84.9	526	81.2	1292	80.5	3193	61.7	6349	62.9	8335	57.0
0.2	139	86.5	456	83.7	934	85.9	1894	77.3	4529	73.5	5888	69.6
0.3	128	87.6	258	90.8	817	87.7	1317	84.2	3611	78.9	5809	70.0
0.4	108	89.5	204	92.7	661	90.0	1288	84.6	3304	80.7	4868	74.9
0.5	108	89.5	196	93.0	657	90.1	919	89.0	2789	83.7	4647	76.0
0.6	108	89.5	184	93.4	522	92.1	918	89.0	2699	84.2	3948	79.6
0.7	103	90.1	143	**94.9**	485	92.7	846	89.9	2437	85.7	3634	81.2
CIF												
Blank	1032	-	2791	-	6613	-	8342	-	17090	-	19362	-
0.1	189	81.7	522	81.3	1442	78.2	2854	65.8	7012	59.0	7491	61.3
0.2	154	85.1	485	82.6	1188	82.0	1850	77.8	5495	67.9	4751	75.5
0.3	141	86.3	389	86.1	983	85.1	1768	78.8	4079	76.1	4641	76.0
0.4	121	88.3	385	86.2	912	86.2	1636	80.4	3743	78.1	4327	77.7
0.5	99	90.4	294	89.5	839	87.3	1232	85.2	3498	79.5	3321	82.9
0.6	99	90.4	268	90.4	811	87.7	1200	85.6	2921	82.9	2989	84.6
0.7	94	90.9	238	**91.5**	762	88.5	1088	87.0	2302	86.5	2957	84.7

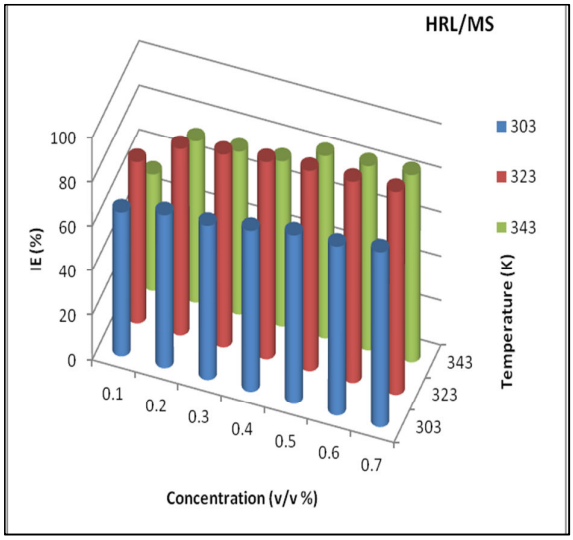

MS/HRL EXTRACT /1 M HCl

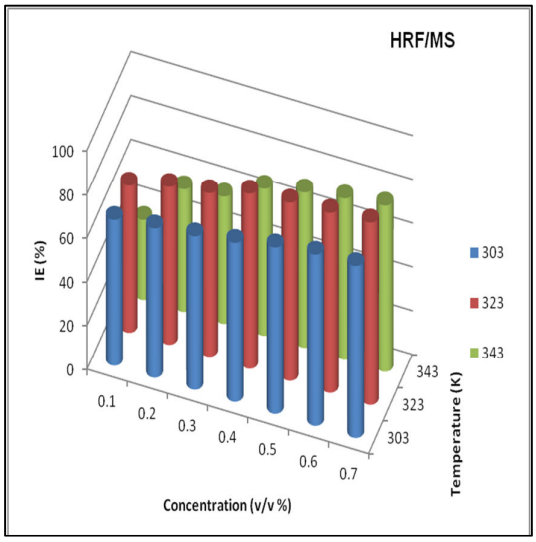

MS/HRF EXTRACT 1 M / HCl

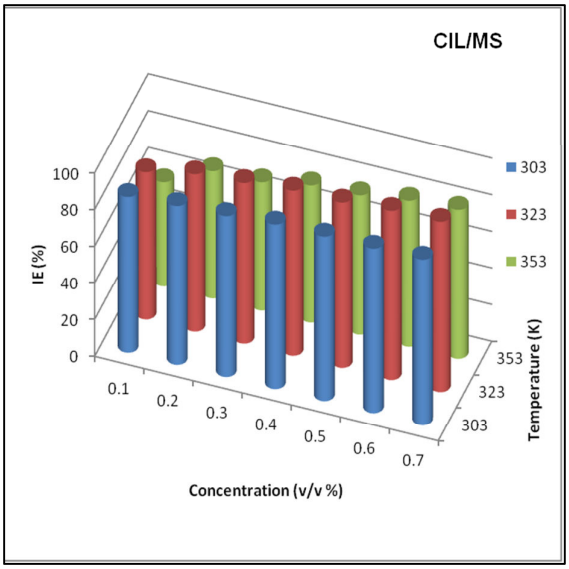

MS/CIL EXTRACT / 1 M HCl

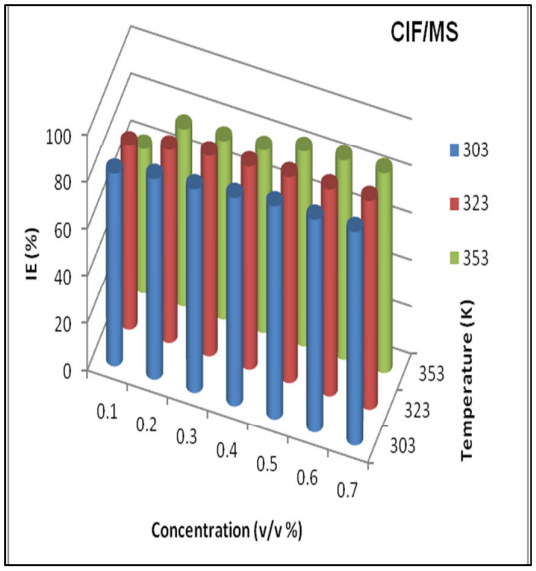

MS/CIF EXTRACT / 1 M HCl

Figure 4.23. Impact of temperature on corrosion rate and inhibition efficiency of HRL/HRF/CIL/CIF extract on MS in 1 M HCl

Examination of Table 4.22 reveals that the presence of inhibitor leads to decrease of the corrosion rate at all studied temperature and at all concentration respectively. As the temperature rises from 303 K to 313 K, inhibition efficiency increases from 90.1% to 94.9 % for CIL and 90.9 %to 91.5 % for CIF respectively. With further increase in temperature IE decreases to 81.2% for CIL and 84.7% for CIF at 353 K in **1 M** HCl at maximum

concentration of 0.7%. This is due to the shift in adsorption-desorption equilibrium in favour of desorption process thereby decreasing the inhibition efficiency to a considerable extent. The observed trend is clearly presented in Figure 4.23.

4.3.3 Effect of concentration of HRL, HRF, CIL, CIF extracts and period of immersion on corrosion of AA1100 in 1 M HCl

The role of exposure time of the metal to the aggressive environment also has an impact on the corrosion of the metal. The corrosion inhibition of AA1100 using HRL, HRF, CIL extracts are studies in 1 M HCl solution and the results are discussed.

4.3.3.1 Effect of concentration and immersion time of HRL extract /AA1100 /1 M HCl

Corrosion behaviour of AA1100 in 1 M HCl containing various concentrations of HRL extract (0.1%-0.7%) is presented in Table 4.23.

Table - 4.23 Inhibition efficiency as a function of immersion time and concentration of HRL/HRF extracts on AA1100/1 M HCl

Conc. %	Immersion Time											
	1/2 h		1h		3h		6h		12h		24h	
	CR (mpy)	IE (%)	CR (mpy)	IE (%)	CR (mpy)	IE (%)	CR (mpy)	IE (%)	CR (mpy)	IE (%)	CR (mpy)	IE (%)
HRL												
Blank	1177	-	2843	-	3727	-	5631	-	3014	-	1521	-
0.1	423	64.1	149	94.8	840	77.5	1686	70.1	979	67.5	530	65.1
0.2	398	66.2	94	96.7	828	77.8	1301	76.9	943	68.7	518	66.0
0.3	315	73.2	68	97.6	792	78.7	906	83.9	762	74.7	494	67.6
0.4	249	78.9	67	97.6	631	83.1	798	85.8	756	74.9	473	68.9
0.5	232	80.3	63	97.8	566	84.8	604	89.3	595	80.3	458	69.9
0.6	216	81.7	31	98.9	587	84.3	589	89.6	511	83.1	441	71.0
0.7	199	83.1	30	**99.0**	510	86.3	530	90.6	482	84.0	399	73.7
HRF												
Blank	1177	-	2843	-	3727	-	5631	-	3014	-	1521	-
0.1	204	82.7	274	90.4	1652	55.7	2969	47.3	1173	61.1	977	35.8
0.2	195	83.5	137	95.2	1252	66.4	2783	50.6	1077	64.3	954	37.3
0.3	185	84.3	114	96.0	927	75.1	2239	60.2	975	67.7	943	38.0
0.4	167	85.8	106	96.3	830	77.7	1974	64.9	951	68.4	938	38.3
0.5	148	87.4	111	96.1	717	80.8	1665	70.4	805	73.3	936	38.5
0.6	130	89.0	63	97.8	703	81.1	1266	77.5	769	74.5	902	40.7
0.7	120	89.8	54	**98.1**	652	82.5	980	82.6	703	76.7	886	41.8

It is clear from the table that the weight loss of the AA1100 decreases as the concentration of HRL extract increases in the solution This directly imparts that the corrosion rate (CR) of AA1100 decreases with increase in concentration of the extract. This is due the fact that more inhibitor molecules are adsorbed on the metal surface at higher concentration, leading to higher surface coverage. (**Singh and Quraishi, 2010**)

The similar trend was observed for all the studied immersion periods. The maximum inhibition efficiency of about 99 % was observed for 1 h immersion period of AA1100 in1 M HCl containing 0.7 % of HRL extract. This clearly depicts the inhibitive effect of HRL extract on AA1100 surface. It also follows from the table that the inhibition efficiency decrease with increase in immersion time from 1 h to 24 h and gets stabilized with 73.7% inhibition efficiency at 24 h of immersion.

4.3.3.2 Effect of concentration and immersion time of HRF extract /AA1100 /1 M HCl

Table 4.23 clearly summarises the role of concentration and immersion period on the corrosion rate and inhibition efficiency of HRF extract on the corrosion of AA1100 in 1 M HCl. The pictorial representation of the CR and IE with concentration is presented in Figure 4.24. The data evidencing the impact of concentration of the HRF extract on the corrosion of AA1100.In the studied inhibitor HRF, the IE increased with immersion period and maximum inhibition efficiency of 98.1 % is obtained for 0.7% HRF extract at 1 h immersion. This is observed due to the formation of adsorbed layer of inhibitor molecules on the metal surface. As the concentration of extract increases the number of available molecules for the adsorption on the AA1100 surface increases which results better surface coverage thereby decreasing the corrosion rate. This indicates that the phytochemical components of the extracts are adsorbed onto the surface resulting blocking of the reaction sites, and protection of AA1100 surface from the attack of the corrosive active ions in the acid medium **(Okafor and Ebenso, 2007; Abiola *et al,* 2009)**. On prolonged immersion the IE decreases and a least value of 42 % was observed for 24 h of immersion. This is due to the porous nature of the formed layer which weakens on longer exposure to the aggressive environment.

4.3.3.3 Effect of concentration and immersion time of CIL extract on AA110 in HCl

The results obtained for the corrosion of AA100 in presence of CIL extract is presented in Table 4.24. The results show that with increase in extract concentration the corrosion rate is found to decrease for all the studied immersion period. The inhibition efficiency increases with immersion time up to 1 h and a maximum protection of 96.6% is

obtained for 0.7%. At higher concentrations the complex formed is insoluble which blocks most of the active sites on the metal surface due to increased surface coverage and results higher values of inhibition efficiency (**Ebenso *et al*, 2003).** The formed layer acts as barrier and protects the metal from aggressive medium. On longer exposure the inhibition efficiency decreases and stabilised to 73.2 % at 24 h.

Table-4.24 Inhibition efficiency as a function of immersion time and concentration of CIL/CIF extract on AA1100/1 M HCl

Conc. %	Immersion Time											
	1/2 h		1h		3h		6h		12h		24h	
	CR (mpy)	IE (%)	CR (mpy)	IE (%)	CR (mpy)	IE (%)	CR (mpy)	IE (%)	CR (mpy)	IE (%)	CR (mpy)	IE (%)
CIL												
Blank	1177	-	2843	-	3727	-	5631	-	3014	-	1521	-
0.1	139	88.2	316	88.9	2127	42.9	3783	32.8	1509	49.9	528	65.3
0.2	115	90.2	210	92.6	1405	62.3	3329	40.9	1295	57.0	512	66.3
0.3	86	92.7	171	94.0	1132	69.6	2892	48.6	1131	62.5	481	68.4
0.4	70	94.1	150	94.7	1051	71.8	2498	55.7	931	69.1	454	70.1
0.5	61	94.8	112	96.1	1003	73.1	2251	60.0	827	72.6	443	70.9
0.6	51	95.7	100	96.5	854	77.1	2235	60.3	793	73.7	421	72.3
0.7	55	95.3	96	**96.6**	788	78.9	2176	61.4	724	76.0	408	73.2
CIF												
Blank	1177	-	2843	-	3727	-	5631	-	3014	-	1521	-
0.1	205	82.6	417	85.3	2302	38.2	2348	58.3	1355	55.1	817	46.3
0.2	114	90.4	180	93.7	1603	57.0	2064	63.4	1148	61.9	800	47.4
0.3	106	91.0	133	95.3	1389	62.7	1725	69.4	854	71.7	770	49.4
0.4	97	91.8	105	96.3	1283	65.6	1476	73.8	802	73.4	747	50.9
0.5	90	92.3	85	97.0	1205	67.7	1266	77.5	685	77.3	745	51.0
0.6	87	92.6	71	97.5	1160	68.9	1133	79.9	574	81.0	722	52.5
0.7	84	92.9	68	**97.6**	961	74.2	1013	82.0	545	81.9	689	54.7

4.3.3.4 Effect of concentration and immersion time of CIF extract on AA1100 in HCl

Similar behaviour of AA1100 is observed in presence of CIF extract. The results are provided in Table 4.24. Addition of extract concentration showed a positive impact on inhibition efficiency. The IE is found to increase with increase in concentration as the number of molecules available for adsorption increases with the concentration of the extract. It provides a maximum of 97.6 % inhibition efficiency at 1 h of immersion. Table 4.24 shows that the IE increases up to 1 h and shows a declination followed by a stabilised value of 54.7 % at 24 h of immersion. On prolonged immersion of AA1100, all the active

sites become saturated with inhibitor and further development of inhibitor layer is gradually slows down. With increased time of exposure it seems that the inhibiting effect decreases probably because of some defects exists on the film leading to the access of aggressive anions to the AA1100/inhibitor interface **(Li and Deng, 2012).** The variation of corrosion rate and IE with concentration of CIF extract is depicted in Figure 4.24.

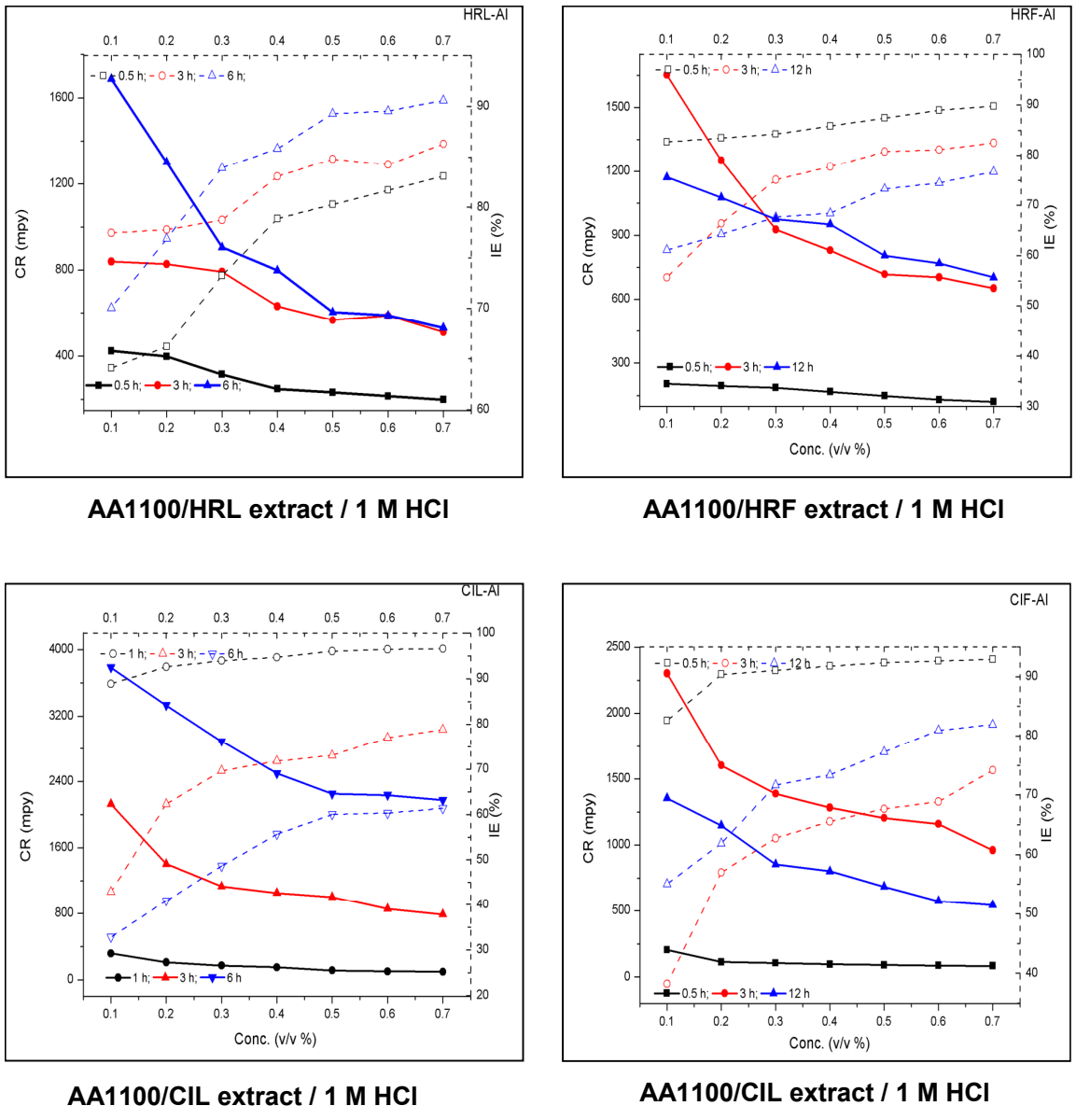

AA1100/HRL extract / 1 M HCl

AA1100/HRF extract / 1 M HCl

AA1100/CIL extract / 1 M HCl

AA1100/CIL extract / 1 M HCl

Fig 4.24 Variation of corrosion rate and inhibition efficiency with concentration of HRL/HRF/CIL/CIF extracts on AA1100

4.3.4 Influence of temperature on the corrosion of AA1100 in the presence of HRL, HRF, CIL and CIF extracts

4.3.4.1 Role of Temperature on HRL and HRF extracts on AA1100/1 M HCl

The results obtained for the experiments carried out for AA1100 corrosion in presence of HRL and HRF extracts at various temperatures from 303 to 353 K is summarized in Table 4.25.

Table 4.25: **Relationship between Inhibition efficiency and concentration for AA1100/1 M HCl/ HRL/HRF extracts at various temperatures**

Conc. %	TEMPERATURE (K)											
	303		313		323		333		343		353	
	CR (mpy)	IE (%)	CR (mpy)	IE (%)	CR (mpy)	IE (%)	CR (mpy)	IE (%)	CR (mpy)	IE (%)	CR (mpy)	IE (%)
HRL												
Blank	1177	-	8761	-	12548	-	27774	-	53359	-	65510	-
0.1	423	64.1	3441	60.7	7264	42.1	12986	53.2	24147	54.8	36616	44.1
0.2	398	66.2	2987	65.9	6290	49.9	12778	54.0	23956	55.1	32009	51.1
0.3	315	73.2	2505	71.4	5056	59.7	12088	56.5	23222	56.5	30672	53.2
0.4	249	78.9	2341	73.3	4347	65.4	11074	60.1	21844	59.1	30467	53.5
0.5	232	80.3	2109	75.9	3971	68.4	10275	63.0	21411	59.9	29139	55.5
0.6	216	81.7	1982	77.4	3882	69.1	9711	65.0	21043	60.6	29054	55.7
0.7	199	83.1	1911	78.2	3565	71.6	9510	65.8	20387	61.8	25418	61.2
HRF												
Blank	1177	-	8761		12548		27774		53359		65510	
0.1	204	82.7	3470	60.4	6041	51.9	8548	69.2	21584	59.6	35553	45.7
0.2	195	83.5	2868	67.3	5352	57.4	8540	69.3	21543	59.6	34931	46.7
0.3	185	84.3	1780	79.7	4428	64.7	8367	69.9	21277	60.1	31716	51.6
0.4	167	85.8	1672	80.9	3747	70.1	7952	71.4	20142	62.3	30481	53.5
0.5	148	87.4	1320	84.9	3297	73.7	7328	73.6	19644	63.2	30323	53.7
0.6	130	89.0	1188	86.4	2773	77.9	6714	75.8	18701	65.0	29370	55.2
0.7	120	89.8	1077	87.7	2316	81.5	6624	76.2	17525	67.2	25732	60.7

Examination of Table 4.25 reveals that the addition of inhibitor leads to decrease of the corrosion rate at all studied temperature and at all concentration respectively. As the temperature rises from 303 K to 353 K, inhibition efficiency decreases from 83.1 to 61.2 % for HRL and 89.8 to 60.7 % for HRF respectively. The observed trend is clearly presented in Figure 4.23. The decrease in inhibition efficiency with rise of temperature is due to the

shift in adsorption-desorption equilibrium. This behaviour can be interpreted on the basis that an increase in temperature results in the desorption of the inhibitor constituents from the surface of the metal, due to the decrease in the strength of adsorption process at higher temperatures (**Abboud *et al,* 2009**).So in the present case, desorption process decreases the inhibition efficiency to a considerable extent.

4.3.4.2 Impact of Temperature on IE of CIL and CIF extracts

The results obtained for the experiments carried out for AA1100 corrosion in the presence of CIL and CIF extracts at various temperatures 303 to 353 K is summarized in Table 4.26

Table 4.26 Relationship between Inhibition efficiency and concentration of CIL/CIF on AA1100 in 1 M HCl systems at various temperatures

Conc. %	TEMPERATURE (K)											
	303		313		323		333		343		353	
	CR (mpy)	IE (%)	CR (mpy)	IE (%)	CR (mpy)	IE (%)	CR (mpy)	IE (%)	CR (mpy)	IE (%)	CR (mpy)	IE (%)
CIL												
Blank	1177	-	8761	-	12548	-	27774	-	53359	-	65510	-
0.1	139	88.2	5134	41.4	8364	33.3	16425	40.9	30833	42.2	38652	41.0
0.2	115	90.2	4801	45.2	7263	42.1	15719	43.4	29991	43.8	38184	41.7
0.3	86	92.7	4344	50.4	7117	43.3	14303	48.5	29608	44.5	37487	42.8
0.4	70	94.1	4182	52.3	6476	48.4	13984	49.7	29365	45.0	37070	43.4
0.5	61	94.8	3903	55.5	6109	51.3	13727	50.6	28878	45.9	36110	44.9
0.6	51	95.7	3812	56.5	5803	53.8	13660	50.8	28801	46.0	35378	46.0
0.7	55	**95.3**	3721	57.5	5692	54.6	13259	52.3	27688	48.1	34783	46.9
CIF												
Blank	1177	-	8761	-	12548	-	27774	-	53359	-	65510	-
0.1	205	82.6	4628	47.2	8102	35.4	17427	37.3	27769	48.0	36760	43.9
0.2	114	90.4	4152	52.6	7337	41.5	17244	37.9	26770	49.8	35811	45.3
0.3	106	91.0	4149	52.6	6502	48.2	17191	38.1	25852	51.6	34682	47.1
0.4	97	91.8	3718	57.6	6008	52.1	16761	39.7	25206	52.8	34611	47.2
0.5	90	92.3	3498	60.1	5957	52.5	16416	40.9	24840	53.5	33796	48.4
0.6	87	92.6	3357	61.7	5471	56.4	15835	43.0	24341	54.4	33518	48.8
0.7	84	**92.9**	3286	62.5	4949	60.6	14220	48.8	23682	55.6	32273	50.7

From the table it is clear that the IE increases with increase in concentration of the extract at the studied higher temperatures also. The impact of temperature on AA1100 increases the corrosion rate thereby decreasing the inhibition efficiency. The IE decreases as the temperature increased from 303 K to 353 K from 95.3% to 46.9 % for CIL and 92.9 to 50.7% for CIF. This is due to the shifting of adsorption – desorption equilibrium towards desorption which leads to the decrease in inhibition efficiency. The variation is clearly depicted in Figure 4.25.

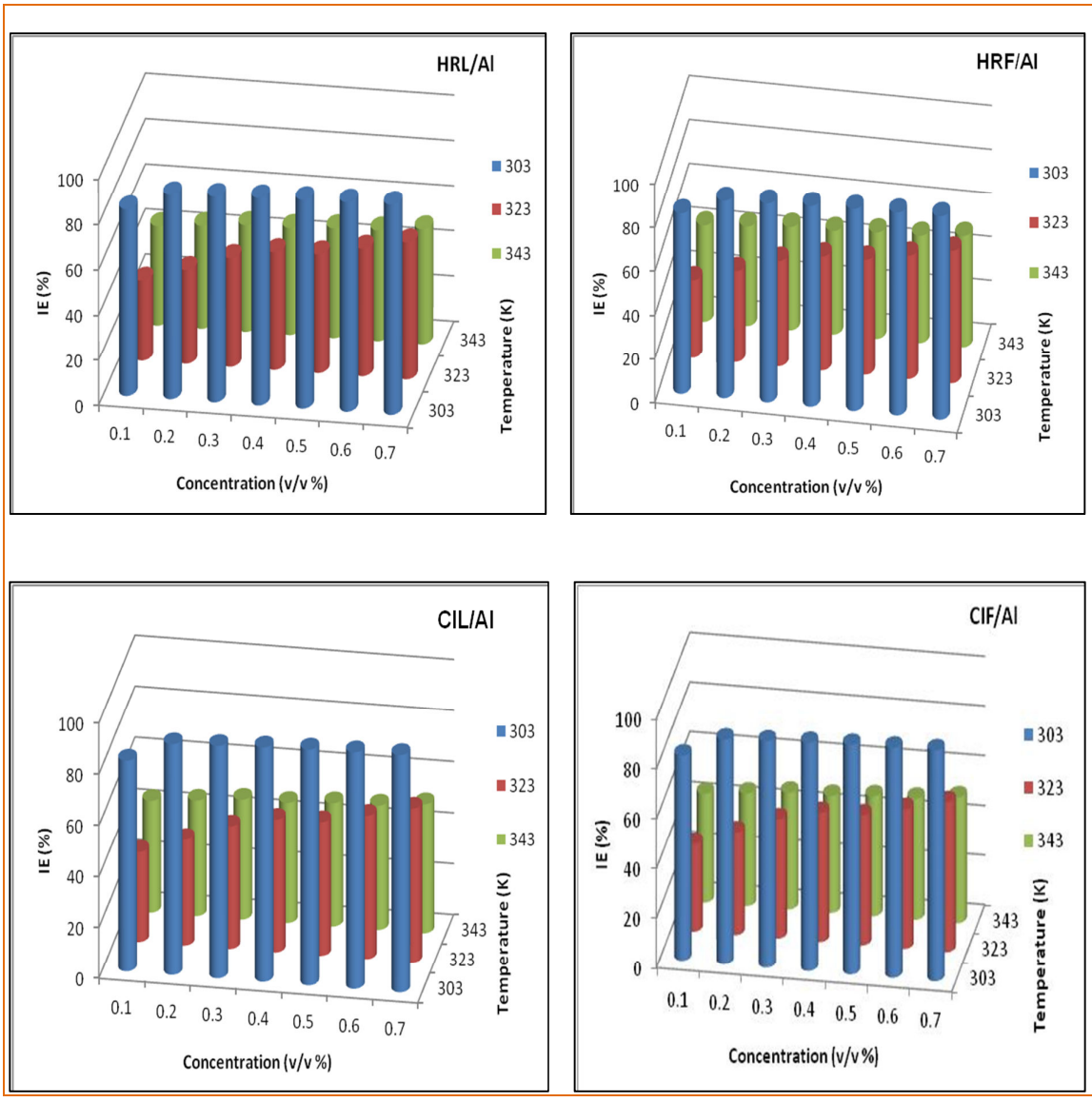

4.25 Impact of temperature on the corrosion inhibition of HRL/HRF/CIL/CIF extract on AA1100 in 1 M HCl

4.3.4.3 Comparison of IE of studied inhibitors using mass loss and electrochemical techniques on Mild steel and AA1100 in 1 M HCl with HRL/HRF/CIL/CIF extracts

Performance evaluation graph of investigated inhibitors using different techniques reveal that all the investigated inhibitors have quite comparable efficiency. Mass loss method furnishes significant raise in IE compared to other techniques (Figure 4.26). This difference may be attributed to the fact that mass loss methods give average corrosion rates, whereas electrochemical methods give instantaneous corrosion rates. This difference may also be expected to arise because of the difference in the time required to form an absorbed layer of the organic compound which can bring down corrosion (**Muralidharan *et al,* 1995**).

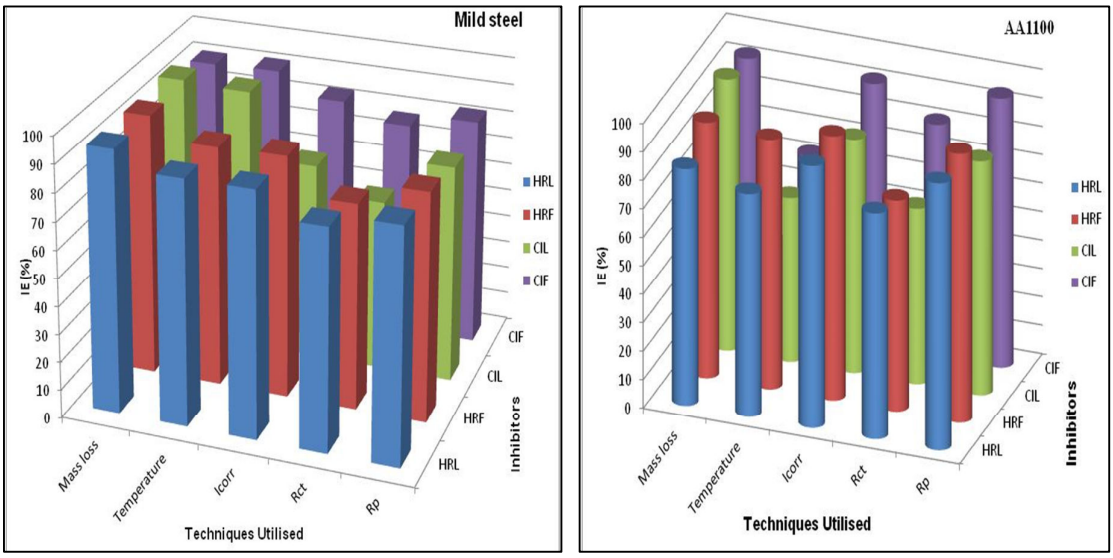

Fig.4.26 Comparison of IE of studied inhibition using mass loss and electrochemical techniques on Mild steel and AA1100 in 1 M HCl with HRL/HRF/CIL/CIF extracts

The results obtained from mass loss, Potentiodynamic polarisation and impedance technique indicate that HRL/HRF/CIL/CIF extracts exhibits significant corrosion inhibition in 1 M HCl. It is worth noticed that the inhibition efficiency obtained from electrochemical measurements are comparable and parallel with those obtained from mass loss method. The selected biomass extracts performed equally well in AA 1100 and Mild steel acid corrosion.The results obtained from all investigated methods are in good agreement.

4.3.4.4 Shelf life performance of HR/CI extracts at room temperature

For industrial purpose the extracts can be prepared in large scale and can be stored for a period of 3 years. This process may help to minimize the labour of the workers. Bearing this in mind, efforts have been taken to prepare the extracts in large scale and portion of it is kept in the room temperature. Mass loss method is best suited method to analyze the inhibitive action of these extracts. Experiments are conducted by selecting an optimum concentration, in the present case 0.7% concentration of HR/CI by mass loss measurements for a period of 3 h immersion. Results pertaining to these studies are pictorially represented in Figure 4.27.

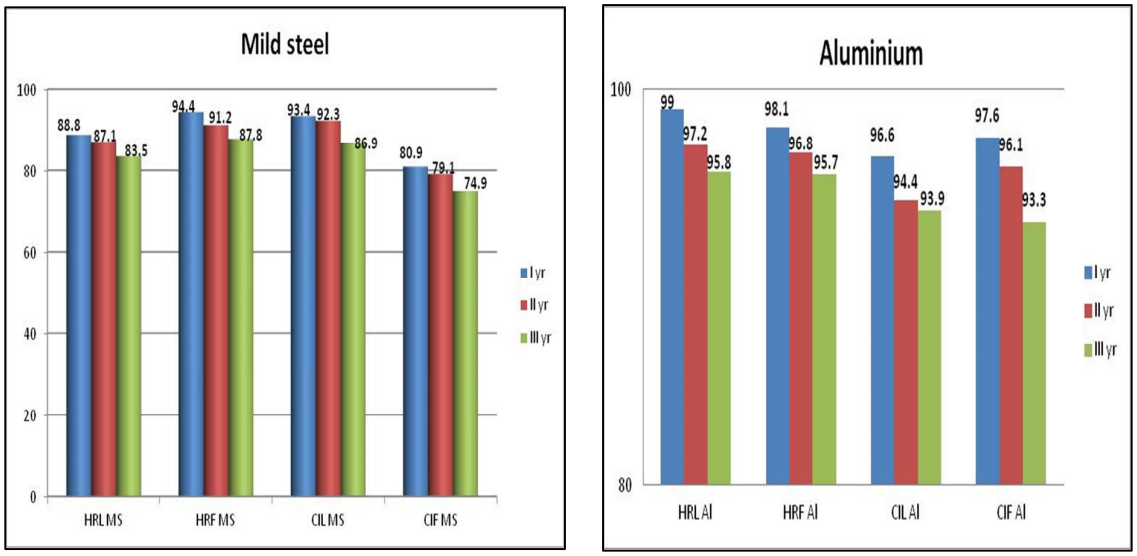

a) MS/HRL/HRF/CIL/CIF **b) AA1100/HRL/HRF/CIL/CIF**

Fig. 4.27 Pictorial representation of durability of investigated inhibitors at room temperature for 3 h of immersion.

Analysis of data reveals that inhibition efficiency (%) is quite comparable for the all the tested inhibitors during the 3 years study period. This test confirms the long lasting capacity of the investigated inhibitors. Results obtained also infer the strong inhibitive action of the inhibitors kept at room temperature for the 3 years. It is up to the interest of industrialist to utilize the inhibitors at room temperature. During storage the extracts are found to be resistant towards fungal and bacterial attack **(El-Etre *et al,* 2005)**. There is no unpleasant odour or evolution of gas during storage. The phytochemical present in these extracts induce the antioxidant characteristics as reflected by very little change of viscosity after two years when stored in room temperature **(Das *et al,* 2004).** Thus these extracts prove to be good performers for 3 years. Thus they can be said to have appreciable shelf life.

4.3.5 Adsorption isotherm

An adsorption isotherm gives the relation between the coverage of an interface with the adsorbed species and the concentration of the species in solution. Interpretation of the performance of the adsorbent type of inhibitor can be enhanced by fitting the data in one of the known adsorption isotherm.

Goodness of Fit:

Data are tested graphically by fitting to various isotherms. Statistical estimation of correlation for the curve fitting of isotherms are used to investigate the goodness of fit of the isotherms **(Schulthess *et al*, 1996).** A measure of the goodness of fit is the square of correlation coefficient R^2 which shows the % of the total variation of the dependent variables can be explained by the independent variable Y. Symbolically

$$R^2 = \frac{\Sigma Y_1^2}{\Sigma Y_1} = \frac{\text{Explained variation}}{\text{Total variation}} \qquad \textbf{(4.11)}$$

The value of R^2 generally lies between 0 and 1 ($0 \leq R^2 \leq 1$). The closer the value of R^2 lies to 1, the better is the regression line to data and vice versa.

To test the overall significance of regression model, the technology of ANOVA is used, which is defined by the F value.

$$F = \frac{\text{Explained sum of square/degrees of freedom}}{\text{Residual sum of squares/ degrees of freedom}} \qquad \textbf{(4.12)}$$

A large F value will be evidence against the null hypothesis, the explanatory variable have no effect of Y.

It is well recognized that the first step in inhibition of metallic corrosion is the adsorption of organic inhibitor molecules at the metal/solution interface. Furthermore, the adsorption depends on the molecules chemical composition, the temperature and the electrochemical potential at the metal/solution interface. So the adsorption of organic inhibitor molecules from the aqueous solution can be regarded as a quasi-substitution process between the organic compounds in the aqueous phase [$Org_{(sol)}$] and water molecules at the electrode surface [$H_2O_{(ads)}$].

$$Org_{(sol)} + x\ H_2O_{(ads)} \longleftrightarrow Org_{(ads)} + x\ H_2O_{(sol)} \quad \textbf{(4.13)}$$

where x is the size ratio, that is, the number of water molecules replaced by one organic inhibitor. Basic information on the interaction between the inhibitor of the mild steel surface can be provided by the adsorption isotherm (**Noor, 2008**). In order to obtain the isotherm, the linear relation between degree of surface coverage (θ) value (θ = %I/100) and inhibitor concentration (C) must be found. Attempts are made to fit θ values to various isotherms including Langmuir, Temkin, Freundlich, Frumkin, Flory-Huggins, El-Awady kinetic thermodynamic and Bockris-Swinkel's adsorption isotherms.

In this section of study, the changes in the surface coverage and thereby the change in the inhibition efficiency is measured using different models at the same level of temperature. These models include Langmuir, Temkin, Freundlich, Frumkin, Flory-Huggins, El Awady kinetic thermodynamic and Bockris-Swinkel's adsorption isotherms.

Langmuir adsorption isotherm can be obtained according to equation (4.14) **(Langmuir, 1917).**

$$\log (C/\theta) = \log C - \log K \quad \textbf{(4.14)}$$

where K is the equilibrium constant, C is the concentration of inhibitor and θ is the degree of surface coverage of the inhibitors. The plots of Langmuir adsorption isotherm is log (C/θ) Vs log C.

Temkin adsorption isotherm can be represented according to equation (4.15) **(Temkin, 1940)**

$$\exp (-2a\theta) = KC \quad \textbf{(4.15)}$$

where 'a' is molecular interaction parameters, θ is the degree of surface coverage, K is the equilibrium constant of adsorption process and C is the concentration of the inhibitors. The plots of Temkin adsorption isotherm is θ Vs ln C.

Frumkin adsorption isotherm can be deduced according to equation (4.16) **(Frumkin, 1964)**

$$\ln [\theta / C (1- \theta)] = \ln K + 2a\ \theta \quad \textbf{(4.16)}$$

where 'a' is the lateral interaction term describing the molecular interaction in the adsorbed layer, θ is the degree of surface coverage, K is the equilibrium constant of

adsorption process and C is the concentration of inhibitors. The plots of Frumkin adsorption isotherm is θ Vs ln [θ/C (1- θ)].

Freundlich adsorption isotherm can be written according to equation (4.17) **(Freundlich *et al,* 1907)**

$$\theta = K C^{1/n} \quad \textbf{(4.17)}$$

where n is the adsorption intensity, C is the inhibitor's concentration and K is the equilibrium constant of adsorption reaction. The plots of Freundlich adsorption isotherm is ln θ Vs ln C.

Flory-Huggins adsorption isotherm can be explained according to equation (4.18) **(Flory, 1941; Huggins, 1941).**

$$\log (\theta/C) = \log K + x \log (1-\theta) \quad \textbf{(4.18)}$$

where θ is the degree of surface coverage, C is the concentration of the system studied x is the number of water molecule replaced by one inhibitor molecule and K is the equilibrium constant for the adsorption process. The plot of Flory-Huggins adsorption isotherm is log (θ/C) Vs log (1-θ).

El-Awady kinetic thermodynamic adsorption isotherm can be described according to equation (4.19) **(El-Awady and Ahmed, 1985)**

$$\log [\theta / (1- \theta)] = \log K' + y \log C \quad \textbf{(4.19)}$$

where C is the concentration of the adsorbate θ is the degree of surface coverage and 1/y is the number of inhibitor molecules occupying one active sites. The plots of El-Awady kinetic thermodynamic adsorption isotherm is log (θ/1- θ) Vs log C.

Bockris-Swinkel's adsorption isotherm can be arrived at using equation (4.20) **(Bockris and Swinkels, 1964)**

$$[\theta / (1-\theta)^x]^{[\theta + x (1- \theta) x-1]} / X^x = KC \quad \textbf{(4.20)}$$

Where θ is the degree of surface coverage, x is the number of water molecules substituted by one molecule of organic absorbate and K is the equilibrium constant of the adsorption process. The plot of Bockris-Swinkel's adsorption isotherm is θ log (θ/1- θ) Vs log C.

A particular model which has highest value of R^2 can be considered as the best model to explain the changes in performance of HR/CI extracts adsorbent-type inhibitors. Similarly, the effect of the level of concentration on the IE can be estimated by coefficient of the equation and can be tested against the hypothesis. The model used takes the following form lny = α + βx, where 'y' is the surface coverage, α is the intercept, β is the slope and 'x' is the concentration. The same model is applied for the seven adsorption isotherms to identify the most suitable model for the problem under study using **Statistical Software Package SPSS 16.**

4.3.5.1 Adsorption isotherm behaviour of investigated inhibitors in acidic media:

Values of adsorption parameters deduced from various adsorption isotherm and the estimated coefficients of studied inhibitors in 1 M HCl for MS and AA1100 are enlisted in Table (4.27-4.34).

Table 4.27 - Adsorption parameters deduced from various adsorption isotherms MS /1 M HCl /HRL

Adsorption isotherms	Temp	Slope	t	intercept	R^2	F
Langmuir	303K	0.902	17.449	0.096	0.999	8.052E3
	313K	0.935	11.677	0.041	1.000	2.108E4
	323K	0.890	1.466 (0.203)	0.013	0.998	3.128E3
	333K	0.874	3.718 (0.014)	0.041	0.997	1.840E3
	343K	0.777	1.319 (0.244)	0.026	0.989	458.277
	353K	0.787	9.863	0.061	0.999	4.896E3
Temkin	303K	0.070	80.494	0.798	0.940	77.803
	313K	0.054	142.196	0.907	0.958	114.002
	323K	0.091	64.671	0.962	0.921	58.482
	333K	0.094	50.782	0.898	0.900	44.863 (0.001)
	343K	0.151	33.649	0.911	0.908	49.284 (0.001)
	353K	0.140	91.033	0.848	0.986	355.360
Frumkin	303K	-0.100	23.373	0.928	0.848	27.844 (0.003)
	313K	0.086	30.535	1.093	0.905	47.481 (0.001)
	323K	-0.231	7.074 (0.001)	1.558	0.666	9.973 (0.025)
	333K	-0.165	9.248	1.207	0.668	10.053 (0.025
	343K	-0.263	3.146 (0.026)	1.332	0.278	1.921 (0.224
	353K	-0.361	11.348	1.400	0.868	32.955 (0.002
Freundlich	303K	0.098	-17.449	-0.220	0.950	94.441
	313K	0.065	-11.677	-0.094	0.954	103.188
	323K	0.110	--1.466 (0.203)	-0.029	0.905	47.818 (0.001
	333K	0.126	-3.718 (0.014)	-0.095	0.884	37.989

Adsorption isotherms	Temp	Slope	t	inter cept	R^2	F
Freundlich	343K	0.223	- 1.319(0.244)	- 0.060	0.883	37.627 (0.002)
	353K	0.213	-9.863	- 0.139	0.986	358.344
Flory-Huggins	303K	3.279	7.566(0.001)	2.177	0.893	41.897 (0.001)
	313K	2.768	14.678	2.695	0.969	158.236
	323K	1.516	16.883	1.771	0.972	174.487
	333K	2.021	9.409	1.800	0.920	57.293 (0.001)
	343K	1.319	8.521	1.167	0.885	38.635 (0.002)
	353K	1.742	14.505	1.243	0.961	124.645
El-Awady kinetic thermodynamic	303K	0.346	23.720	0.584	0.921	58.592 (0.001)
	313K	0.394	57.709	0.943	0.972	172.699
	323K	0.685	43.443	1.158	0.975	196.475
	333K	0.530	24.714	0.856	0.933	69.562
	343K	0.761	16.613	0.854	0.929	65.216
	353K	0.649	29.842	0.681	0.980	241.042
Bockris-Swinkles	303K	0.312	18.404	0.456	0.904	47.202 (0.001)
	313K	0.415	50.255	0.842	0.973	182.576
	323K	0.720	44.148	1.072	0.981	261.674
	333K	0.512	24.523	0.732	0.946	87.192
	343K	0.666	15.849	0.706	0.930	66.570
	353K	0.534	19.761	0.529	0.960	118.502

Figure within ( ) give t values; F Figure within [ ] give F ratio.

Table 4.28 - Adsorption parameters deduced from various adsorption isotherms MS /1 M HCl /HRF

Adsorption isotherms	Temp	Slope	t	intercept	R^2	F
Langmuir	303K	0.909	13.553	0.096	0.999	4.911E3
	313K	0.828	13.736	0.081	0.999	5.916E3
	323K	0.885	14.423	0.059	1.000	1.380E4
	333K	0.759	2.334 (0.067)	0.036	0.993	716.799
	343K	0.638	2.123 (0.087)	0.044	0.983	285.329
	353K	0.713	7.272 (0.001)	0.109	0.993	672.149
Temkin	303K	0.066	64.154	0.799	0.898	44.244 (0.001)
	313K	0.113	110.243	0.816	0.987	369.049
	323K	0.086	114.517	0.866	0.976	205.289
	333K	0.167	32.931	0.898	0.922	58.980 (0.001)
	343K	0.198	48.806	0.841	0.977	208.768
	353K	0.159	31.745	0.751	0.934	70.818
Frumkin	303K	-0.090	19.423	0.914	0.766	16.390 (0.010)
	313K	-0.229	25.547	1.134	0.953	101.015
	323K	-0.156	21.320	1.137	0.905	47.665 (0.001)
	333K	-0.101	1.968 (0.106)	0.928	0.039	0.202 (0.672)
	343K	-0.718	3.133 (0.026)	1.795	0.456	4.185 (0.096)
	353K	-0.306	5.372 (0.003)	1.014	0.522	5.464 (0.067)
Freundlich	303K	0.091	-13.553	-0.221	0.909	49.663 (0.001)
	313K	0.172	-13.736	-0.186	0.981	255.157
	323K	0.115	-14.423	-0.137	0.979	231.698
	333K	0.241	-2.334 (0.067)	-0.083	0.935	72.411

Adsorption isotherms	Temp	Slope	t	inter cept	R^2	F
Freundlich	343K	0.362	-2.123 (0.087)	-0.101	0.948	91.478
	353K	0.287	-7.272 (0.001)	-0.251	0.956	109.174
Flory-Huggins	303K	3.239	6.200 (0.002)	2.180	0.849	28.050 (0.003)
	313K	2.362	22.326	1.547	0.985	329.702
	323K	2.353	12.696	1.899	0.956	108.713
	333K	1.045	6.609 (0.001)	0.932	0.804	20.520 (0.006)
	343K	1.267	14.593	0.827	0.957	110.555
	353K	1.656	6.656 (0.001)	0.872	0.840	26.164 (0.004)
El-Awady kinetic thermodynamic	303K	0.333	19.792	0.588	0.882	37.297 (0.002)
	313K	0.518	47.633	0.607	0.990	492.935
	323K	0.476	36.546	0.766	0.968	153.514
	333K	0.846	11.327	0.833	0.887	39.423
	343K	0.853	22.037	0.638	0.981	258.649
	353K	0.661	10.021	0.457	0.926	62.686 (0.001)
Bockris-Swinkles	303K	0.305	15.909	0.462	0.868	32.838 (0.002)
	313K	0.424	37.988	0.461	0.986	362.997
	323K	0.459	28.533	0.642	0.961	123.850
	333K	0.752	8.975	0.693	0.850	28.257 (0.003)
	343K	0.550	16.720	0.437	0.963	131.883
	353K	0.415	7.481 (0.001)	0.299	0.865	32.035

Figure within ( ) give t values; F Figure within [ ] give F ratio.

Table 4.29 - Adsorption parameters deduced from various adsorption isotherms MS /1 M HCl/ CIL

Adsorption isotherms	Temp	Slope	t	intercept	R^2	F
Langmuir	313K	0.915	1.124 (0.312)	0.006	0.999	7.480E3
	323K	0.929	8.777	0.021	1.000	4.641E4
	333K	0.814	0.018 (0.986)	0.000	0.995	963.060
	343K	0.844	4.458 (0.007)	0.034	0.999	3.700E3
	353K	0.829	6.577(0.001)	0.061	0.998	2.363E3
	303K	0.028	267.729	0.912	0.955	105.230
Temkin	313K	0.075	85.116	0.981	0.931	66.958
	323K	0.061	220.831	0.950	0.985	319.628
	333K	0.141	45.583	0.976	0.932	68.935
	343K	0.116	88.784	0.911	0.976	201.175
	353K	0.117	66.241	0.853	0.963	130.626
	303K	0.064	267.729	0.912	0.955	105.230
Frumkin	313K	0.173	85.116	0.981	0.931	66.958
	323K	0.141	220.831	0.950	0.985	319.628
	333K	0.326	45.583	0.976	0.932	68.935
	343K	0.267	88.784	0.911	0.976	201.175
	353K	0.270	66.241	0.853	0.963	130.626
	303K	0.032	-23.584	0.091	0.955	107.194
Freundlich	313K	0.085	-1.124 (0.312)	-0.015	0.929	65.371
	323K	0.071	-8.777	-0.048	0.982	268.762
	333K	0.186	-0.018 (0.986)	0.000	0.910	50.580 (0.001)
	313K	0.915	1.124 (0.312)	0.006	0.999	7.480E3

Adsorption isotherms	Temp	Slope	t	intercept	R^2	F
Freundlich	343K	0.156	-4.458 (0.007)	-0.078	0.962	126.375
	353K	0.171	-6.577 (0.001)	-0.141	0.952	99.971
Flory-Huggins	303K	4.052	10.168	4.201	0.944	84.284
	313K	1.240	10.402	1.719	0.927	63`523 (0.001)
	323K	1`840	16.954	2.180	0.975	191.825
	333K	1.145	15.156	1.296	0.960	120.625
	343K	1.717	32.877	1.549	0.992	656.881
	353K	1.978	12.121	1.472	0.948	91.872
El-Awady kinetic thermodynamic	303K	0.258	68.278	1.001	0.948	92.060
	313K	0.773	28.336	1.361	0.939	77.148
	323K	0.563	59.085	1.170	0.980	241.038
	333K	0.877	31.327	1.123	0.973	178.293
	343K	0.645	69.083	0.887	0.993	751.696
	353K	0.571	26.843	0.705	0.966	140.817
Bockris-Swinkles	303K	0.280	56.659	0.909	0.948	90.875
	313K	0.840	24.773	1.303	0.938	75.977
	323K	0.609	49.161	1.093	0.978	223.870
	333K	0.867	32.083	1.015	0.978	223.951
	343K	0.618	75.687	0.762	0.996	1.122E3
	353K	0.498	22.170	0.563	0.958	114.518

Figure within ( ) give t values; F Figure within [ ] give F ratio.

Table 4.30 - Adsorption parameters deduced from various adsorption isotherms MS/ 1 M HCl /CIF

dsorption isotherms	Temp	Slope	t	intercept	R^2	F
Langmuir	303K	0.943	16.138	0.031	1.000	7.196E4
	313K	0.936	7.780 (0.001)	0.032	1.000	1.543E4
	323K	0.936	19.709	0.041	1.000	6.118E4
	333K	0.865	3.990	0.034	0.998	2.982E2
	343K	0.810	5.447 (0.003)	0.034	0.999	4.918E3
	353K	0.843	3.418 (0.019)	0.039	0.997	1.650E3
Temkin	303K	0.049	234.277	0.929	0.980	243.193
	313K	0.055	109.087	0.927	0.929	65.307
	323K	0.053	252.185	0.908	0.986	347.665
	333K	0.103	66.602	0.913	0.947	89.277
	343K	0.136	94.323	0.905	0.985	318.776
	353K	0.115	52.532`	0.900	0.934	71.294
Frumkin	303K	0.113	234.277	0.929	0.980	243.193
	313K	0.126	109.087	0.927	0.929	65.307
	323K	0.123	252.185	0.908	0.986	347.665
	333K	0.237	66.602	0.913	0.947	89.227
	343K	0.314	94.323	0.905	0.985	318.776
	353K	0.265	52.532	0.900	0.934	71.294
Freundlich	303K	0.902	17.449	0.096	0.999	8.052E3
	313K	0.935	11.677	0.041	1.000	2.108E4
	323K	0.890	1.466 (0.203)	0.013	0.998	3.128E3
	333K	0.874	3.778 (0.014)	0.041	0.997	1.840E3

Adsorption isotherms	Temp	Slope	t	intercep t	R^2	F
Freundlich	343K	0.777	1.319 (0.244)	0.026	0.989	458.277
	353K	0.787	9.863	0.061	0.999	4.896E3
Flory-Huggins	303K	2.394	12.537	2.615	0.958	112.901
	313K	2.008	7.219(0.001)	2.208	0.876	35.205 (0.002)
	323K	2.795	30.492	2.7320	0.993	685.538
	333K	1.729	11.649	1.623	0.943	83.254
	343K	1.445	12.743	1.2740	0.948	90.636
	353K	1.685	10.215	1.4860	0.926	62.467 (0.001)
El-Awady kinetic thermodynamic	303K	0.902	17.449	0.096	0.999	8.052E3
	313K	0.935	11.677	0.041	1.000	2.108E4
	323K	0.890	1.466 (0.203)	0.013	0.998	3.128E3
	333K	0.874	3.718 (0.014)	0.041	0.997	1.840E3
	343K	0.777	1.319 (0.244)	0.026	0.989	458.277
	353K	0.787	9.863	0.061	0.999	4.896E3
Bockris-Swinkles	303K	0.470	43.233	0.980	0.962	127.978
	313K	0.512	21.123	0.969	0.890	40.638 (0.001)
	323K	0.420	103.164	0.851	0.994	772.214
	333K	0.602	25.197	0.795	0.956	108.299
	343K	0.669	19.205	0.724	0.949	93.619
	353K	0.591	20.883	0.723	0.945	86.701

Figure within ( ) give t values; F Figure within [ ] give F ratio.

Table 4.31 - Adsorption parameters deduced from various adsorption isotherms – AA 1100/1 M HCl /HRL

dsorption isotherms	Temp	Slope	t	intercept	R^2	F
Langmuir	303K	0.851	6.292 (0.001)	0.055	0.998	2.843E3
	313K	0.865	26.094	0.082	1.000	2.273E4
	323K	0.714	8.264	0.088	0.996	1.341E3
	333K	0.879	17.102	0.169	0.998	2.365E3
	343K	0.934	37.034	0.204	0.999	8.556E3
	353K	0.905	8.412	0.229	0.985	328.836
Temkin	303K	0.109	58.524	0.871	0.944	84.106
	313K	0.094	171.556	0.820	0.992	605.658
	323K	0.160	61.592	0.782	0.980	249.863
	333K	0.071	47.981	0.674	0.891	40.765
	343K	0.038	83.326	0.624	0.892	41.476
	353K	0.048	17.665	0.586	0.393	3.242 (0.132)
Frumkin	303K	-0.209	9.143	1.222	0.714	12.481 (0.017)
	313K	-0.168	40.515	1.061	0.972	176.417
	323K	-0.433	9.853	1.277	0.844	27.118 (0.003)
	333K	-0.094	21.369	0.736	0.781	17.851
	343K	-0.044	50.830	0.645	0.849	28.040 (0.003)
	353K	-0.034	11.590	0.577	0.145	0.845 (0.400)
Freundlich	303K	0.149	-6.310 (0.008)	-0.126	0.946	87.485
	313K	0.135	-26.045	-0.188	0.991	551.757
	323K	0.286	-8.265	-0.203	0.977	214.051
	333K	0.121	-17.136	-0.388	0.900	44.986 (0.001)

Adsorption isotherms	Temp	Slope	t	intercept	R^2	F
Freundlich	343K	0.066	-37.187	-0.4700	0.897	43.632
	353K	0.094	-8.409	-0.528	0.417	3.575 (0.117)
Flory-Huggins	303K	1.856	9.246	1.507	0.913	52.618 (0.001)
	313K	2.698	21.186	1.835	0.984	311.038
	323K	1.805	14.736	1.009	0.963	131.317
	333K	4.302	5.908 (0.002)	1.955	0.844	27.142
	343K	8.964	6.191 (0.002)	3.642	0.871	33.697 (0.002)
	353K	2.861	1.568 (0.00178)	1.155	0.256	1.720 (0.247)
El-Awady kinetic thermodynamic	303K	0.902	17.449	0.096	0.999	8.052E3
	313K	0.935	11.677	0.041	1.000	2.108E4
	323K	0.890	1.466 (0.203)	0.013	0.998	3.128E3
	333K	0.874	3.718 (0.014)	0.041	0.997	1.840E3
	343K	0.777	1.319 (0.244)	0.026	0.989	458.277
	353K	0.787	9.863	0.061	0.999	4.896E3
Bockris-Swinkles	303K	0.902	17.449	0.096	0.999	8.052E3
	313K	0.935	11.677	0.041	1.000	2.108E4
	323K	0.890	1.466 (0.203)	0.013	0.998	3.128E3
	333K	0.874	3.718 (0.014)	0.041	0.997	1.840E3
	343K	0.777	1.319 (0.244)	0.026	0.989	458.277
	353K	0.787	9.863	0.061	0.999	4.896E3

Figure within ( ) give t values; F Figure within [ ] give F ratio.

Table 4.32 - Adsorption parameters deduced from various adsorption isotherms - AA 1100/1 M HCl /HRF

dsorption isotherms	Temp	Slope	t	intercept	R^2	F
Langmuir	303K	0.956	11.171	0.045	1.000	1.689E4
	313K	0.797	1.479 (0.199)	0.015	0.997	1.869E3
	323K	0.761	7.853 (0.001)	0.059	0.998	3.085E3
	333K	0.947	16.420	0.117	0.999	5.276E3
	343K	0.941	22.301	0.177	0.999	4.171E3
	353K	0.866	18.518	0.219	0.997	1.598E3
Temkin	303K	0.038	110.255	0.901	0.869	33.227 (0.0022)
	313K	0.149	55.577	0.944	0.964	135.436
	323K	0.156	54.046	0.851	0.969	154.355
	333K	0.038	63.695	0.764	0.765	16.270 (0.01000)
	343K	0.037	56.640	0.664	0.759	15.705 (0.0111)
	353K	0.070	38.505	0.600	0.863	31.439 (0.002)
Frumkin	303K	-0.090	19.423	0.914	0.766	16.390 (0.010)
	313K	-0.229	25.547	1.134	0.953	101.015
	323K	-0.156	21.320	1.137	0.905	47.665 (0.001)
	333K	-0.101	1.968 (0.106)	0.928	0.039	0.202 (0.672)
	343K	--0.718	3.133 (0.026)	1.765	0.456	4.185 (0.096)
	353K	-0.306	5.372 (0.003)	1.014	0.522	5.464 (0.067)
Freundlich	303K	0.044	-11.152	-0.103	0.875	35.004 (0.002)
	313K	0.203	-1.480	-0.034	0.960	120.574
	323K	0.239	-7.877 (0.001)	-0.135	0.984	305.445
	333K	0.053	-16.469	-0.269	0.770	16.739 (0.0099)

Adsorption isotherms	Temp	Slope	t	intercept	R^2	F
Freundlich	343K	0.059	-22.348	-0.408	0.768	16.520 (0.010)
	353K	0.134	-18.502	-0.504	0.885	38.472 (0.002)
Flory-Huggins	303K	2.902	5.491 (0.003)	2.910	0.818	22.531 (0.005)
	313K	1.202	13.591	1.202	0.951	96.368
	323K	1.424	8.834	1.039	0.894	42.348 (0.001)
	333K	4.987	4.028 (0.010)	3.112	0.723	13.055 (0.015)
	343K	6.879	3.816 (0.012)	3.197	0.711	12.309 (0.017)
	353K	4.817	4.803 (0.005)	1.754	0.789	18.703 (0.008)
El-Awady kinetic thermodynamic	303K	0.316	27.939	0.946	0.838	25.842 (0.004)
	313K	0.838	26.938	0.984	0.969	156.724
	323K	0.723	16.178	0.688	0.945	85.929
	333K	0.193	18.942	0.507	0.756	15.494 (0.011)
	343K	0.159	13.302	0.296	0.752	15.162(0.011)
	353K	0.280	6.313 (0.001)	0.175	0.859	30.493 (0.003)
Bockris-Swinkles	303K	0.340	22.960	0.849	0.834	25.191 (0.004)
	313K	0.800	22.081	0.860	0.962	125.559
	323K	0.590	11.222	0.536	0.901	45.527 (0.001)
	333K	0.177	15.393	0.386	0.748	14.880 (0.012)
	343K	0.119	11.254	0.195	0.736	13.944 (0.014)
	353K	0.151	5.369 (0.003)	0.098	0.805	20.606 (0.006)

Figure within ( ) give t values; F Figure within [ ] give F ratio.

Table 4.33 - Adsorption parameters deduced from various adsorption isotherms - AA1100/1 M HCl/ CIL

dsorption isotherms	Temp	Slope	t	intercept	R^2	F
Langmuir	303K	0.956	6.144 (0.002)	0.011	1.000	8.797E4
	313K	0.822	41.370	0.209	0.999	7.876E3
	323K	0.747	25.231	0.217	0.998	25.231
	333K	0.869	37.896	0.258	0.999	4.833E3
	343K	0.942	72.908	0.319	1.000	1.379E4
	353K	0.931	56.735	0.326	0.999	7.801E3
Temkin	303K	0.041	263.129	0.974	0.975	191.462
	313K	0.088	94.510	0.608	0.983	293.459
	323K	0.110	68.517	0.586	0.981	261.547
	333K	0.061	77.122	0.546	0.959	115.796
	343K	0.026	98.358	0.479	0.899	44.456 (0.001)
	353K	0.030	77.281	0.471	0.886	38.842 (0.002)
Frumkin	303K	-0.088	19.121	1.259	0.834	25.153
	313K	-0.134	45.445	0.664	0.961	121.800
	323K	-0.196	29.127	0.653	0.940	77.979
	333K	-0.079	51.162	0.559	0.928	64.350
	343K	-0.028	93.812	0.476	0.874	34.828
	353K	-0.034	73.958	0.466	0.853	28.907 (0.003)
Freundlich	303K	0.044	-6.233 (0.002)	-0.025	0.975	194.435
	313K	0.178	-41.333	-0.481	0.987	370.384
	323K	0.253	-25.199	-0.500	0.981	256.511
	333K	0.131	-37.910	-0.595	0.956	109.718

Adsorption isotherms	Temp	Slope	t	intercept	R^2	F
Freundlich	343K	0.058	-72.856	-0.735	0.912	51.070 (0.001)
	353K	0.069	-56.750	-0.751	0.896	43.201 (0.001)
Flory-Huggins	303K	1.680	12.677	2.427	0.956	109.582
	313K	4.575	14.144	1.618	0.970	162.253
	323K	3.621	12.613	1.137	0.963	128.620
	333K	7.299	10.059	2.233	0.947	89.067
	343K	17.741	6.099 (0.002)	4.745	0.876	35.368 (0.002)
	353K	15.056	5.727 (0.002)	3.886	0.861	31.054 (0.003)
El-Awady kinetic thermodynamic	303K	0.589	49.424	1.429	0.961	123/638
	313K	0.353	16.978	0.188	0.984	302.389
	323K	0.453	10.344	0.154	0.982	275.549
	333K	0.244	6.484(0.001)	0.080	0.959	116.122
	343K	0.105	-4.361 (0.007)	-0.0370	0.902	45.875 (0.001)
	353K	0.123	-4.734 (0.005)	-0.050	0.888	39.826 (0.001)
Bockris-Swinkles	303K	0.646	43.596	1.379	0.961	24.024
	313K	0.173	12.482	0.098	0.966	144.167
	323K	0.175	6.422 (0.001)	0.063	0.949	93.139
	333K	0.105	6.717 (0.001)	0.035	0.959	118.254
	343K	0.042	-4.791 (0.005)	-0.019	0.872	33.987 (0.002)
	353K	0.046	-5.599 (0.005)	-0.025	0.863	31.467 (0.002)

Figure within ( ) give t values; F Figure within [ ] give F ratio.

Table 4.34- Adsorption parameters deduced from various adsorption isotherms AA1100/1 M HCl/ CIF

dsorption isotherms	Temp	Slope	t	intercept	R^2	F
Langmuir	303K	0.945	2.902 (0.034)	0.018	0.999	7.102E3
	313K	0.852	24.690	0.182	0.999	3.996E3
	323K	0.731	24.157	0.185	0.998	2.726E3
	333K	0.888	16.962	0.339	0.992	590.109
	343K	0.925	114.720	0.247	1.000	5.479E4
	353K	0.932	71.271	0.293	1.000	1.530E4
Temkin	303K	0.048	79.711	0.957	0.832	25.375 (0.004)
	313K	0.081	64.380	0.651	0.953	101.048
	323K	0.125	56.769	0.631	0.976	199.145
	333K	0.047	22.352	0.458	0.619	8.118 (0.036)
	343K	0.038	186.714	0.564	0.981	255.415
	353K	0.032	104.512	0.508	0.932	68.453
Frumkin	303K	-0.073	11.768	1.152	0.562	6.419 (0.052)
	313K	-0.116	28.759	0.719	0.895	42.804 (0.001)
	323K	-0.242	19.174	0.752	0.903	46.690 (0.001)
	333K	-0.048	20.807	0.442	0.439	3.915 (0.105)
	343K	-0.045	132.592	0.575	0.973	180.930
	353K	-0.036	89.093	0.509	0.911	50.989 (0.001)
Freundlich	303K	0.055		-0.041	0.827	23.865 (0.005)
	313K	0.148	-24.699	-0.418	0.960	120.487
	323K	0.269	-24.143	-0.425	0.987	367.762
	333K	0.112	-16.954	-0.779	0.650	9.289 (0.028)

Adsorption isotherms	Temp	Slope	t	intercept	R^2	F
Freundlich	343K	0.075	-114.119	-0.570	0.986	351.719
	353K	0.068	-70.826	-0.675	0.942	81.187
Flory-Huggins	303K	1.982	7.610 (0.001)	2.4960	0.890	40.334 (0.001)
	313K	4.389	8.806	1.812	0.924	61.084(0. 001)
	323K	2.879	10.092	1.030	0.939	76.349
	333K	6.091	2.366 (0.064)	1.472	0.504	5.086 (0.074)
	343K	11.328	13.609	3.829	0.971	168.206
	353K	14.124	7.446 (0.001)	4.085	0.912	51.751 (0.001)
El-Awady kinetic thermodynamic	303K	0.483	30.828	1.227	0.898	43.835 (0.001)
	313K	0.329	14.672	0.267	0.951	97.705
	323K	0.509	12.006	0.231	0.977	208.543
	333K	0.192	-1.997 (0.102)	-0.072	0.627	8.389 (0.034)
	343K	0.154	20.969	0.111	0.980	251.029
	353K	0.129	1.712 (0.148)	0.014	0.933	69.478
Bockris-Swinkles	303K	0.526	27.070	1.157	0.900	45.019 (0.001)
	313K	0.197	12.226	0.161	0.931	67.183
	323K	0.227	6.780 (0.001)	0.114	0.916	54.335(0. 001)
	333K	0.065	-2.317 (0.068)	-0.033	0.552	6.162 (0.056)
	343K	0.080	16.357	0.060	0.968	149.300
	353K	0.057	1.261 (0.263)	0.006	0.908	49.555 (0.001)

Figure within ( ) give t values; F Figure within [ ] give F ratio.

Analysing the values of F, the following table has been arrived at and the adsorption models followed by the studied inhibitors are represented in Table 4.35. The highest values of F are also highlighted in Table 4.35.

Table 4.35 The results of statistical SPSS 16 package on adsorption isotherms and the various adsorption models obeyed by the investigated inhibitors and their highest F values

Inhibitors	MS			AA1100		
	Adsorption models	Highest F values	R^2	Adsorption models	Highest F values	R^2
HRL	Langmuir	21080	1	Langmuir	22730	1
HRF	Langmuir	13800	1	Langmuir	16890	1
CIL	Langmuir	46410	1	Langmuir	87970	1
CIF	Langmuir	71960	1	Langmuir	54790	1

4.3.5.2 Langmuir Adsorption model for investigated inhibitors:

Analysis of the results of statistical data reveals that HRL/HRF/CIL/CIF extract / Mild steel /AA1100 are best described by Langmuir adsorption isotherm model in 1 M HCl.

Langmuir Adsorption Isotherm:

Langmuir adsorption equation relates degree of surface coverage to concentration of inhibitor according to equation (4.21)

$$\text{Log } (C/\theta) = \log C - \log K \qquad \textbf{(4.21)}$$

A plot of log (θ/1-θ) versus log C from mass loss data obtained for studied inhibitors yields straight lines as represented in Figure 4.28. The slope deviates from unity. This deviation may be explained on the basis of the interaction among adsorbed species on the metal surface. It has been postulated in the derivation of Langmuir adsorption isotherm

equation that adsorbed molecules do not interact with one another, but this is not the case of large organic molecules having polar atoms (or) groups which can adsorbed on the cathodic and anodic sites of the metal surface such adsorbed species interact by mutual repulsion or attraction **(Eddy *et al,* 2010, Solomon *et al,* 2010).** It is also possible that the inhibitor studied can be adsorbed on the anodic and cathodic sites resulting in deviation from unit gradient.

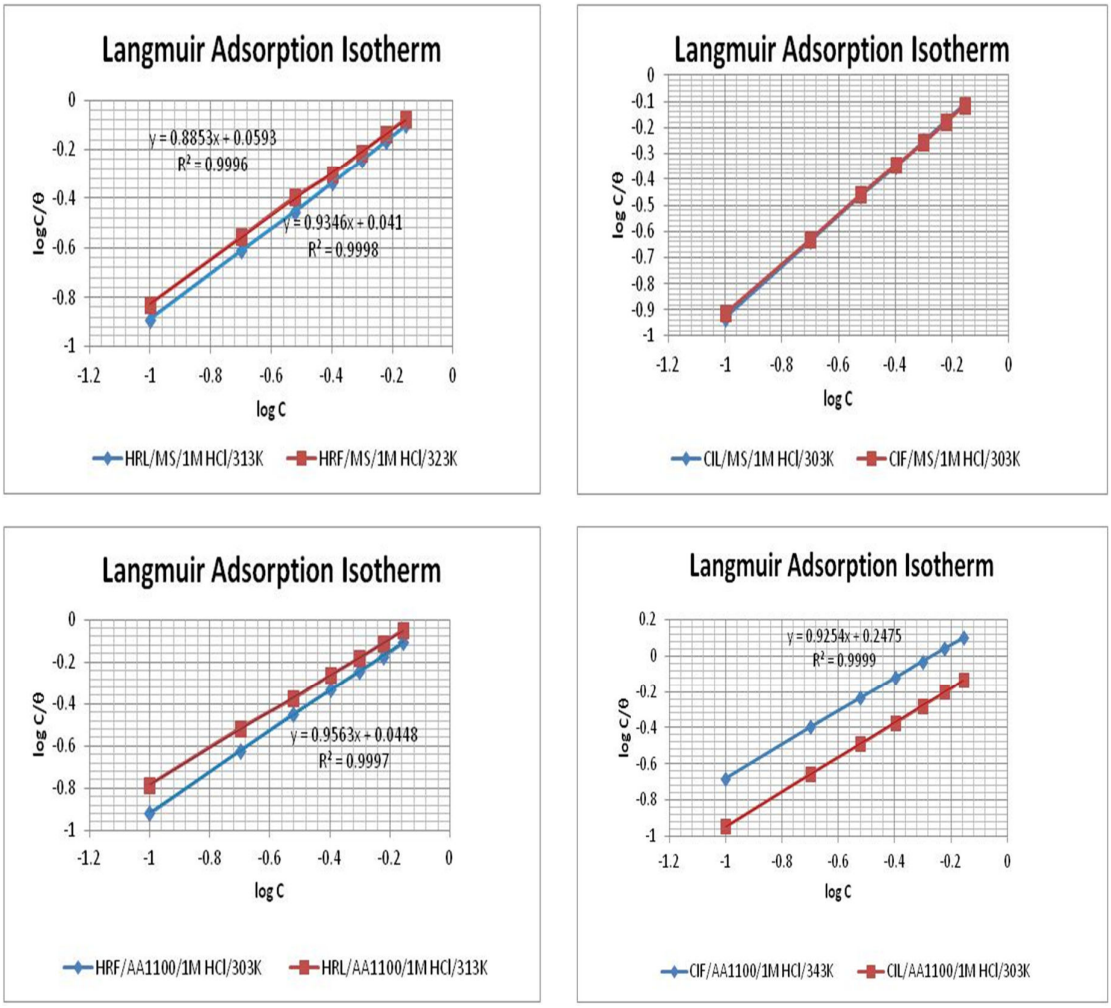

Figure 4.28 Langmuir Adsorption Isotherms for MS, AA1100/HRL/HRF/CIL/CIF extract /1 M HCl systems

4.3.6 Activation Parameters for inhibition process

4.3.6.1 Energy of Activation:

Temperature has a prominent role on the corrosion process of a metal or an alloy and also on the corrosion inhibition process of various inhibitors (**Popova *et al* , 2003**). The impact of the temperature depends on the nature of the medium. In acidic environment the corrosion rate rapidly increases exponentially with temperature as the hydrogen evolution process increases rapidly.

Effect of the temperature on the corrosion process of MS/AA1100 in 1 M HCl in the absence and presence of various concentrations of studied inhibitors HRL,HRF, CIL and CIF extract has been studied for ½ h exposure and the obtained CR and IE are processed to get various kinetic parameters of the corrosion process as per the Arrhenius equation,

$$\log CR = \log A - Ea/2.303RT \quad (4.22)$$

where CR is the corrosion rate of MS/AA1100, A is Arrhenius pre-exponential factor, E_a is the activation energy, R is the universal gas constant and T is the temperature .

The Arrhenius plots for the corrosion process of MS/AA1100 in the absence and presence of various concentrations of HRL, HRF, CIL and CIF extract are depicted in Figure 4.29. The activation energy of the studied inhibitor was calculated from the slope of the Arrhenius plots. The intercept values are used to find the Arrhenius pre-exponential factors. The obtained values for MS/AA1100 for the studied inhibitors are provided in Table 4.36.

It is found from the Table 4.36 that the value of activation energy E_a is higher in presence of the studied inhibitors than in the absence. The increase in activation energy in presence of the inhibitors is due to the formation of a protective layer on the surface of the metal there by blanketing the metal from the corrosive attack of the acid medium, (**Tebbji *et al*, 2007**). The higher activation energy in presence of the inhibitors also suggests the physical adsorption of the studied inhibitor molecules on the metal surface. The similar behaviour was reported in earlier studies (**Fu *et al*, 2010, Solomon *et al*, 2010; Ahamad *et al*, 2010**). The higher values of activation energy also implies that the energy barrier for the corrosion process increased in the presence of HRL, HRF, CIL and CIF extracts, **(Singh and Quraishi, 2010).** This supports the existence of electrostatic attraction between the adsorbed molecules and the metal surface.

Table 4.36 Activation parameters of MS/AA1100 corrosion in 1 M HCl in the absence and presence of different concentration of HRL / HRF / CIL / CIF extracts

Conc (%)	E_a(kJ/mol)							
	HRL		HRF		CIL		CIF	
	MS	AA1100	MS	AA1100	MS	AA1100	MS	AA1100
Blank	52	68	52	68	52	68	52	68
0.1	62	74	62	81	72	89	69	83
0.2	58	73	61	83	67	91	64	91
0.3	58	78	60	87	70	95	64	92
0.4	58	81	59	88	71	98	65	94
0.5	55	83	58	91	69	100	65	95
0.6	54	82	56	93	68	103	63	95
0.7	55	86	55	93	68	101	62	95
Average	**56**	**78**	**58**	**86**	**67**	**93**	**63**	89

Close examination of the data showed that activation energy is higher for AA1100 compared to MS in presence of all studied extracts. This clearly explains the formation of a protective layer on AA1100 is more adherent than that formed on mild steel. It can also be seen from Table 4.36 that among the studied inhibitors CIL extract shows much pronounced increase in activation energy for both MS and AA1100.

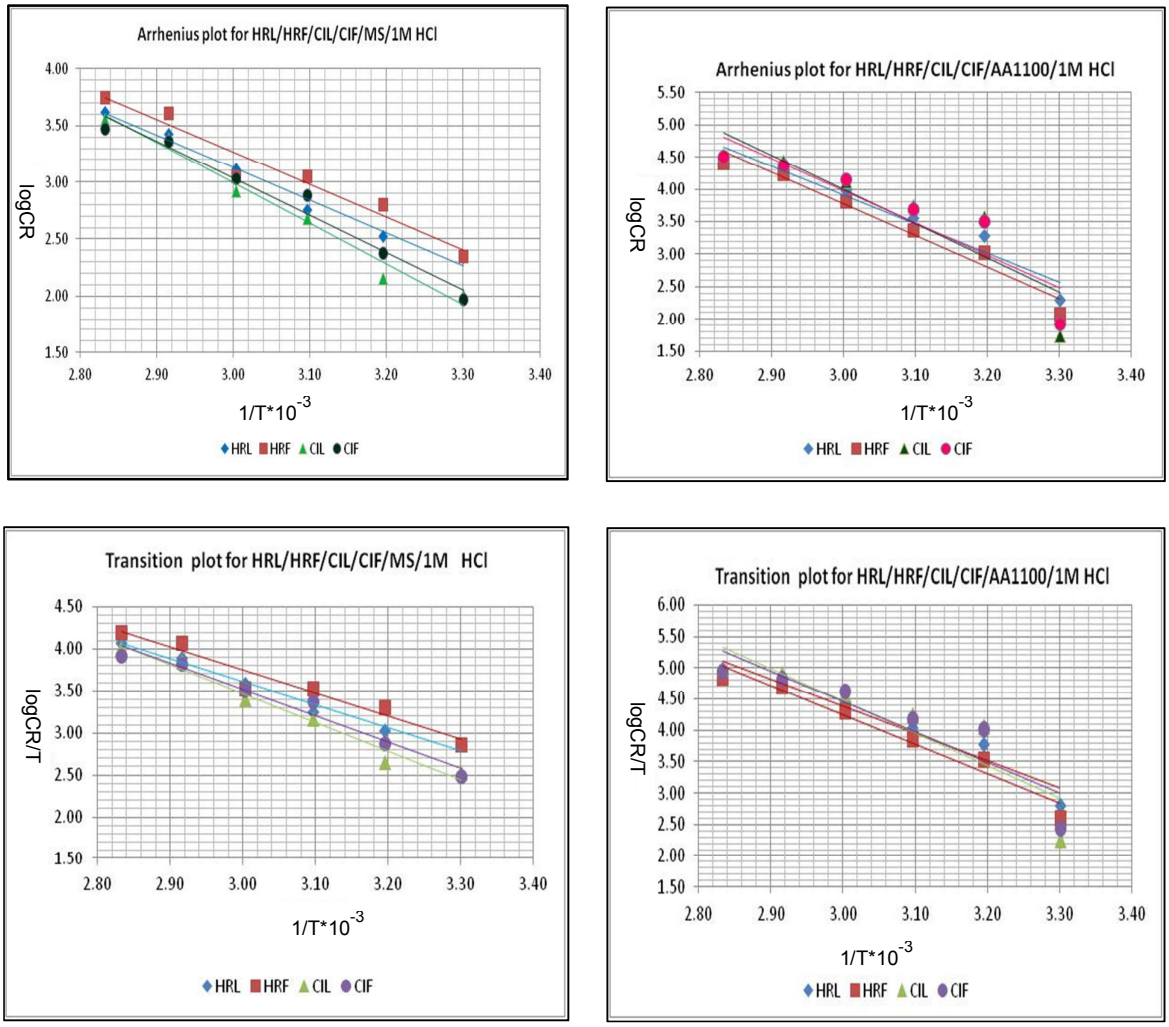

Figure 4.29 Arrehenius plot and Transition plot for MS / AA1100 / HRL / HRF / CIL / CIF extracts/1 M HCl

4.3.6.2 Activation parameters – Entropy of Activation and Enthalpy of Activation

The enthalpy of activation, ΔH_a and entropy of activation ΔS_a are obtained from Eyring and transition state equation which relates the CR/T versus 1/T. The relationship between log (CR/T) versus 1/T for mild steel and AA1100 corrosion in the absence and presence of different concentrations of HRL, HRF, CIL, CIF extracts is shown in Figure

4.29. Straight lines are obtained with slope of ($-\Delta H_a/2.303R$) and an intercept of ($\log R/Nh + \Delta S_a/2.303R$) from which the values of ΔH_a and ΔS_a are computed respectively and listed in Table 4.37.

Analyzing the values of activation parameters for the mild steel and AA1100 corrosion in HRL, HRF, CIL, CIF extracts listed in Table 4.37, it can be seen that all the studied inhibitors towards both MS and AA1100 furnished positive values of ΔH_a. The positive value of the enthalpies (ΔH_a) reflects the endothermic nature of the MS/AA1100 dissolution process meaning that dissolution of the metal becomes difficult in presence of inhibitors **(Shukla, *et al,* 2011; Ebenso *et al,* 2008).**

Table 4.37 Average values of activation parameters of MS/AA1100 corrosion in 1 M HCl in the absence and presence of different concentration of HRL/HRF/CIL/CIF extracts

Inhibitor	E_a(kJ/mol)		ΔH_a kJ/mol		ΔS_a J/Kmol	
	MS	AA1100	MS	AA1100	MS	AA1100
Blank	52	68	49	65	35	90
HRL	56	78	54	75	37	115
HRF	58	86	55	83	44	135
CIL	67	93	65	90	67	161
CIF	63	89	60	86	56	148

The values of activation energy and enthalpy are closer to each other in the absence and presence of the inhibitors as expected from the transition state theory. However, the enthalpy values are found to be somewhat less than the activation energies, **(Ekanem *et al*, 2010; Noor, 2007)**. The difference in the activation energy and enthalpy values is a constant for the particular temperature**.**

The entropies in the presence of studied inhibitors in 1 M HCl for MS/AA1100 corrosion are positive. The positive values of entropies (ΔS_a) in the presence of all studied inhibitors in 1 M HCl implying that the adsorption process is accompanied by an increase in entropy, which is the driving force for the adsorption of inhibitor molecules present in the extract on the metal surface. Therefore increase in disorderliness takes place on going from reactants to the activation complex **(Elachouri *et al,* 1996).**

4.3.7 Thermodynamic Adsorption Parameters

Adsorption of any substance in the interface of the material is accompanied by a change in Gibbs energy and in enthalpy of the system. The adsorption energy is the algebraic sum of all energy effects associated with the formation of adsorbent–adsorbate bonds, desorption of other components, bond breaking and other types of system reorganization.

The impact of the temperature of the system allows the determination of thermodynamic adsorption parameters in absence and in presence of inhibitors. The obtained results can elucidate the mechanism of corrosion inhibition. In the present work, further insight into the adsorption mechanism is offered by considering the thermodynamic functions for the MS/AA1100 dissolution in 1 M HCl solution in the absence and presence of different concentrations of HRL, HRF, CIL, and CIF extracts.

4.3.7.1 ΔG^{o}_{ads}

A plot of ΔG^{o}_{ads} versus T is linear (Figures 4.30 and 4.31) for mild steel acid corrosion in the presence of various concentrations of investigated extracts. The slope of the straight lines is equal to ΔS^{o}_{ads} and intercept equal to ΔH^{o}_{ads}. Figure 4.30 and 4.31 clearly shows the good correlation exist on the ΔG^{o}_{ads} values on T. The values of ΔG^{o}_{ads} are found to be negative which ensure the spontaneity of the adsorption process. This also reveals the stability of the adsorbed layer on the metal surface. The enthalpy and entropy of adsorption for metal corrosion in the absence and presence of the studied inhibitors are deduced from the basic thermodynamic basic equation (3.23).

Table 4.38 –Thermodynamic adsorption parameters for MS/AA 1100 corrosion in 1 M HCl in the absence and presence of different concentrations of HRL/HRF /CIL/CIF extracts

Inhibitor	Free energy of adsorption $-\Delta G^{o}_{ads}$ (kJ/mol)						$-\Delta S^{o}_{ads}$ J/mol	$-\Delta H^{o}_{ads}$ kJ/mol
	303K	313K	323K	333K	343K	353K		
MS								
HRL	15.3	17.2	17.7	16.3	15.7	15.0	20.7	23.0
HRF	15.3	14.9	16.0	15.3	14.2	13.7	31.8	25.3
CIL	17.9	18.6	18.1	16.9	16.2	15.4	60.6	37.1
CIF	17.8	17.7	17.3	16.5	15.8	16.1	43.3	31.1
AA1100								
HRL	15.7	15.2	14.0	13.8	13.7	13.2	50.3	30.8
HRF	17.5	16.2	14.8	15.2	14.1	13.1	79.8	41.3
CIL	19.5	13.0	12.5	12.6	12.3	12.2	109.3	49.5
CIF	18.6	13.5	12.8	11.9	13.1	12.6	92.8	44.2

The calculated mean values of ΔG^{o}_{ads}, ΔH^{o}_{ads}, ΔS^{o}_{ads} at all the studied temperatures (303K-353K) using different concentrations of HRL/HCF/CIL/CIF extracts are represented in Table 4.38. The values of ΔG^{o}_{ads} presented in Table 4.38 are negative which suggests adsorption of organic molecules present in the extract on to the metal surface is a spontaneous process.

As, observed, the studied inhibitors obey the general rule that the effectiveness of corrosion inhibition increases with increasing the negative value of $\Delta G^{o}_{ads.}$ Generally, values of ΔG^{o}_{ads} around -20 $kJmol^{-1}$ or lower are consistent with the electrostatic interaction between the charged molecules and the charged metal (physisorption); those around -40 $kJmol^{-1}$ or higher involve charge sharing or transfer from organic molecules to the metal surface to form a coordinate type of bond (chemisorption) (**Donahue and Nobe, 1965; Khamis and Ateya, 1994**). In the present work, the calculated ΔG^{o}_{ads} values are almost slightly less negative than -20 $kJmol^{-1}$ ranging from -11 to -19 $kJmol^{-1}$. Hence it may be assumed that the adsorption of the inhibitor molecules is obeying physical adsorption however chemical adsorption may not be excluded due to the complex nature of the corrosion inhibiting process **(Ahamad *et al,* 2010).**

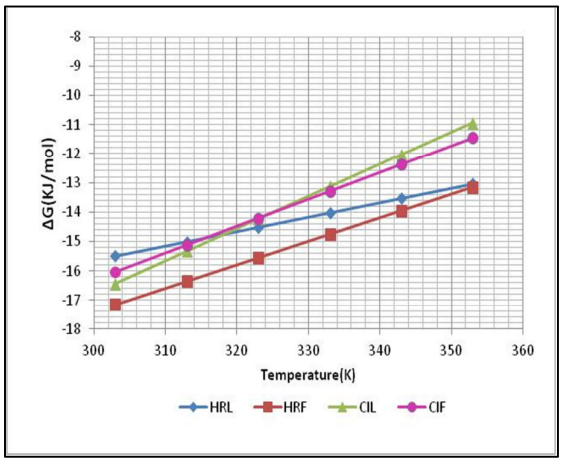

Figure 4.30 : Best fit curves of $-\Delta G^{\circ}_{ads}$ Vs T for MS/ HRL/HRF/CIL /CIF extract /1 M HCl

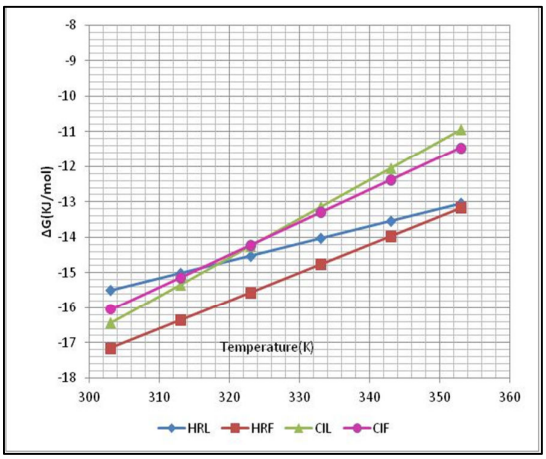

Figure 4.31: Best fit curves of $-\Delta G^{\circ}_{ads}$ Vs T for AA1100/ HRL/HRF/CIL /CIF extract /1 M HCl

4.3.7.2 ΔH^{o}_{ads} and ΔS^{o}_{ads}

The negative sign of enthalpy of adsorption indicate heat is released from the process and it is exothermic adsorption process. Generally, an exothermic adsorption process signifies either physisorption or chemisorption by considering the absolute value of adsorption. Typically, the enthalpy of a physisorption process is lower than 41.86 kJ mol^{-1},

while that of a chemisorption process approaches 100 kJ mol^{-1}(**Martinez *et al,* 2002**). In the present work, the absolute values reflected the physisorption process (Table 4.38).

The negative entropy of adsorption suggests that the exothermic adsorption accompanied with the decrease in disorder during the adsorption process. This can be explained by the fact that initially inhibitor molecules freely move in the bulk solution and adsorbed on MS/AA but with the progress in the adsorption, inhibitor molecules were orderly adsorbed onto the steel surface, as a result a negative entropy is observed **(Mu *et al*, 2004**). Inspection of Table 4.38 reveals that decrease in enthalpy and entropy is the driving force for the adsorption of HR and CI on MS/AA1100 surface **(Umoren *et al,* 2007b).**

4.4 SURFACE ANALYTICAL TECHNIQUES

The use of surface analytical techniques will enable the characterization of the active materials in the adsorbed layer and assist in identifying the most active ingredients in the extract of plant materials. The following surface analytical techniques are used to study the surface of the mild steel and AA1100 in the presence and absence of the investigated inhibitors.

4.4.1 UV Visible spectral Analysis (UV)
4.4.2 FT-IR Spectral studies (FT-IR)
4.4.3 Scanning Electron Microscopic studies (SEM)
4.4.4 Energy dispersive X-ray analysis (EDX)
4.4.5 X-ray diffraction Analysis (XRD) 3D optical profilometry

4.4.1 UV Visible spectral Analysis

The plant extracts contain major active components which are responsible for the inhibiting action. They form complex chemical composition with the metal surface during inhibition process. The formation of metal complexes is often obtained by UV-visible spectrum. UV-Visible spectroscopy provides a strong evidence for the formation of a metal complex (**Quraishi *et al,* 2012**).The change in position of the absorbance maximum and change in the value of absorbance indicate the formation of a complex between two species in solution **(Abboud *et al,* 2007).**

- **HRL/HRF /CIL/CIF extract/ MS in 1 M HCl**

UV-Visible absorption spectra obtained from crude plant extract and solution of mild steel /1 M HCl /0.7% concentration of the HRL/HRF /CIL/CIF/ extracts after 3h

immersion are shown in Figure 4.32. The absorption bands of HR/CI extracts are listed in Table 4.39.

Table 4.39 : UV spectral details of for crude plant extracts, corrodent solution on MS in 1 M HCl

Inhibitor	Absorption bands (nm)		
	Crude plant extract	MS+1 M HCl+ inhibitors	Transitions
HRL	246,349	219,346,380,370,236	n → π* π → π*
HRF	243,274,298,346,	320,298	
CIL	344,238	222,270,310,375,354,298,	
CIF	260,375,318,291,344,224	305,265	

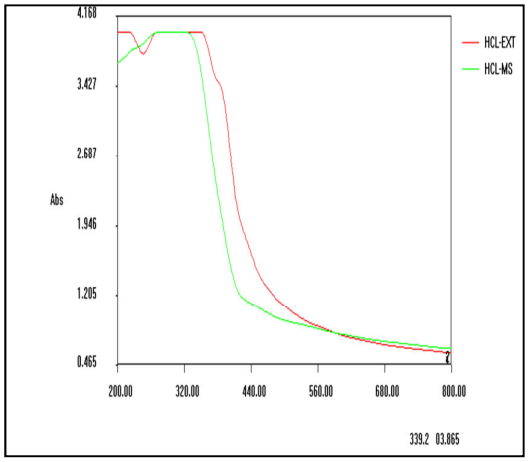

MS / HRL extract/ 1 M HCl

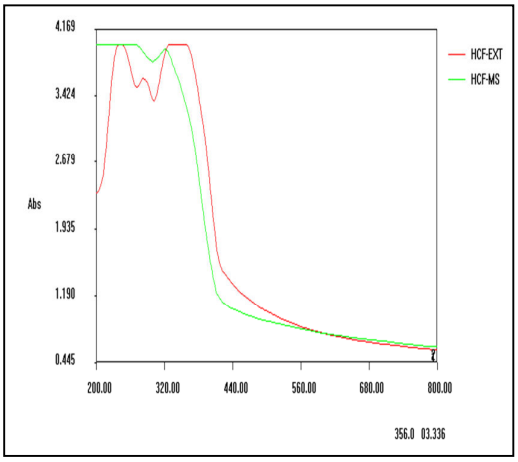

MS /HRF extract / 1 M HCl

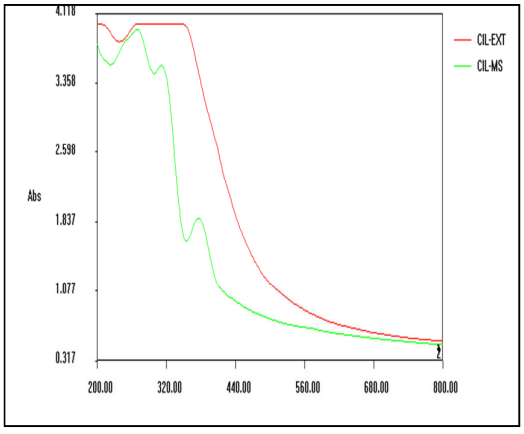

MS /CIL extract / 1 M HCl

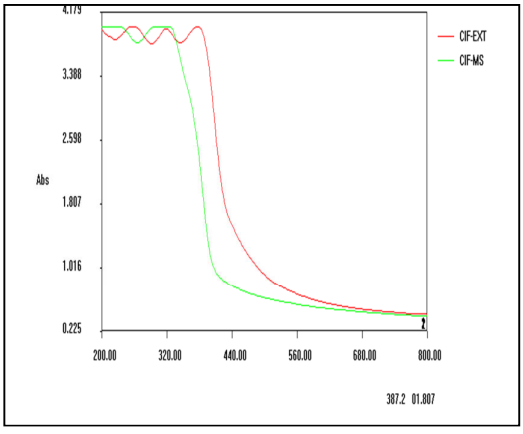

MS /CIF extract / 1 M HCl

Figure 4.32 : UV-Vis spectra for crude plant extracts HRL/HRF /CIL/CIF, corrodent solution on MS in 1 M HCl

From Table 4.39 and Figure 4.32, it is seen that a deviation in the absorbance values and their intensities were obtained. These deviation in absorption bands may be due to π-π* and n- π* transitions with a considerable charge transfer character. This change in the position of absorption maximum or change in the values of absorbance indicate the formation of a complex between Fe^{2+} and the phytoconstituents of the plant extracts.

The UV spectral data reveals that the band in the region of 300-350 nm is due to the carbonyl groups which are held up in the complex with Fe. It is clearly seen that the band maximum of the n→ π* and π→ π* transition, indicating that the carbonyl group are held up in the complex with Fe. (**Abboud *et al,* 2007**). Formation of this complex may be responsible for the observed deviation in the absorbance and its intensity value and this may be responsible for plant extracts anti-corrosion activity. Similar assertion has been reported by **Raja and Sethuraman, 2009**. It is also noted that there is no significant difference in the shape of the spectra before and after the immersion of plant extracts showing a possibility of weak interaction between the extracts and mild steel.

- **HRL/HRF /CIL/CIF extract/ AA1100 in 1 M HCl**

The UV visible spectrum of the corrosion product on the surface of AA1100 in the absence and presence of HRL/HRF /CIL/CIF/ extracts in 1 M HCl are listed in Figure 4.33 and the details are given in Table 4.40. On comparing both these spectra, it may be noted that the bands observed for crude plant extracts shifts to higher wavelength region (Bathochromic shift or red shift) viz 360nm. The observed results conclude the co-ordination between the hetero atoms (oxygen and nitrogen) present in the inhibitor and surface of the metal ion. **(Petchiammal *et al*,2013).**

Table 4.40 : UV spectral details of for crude plant extracts, corrodent solution On AA1100 in 1 M HCl

Inhibitor	Absorption bands (nm)		
	Crude plant extract	AA 1100+1 M HCl+ inhibitors	Transitions
HRL	246,349	325,338,342	n → π* π → π*
HRF	243,274,298,346,	280,313	
CIL	344,238	348,383	
CIF	260,375,318,291,344,224	380,423	

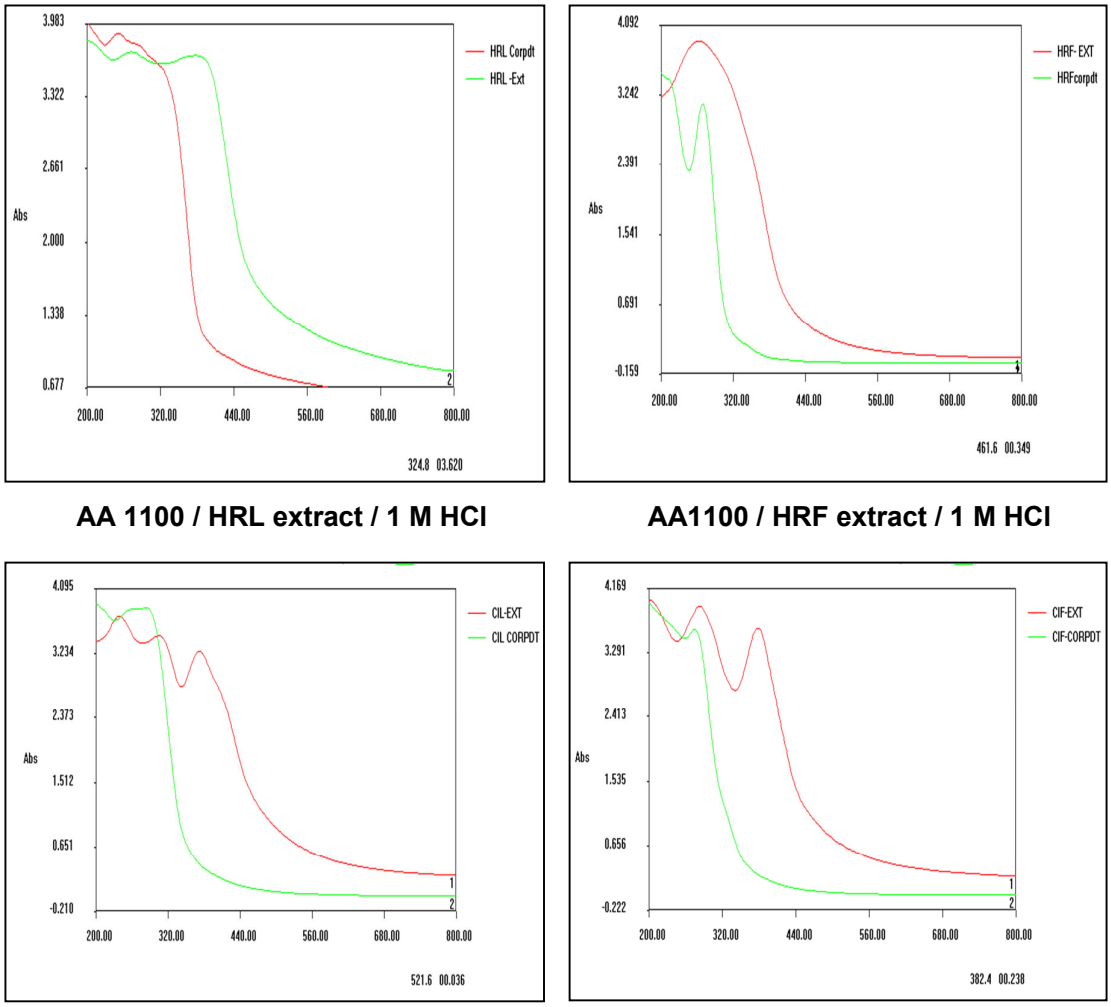

AA 1100 / HRL extract / 1 M HCl **AA1100 / HRF extract / 1 M HCl**

AA 1100 / CIL extract / 1 M HCl **AA 1100 / CIF extract / 1 M HCl**

Figure 4.33: UV-Vis spectra for crude plant extracts HRL/HRF /CIL/CIF, corrodent solution on AA 1100 in 1 M HCl

4.4.2 FT-IR Spectral studies

FT-IR spectrometry is a powerful tool that can be used to determine the type of bonding present in organic inhibitors/ phytochemical constituents. FT-IR studies help to predict the functional groups of the adsorption bands and the arrangement of the inhibitor molecules on the surface of the metal. It also provides information regarding new bonding on the metal surface after immersion in inhibited acid solutions.

In the present study, FT-IR spectra obtained for concentrated crude plant extract, Mild steel/AA1100/1 M HCl/ 0.7% concentration of the HRL/HRF/CIL/CIF extracts after 3h of immersion are shown in Figure 4.34.

4.4.2.1 FT-IR analysis of HRL/HRF extracts with MS as the electrode

i) HRL extract /MS/1 M HCl

The FT-IR spectrum of HRL extract (Figure 4.34a) indicates a strong band at 3411 cm^{-1} and 3395 cm^{-1} (N-H/O-H), 2924 cm^{-1} (CH_2), 1632 cm^{-1} (C=O) stretching. These characteristic peaks of the compounds present in the extract are shifted to higher frequency regions on adsorption over the mild steel surface after exposure of the specimens to the extract. The MS exposed to the HRL extract shows peaks at 3513 cm^{-1} and 3603 cm^{-1}. The band observed at 3411 cm^{-1} and 3395 cm^{-1} of the extract is shifted to 3513 cm^{-1} and 3603 cm^{-1}. The $–CH_2$ asymmetric band at 2924 cm^{-1} is shifted to 3065 cm^{-1}. The absorption band at 1632 cm^{-1} (C=O stretching) diminishes and shifts to 1649 cm^{-1}. The bands at these regions of the MS surface indicate the adsorption of the phytochemical constituents present in the extract on the surface.

Table 4.41: FT-IR spectral details of HR crude plant extract and corrosion product on MS in 1 M HCl

Observed IR Frequency , (cm^{-1}) and Peak assignment					
HRL			HRF		
Crude plant extract	Corrosion product/ Mildsteel/1 M HCl	Frequency Assignment	Crude plant extract	Corrosion product/ Mildsteel/1 M HCl	Frequency Assignment
3411	3513	O-H stretch	3450	3492	O-H stretch
3395	3603	N-H / O-H stretch	3395	3307	N-H / O-H stretch
2924	3065	C-H stretch	2376	2302	C≡ N
1632	1649	C=O stretch	1628	1622	C=O stretch
-			1427	1519	C-H bend
1379	-	C-O-C stretch	1381	-	C-O-C stretch
1065	-	C-O stretch	1265	-	C-O stretch
633	-	C=C bending”	1065	1017	Aromatics
	687	γ-Fe_2O_3	772	823	OH bend
				683	γ-Fe_2O_3

ii) HRF extract /MS/1 M HCl

The FT-IR spectrum of HRF extract indicates a strong band at 3950 cm^{-1} and 3395 cm^{-1} (N-H /OH), 2376 (– CH_2), and a strong band at 1628 cm^{-1} corresponds to

C=O stretching. The band observed at 3950 cm^{-1} and 3395 cm^{-1} is shifted to 3492 cm^{-1} and 3307 cm^{-1}. A band at 2376 cm^{-1} attributed to C ≡ N stretching observed in the plant spectra shifts to 2302 cm^{-1} in the HRF extract / MS. The absorption band at 1628 cm^{-1} (C=O stretching) diminishes and shifts to 1622 cm^{-1}.The absorption band at 772 cm^{-1}(OH bend) diminishes and shifts to 823cm^{-1}. The MS exposed to HRF extract shows the retention of the characteristic peaks of HRF extract and is found to be shifted which is due to the participation of the compounds present in the extract in the corrosion inhibition process.

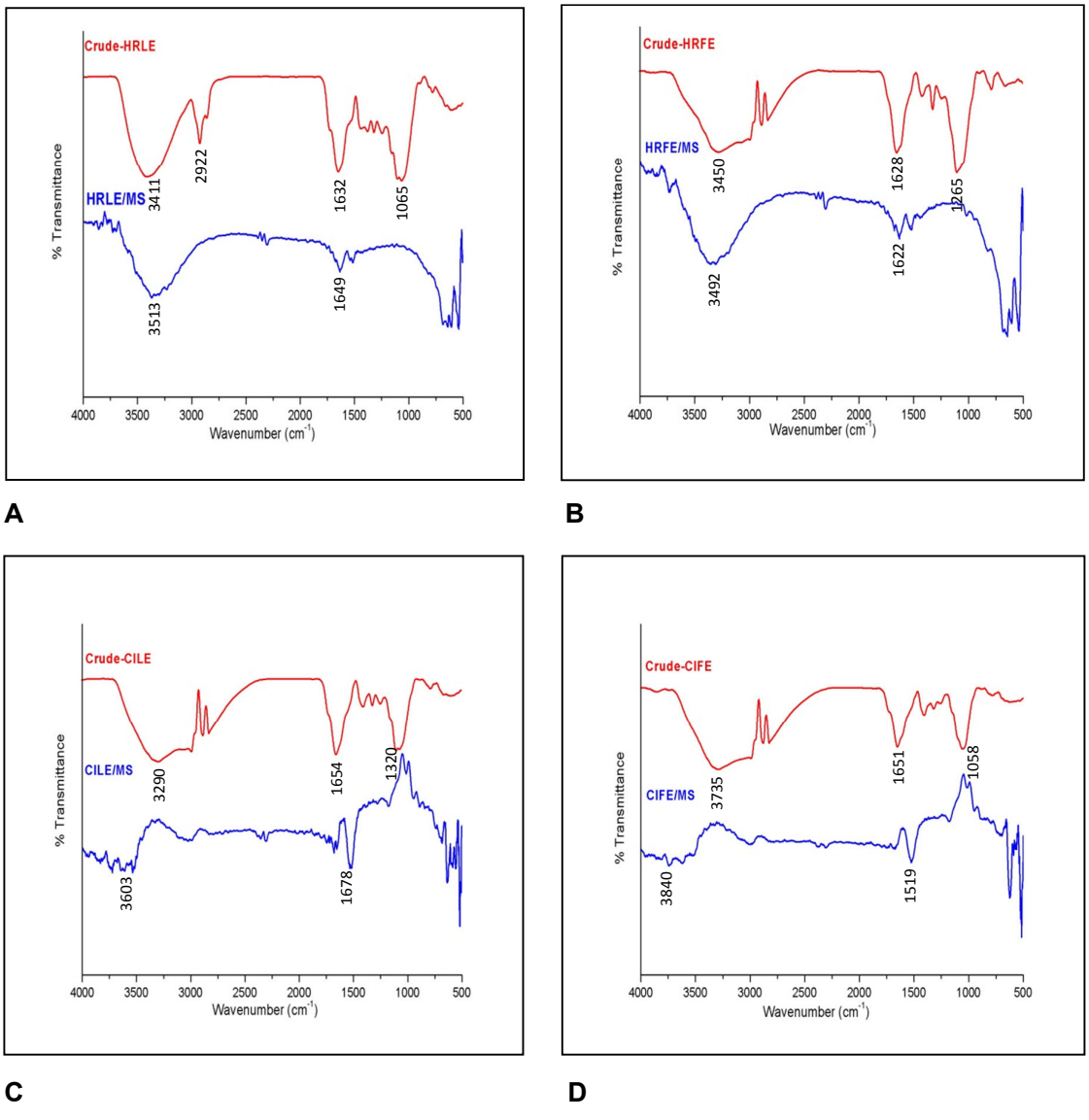

Figure 4.34 FT-IR Spectrum of (a) HRL and corrosion products in the presence of HRL extract (b) HRF and corrosion products in the presence of HRF extract (c) CIL and corrosion products in the presence of CIL extract (d) CIF and corrosion products in the presence of CIF extract on mild steel.

4.4.2.2 FT-IR results of extract of CIL / CIF / MS/ 1 M HCl

i) CIL extract /MS/1 M HCl

The FT IR spectrum of the corrosion product after 3h of immersion in 1 M HCl in the presence of the inhibitor reflects peaks at 3959 cm^{-1} and 3603 cm^{-1}. The band observed at 3290 cm^{-1} is shifted to 3603 cm^{-1}. The absorption band at 1654 cm^{-1} (C=O stretching) diminishes and shifts to 1678 cm^{-1}. The shift in the absorption frequencies of the inhibitor on the metal surface strongly supports the interaction between the phytochemical compounds of the inhibitor and metal surface. Some bonds are missing in the spectrum of the corrosion product indicating that these bonds might have been involved in bonding. Bands at 683 cm^{-1} probably originates mainly from γ -Fe_2O_3. This indicates that there is interaction (Fe-CI complex formation) between the leaves extract of CI and the surface of MS.

Table 4.42: FT-IR spectral details of CI crude plant extract and corrosion product on MS in 1 M HCl

Observed IR Frequency , (cm^{-1}) and Peak assignment					
CIL			CIF		
Crude plant extract	Corrosion product/ /Mildsteel/1 M HCl	Frequency Assignment	Crude plant extract	Corrosion product/ /Mildsteel/1 M HCl	Frequency Assignment
			3850	3956	O-H stretch
3290	3603	N-H / O-H stretch	3735	3840	N-H / O-H stretch
2924	2987	C-H stretch	2879	2309	C≡ N
1654	1678	C=O stretch	1651	1747	C=O stretch
-			1406	1519	C-H bend
1320	-	C-O-C stretch	1319	-	C-O-C stretch
1072	-	C-O stretch	1260	-	C-O stretch
	-	C=C bending”	1058	1017	Aromatics
784	-	OH bend	779	823	OH bend
	635	γ-Fe_2O_3	622	-	C=C bending

ii) CIF extract /MS/1 M HCl

FT IR spectrum of the corrosion product after 3h of immersion in 1 M HCl in the presence of the inhibitor reflected peaks at 3956 cm^{-1} and 3840 cm^{-1}. The band observed at 3850 cm^{-1} and 3735 cm^{-1} is shifted to 3956 cm^{-1} and 3840 cm^{-1}. The $-CH_2$ asymmetric band at 2879 cm^{-1} is shifted to 3505 cm^{-1}. The absorption band at 1651 cm^{-1} (C=O stretching) diminishes and shifts to 1747 cm^{-1}. The shift in the absorption frequencies

of the inhibitor on the metal surface strongly supports the interaction between the phytochemical compounds of the inhibitor and metal surface. Some bonds are missing in the spectrum of the corrosion product indicating that these bonds might have been involved in bonding .This indicates that there is interaction (Fe-Cl complex formation) between the flower extract of Cl and the surface of MS.

4.4.2.3 FT-IR results of HRL/HRF extracts in the presence of AA1100 electrode

i) HRL/AA1100/1 M HCl

The FT IR spectrum of the corrosion product after 3h of immersion in 1 M HCl in the presence of the inhibitor reflected peaks at 3742 cm^{-1} and 3513 cm^{-1}. The band observed at 3411 cm^{-1} and 3395 cm^{-1} is shifted to 3742 cm^{-1} and3513 cm^{-1}. The $-CH_2$ asymmetric band at 2924 cm^{-1} is shifted to 2259 cm^{-1}. A peak noticed for C-O stretching at 1065 cm^{-1} shifts to 943 cm^{-1}.The shift in the absorption frequencies of the inhibitor on the metal surface strongly supports the interaction between the phytochemical compounds of the inhibitor and metal surface. Some bonds are missing in the spectrum of the corrosion product indicating that these bonds might have been involved in bonding .This indicates that there is interaction between the leaves extract of HR and the surface of Al. **(Kamal and Sethuraman, 2012; Gopiraman *et al,* 2012).**

Table 4.43: FT-IR spectral details of HR for crude plant extract and corrosion product on AA1100 in 1 M HCl

Observed IR Frequency , (cm^{-1}) and Peak assignment					
HRL			HRF		
Crude plant extract	Corrosion product/ AA1100/1 M HCl	Frequency Assignment	Crude plant extract	Corrosion product/ AA1100/1 M HCl	Frequency Assignment
3411	3742	O-H stretch	3950	3722	O-H stretch
3395	3513	N-H / O-H stretch	3395	3497	N-H / O-H stretch
2924	2259	C-H stretch	2376	2457	C≡ N
1632	-	C=O stretch	1628	-	C=O stretch
-			1427	1519	C-H bend
1379	1500	C-O-C stretch	1381	-	C-O-C stretch
1065	943	C-O stretch	1065	1017	C-O stretch
633	-	C=C bending”	-	-	Aromatics
			772	-	OH bend

ii) HRF extract /AA1100/1 M HCl

The FT IR spectrum of the corrosion product after 3h of immersion in 1 M HCl in the presence of the inhibitor reflected peaks at 3722 cm^{-1} and 3497 cm^{-1}. The band observed at 3950 cm^{-1} and 3395 cm^{-1} is shifted to 3722 cm^{-1} and 3497 cm^{-1} . The $-CH_2$ asymmetric band at 2376 cm^{-1} is shifted to 2457 cm^{-1}. A peak noticed for C-O stretching at 1065 cm^{-1} shifts to 1017 cm^{-1}. The shift in the absorption frequencies of the inhibitor on the metal surface strongly supports the interaction between the phytochemical compounds of the inhibitor and metal surface. Some bonds are missing in the spectrum of the corrosion product indicating that these bonds might have been involved in bonding .This indicates that there is interaction (Al-HR complex formation) between the flower extract of HR and the surface of Al.

4.4.2.4 FT-IR results of CIL/CIF extracts in the presence of AA1100 electrode

i) CIL extract /AA1100/1 M HCl

The FT IR spectrum of the corrosion product after 3h of immersion in 1 M HCl in the presence of the inhibitor reflected peaks at 3956 cm^{-1} and 3840 cm^{-1}. The band observed at 3850 cm^{-1} and 3735 $cm^{-1}$is shifted to 3956 cm^{-1} and 3840 cm^{-1}. A band at 2879 cm^{-1} attributed to C ≡ N stretching observed in the plant spectra shifts to 2309 cm^{-1} in the corrosion product. The absorption band at 1651 cm^{-1} (C=O stretching) diminishes and shifts to 1747 cm^{-1}. The shift in the absorption frequencies of the inhibitor on the metal surface strongly supports the interaction between the phytochemical compounds of the inhibitor and metal surface. Some bonds are missing in the spectrum of the corrosion product indicating that these bonds might have been involved in bonding .This indicates that there is interaction (Al-Cl complex formation) between the leaves extract of CI and the surface of Al.

ii) CIF extract/AA1100/1 M HCl

The FT IR spectrum of the corrosion product after 3h of immersion in 1 M HCl in the presence of the inhibitor reflected peaks at 3956 cm^{-1} and 3840 cm^{-1}. The bands observed at 3850 cm^{-1} and 3735 cm^{-1} are shifted to 3956 cm^{-1} and 3840 cm^{-1} . A band at 2879 cm^{-1} attributed to C ≡ N stretching observed in the plant spectra shifts to 2309 cm^{-1} in the corrosion product. The absorption band at 1651 cm^{-1} (C=O stretching) diminishes and shifts to 1747 cm^{-1}. The shift in the absorption frequencies of the inhibitor on the metal surface strongly supports the interaction between the phytochemical compounds of the inhibitor and metal surface. Some bonds are missing in the spectrum of the corrosion product indicating that these bonds might have been involved in bonding .This indicates that there is interaction between the flower extract of CI and the surface of Al.

Table 4.44 : FT-IR spectral details of CI for crude plant extract and corrosion product on AA1100 in 1 M HCl

Observed IR Frequency , (cm^{-1}) and Peak assignment					
CIL			CIF		
Crude plant extract	Corrosion product/ AA1100/1 M HCl	Frequency Assignment	Crude plant extract	Corrosion product/ AA1100/1 M HCl	Frequency Assignment
			3850	3956	O-H stretch
3290	3603	N-H / O-H stretch	3735	3840	N-H / O-H stretch
2924	2987	C-H stretch	2879	2309	C≡ N
1654	1678	C=O stretch	1651	1747	C=O stretch
-			1406	1519	C-H bend
1320	-	C-O-C stretch	1319	-	C-O-C stretch
1072	-	C-O stretch	1260	-	C-O stretch
	-	C=C bending"	1058	1017	Aromatics
784	-	OH bend	779	823	OH bend
			622	-	C=C bending

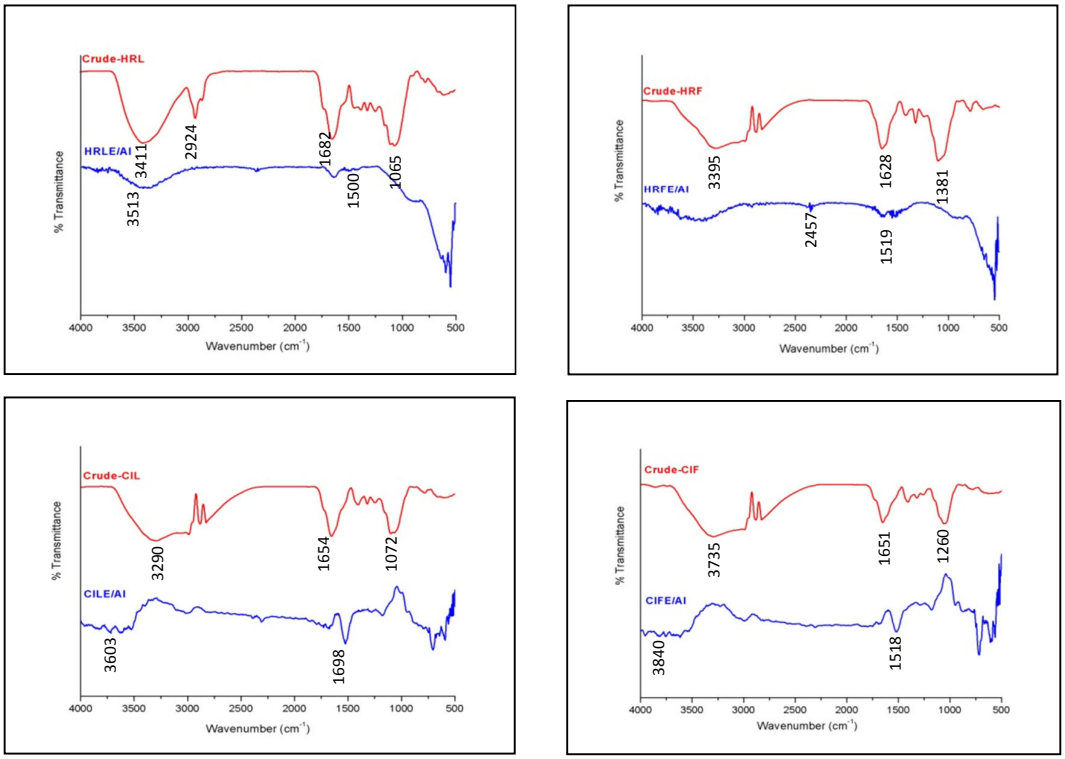

Figure 4.35 FT-IR Spectrum of (a) crude HRL and corrosion products in the presence of HRL extract (b) crude HRF and corrosion products in the presence of HRF extract (c) crude CIL and corrosion products in the presence of CIL extract (d) crude CIF and corrosion products in the presence of CIF extract on AA1100

4.4.3 Scanning Electron Microscopic studies (SEM)

The surface morphology of Mild steel/AA1100 surface has been studied by scanning electron microscope. In the present investigation, SEM micrograph of mild steel specimen exposed to the uninhibited and inhibited solutions has been under taken to supplement the results.

4.4.3.1 Scanning electron micrograph of mild steel in the presence of HRL/HRF Extract in 1 M HCl

Surface examination using SEM has been carried out to investigate the effect of HRL/HRF extracts on mild steel surface in 1 M HCl. Figure. 4.36 (c) and 4.36 (d) shows SEM image of the surface of the mild steel specimens after immersion in 1 M HCl solution with HRL/HRF extracts for 3 h. It can be seen from the image that the surface damage has diminished in presence of the inhibitors. It is revealed that the metal surface is highly covered with the protective layer formed by HRL/HRF extracts which prevents the metal from further attack of acid media thus inhibiting corrosion **(Raja, 2009)**. SEM images prove that HRL/HRF extracts adsorb onto steel surface to form a dense and more tightly protective film. The film covered with anodic and cathodic reactive sites on the steel surface and inhibited both reactions at the same time.

4.4.3.2 Scanning electron micrograph of mild steel in the presence of CIL/CIF extracts in 1 M HCl

SEM photographs obtained for mild steel surface immersed in 1 M HCl solutions at room temperature for 3 h immersion in the absence and presence of 0.7% of optimum concentration of CIL/CIF extracts are shown in Figure 4.36 (e) and 4.36 (f) it can be noted it that the smooth surface observed in plain mild steel is highly corroded with etched grain boundaries and corrosion products after its immersion in 1 M HCl. But in the presence of extracts CIL/CIF /mild steel/1 M HCl, SEM images reveal that a good protective adsorbed film formed on the specimen surface, which suppresses the rate of corrosion. This observation clearly proves that the inhibition is due to the formation of an insoluble stable film through the process of adsorption of the phytoconstituents present in extract on the metal surface **(Achary *et al,* 2008)**

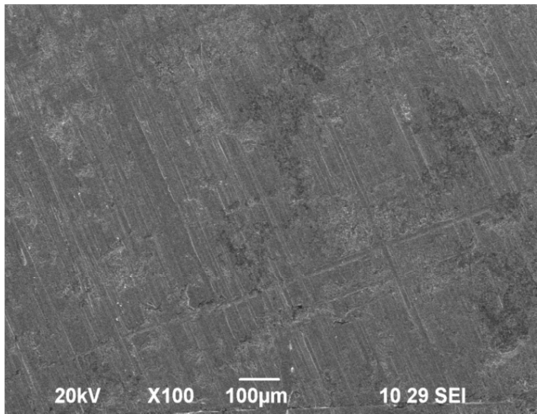

a. Plain Mild steel

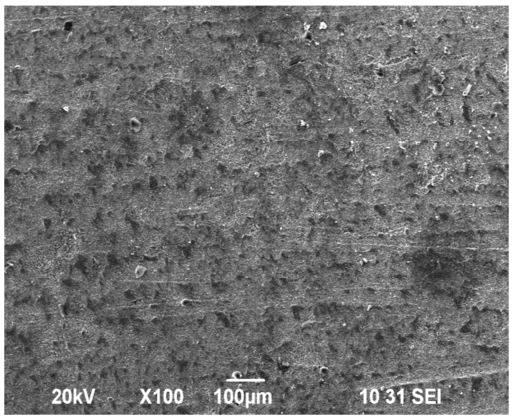

b.Blank

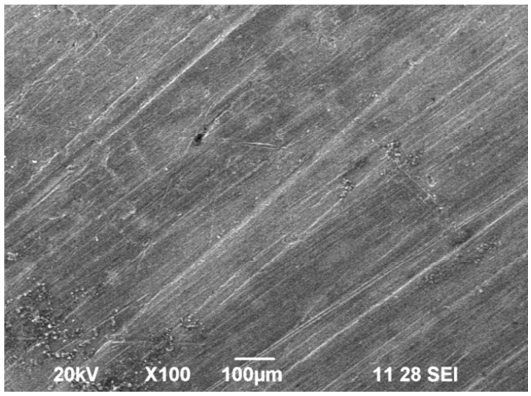

c. Mild steel /HRL extract/ 1 M HCl

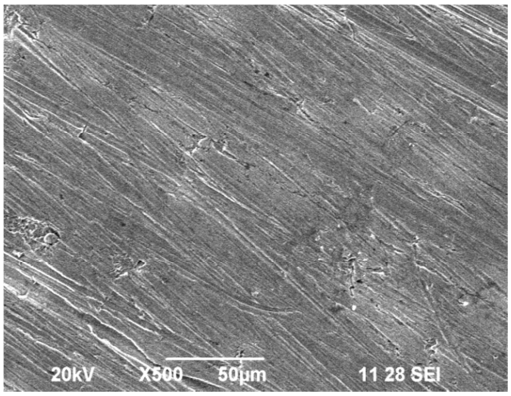

d. Mild steel /HRF extract / 1 M HCl

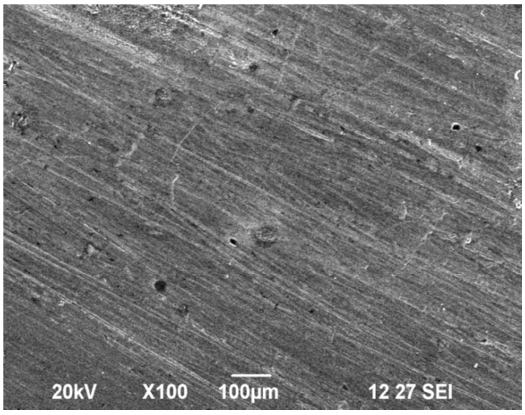

e. Mild steel /CIL extract / 1 M HCl

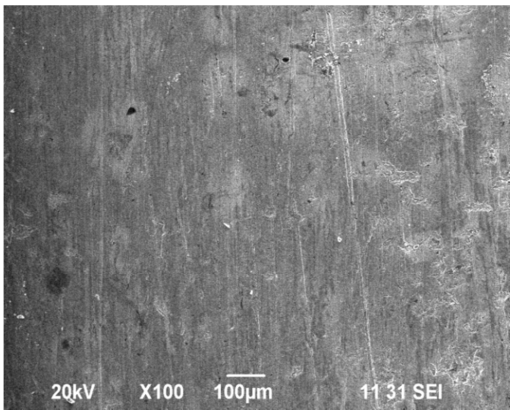

f. Mild steel /CIF extract / 1 M HCl

Figure 4.36 : SEM images of MS corrosion in absence and presence of (c) HRL (d) HRF (e) CIL (f) CIF extract in 1 M HCl

4.4.3.3 Scanning electron micrograph of AA1100 in the presence of HRL/HRF extracts in 1 M HCl

Surface morphology of the HRL/HRF extracts AA1100 sample immersed in 1 M HCl with and without inhibitor is shown in Figure 4.37 (c) and 4.37 (d). When AA1100 is exposed to the blank HCl solution, metal dissolution rate became high which causes formation of stress raisers and more active sites available for corrosion (blank HCl) in comparison to the surface of pure steel (Plain mild steel). When inhibitor is introduced to the system (0.7% of HRL/HRF extracts), a protective layer is formed which decreases the mild steel dissolution in HCl and less corrosion can be seen from the SEM image. SEM images reveal that the AA1100 specimens immersed in inhibited solution is in better condition having smooth surface, while the metal surface immersed in blank acid solution is rough covered with corrosion products and appear like full of pits and cavities. The smooth surface of AA1100 in inhibited solution may be due to the phytochemical constituents present in the extracts hindering the dissolution of iron by forming protective film on metal surface and thereby reducing the corrosion rate **(Bothi Raja and Sethuraman, 2010).**

4.4.3.4 Scanning electron micrograph of AA1100 in the presence of CIL/CIF extracts in 1 M HCl

SEM micrographs of the AA1100 sample exposed to inhibited solutions (CIL/CIF extracts) are displayed in Figure 4.37(e) and 4.37 (f). The corroded metal surface with etched grain boundaries is clearly seen in blank HCl. The SEM photograph of extracts CIL/CIF / AA1100/1 M HCl shows the formation of a film by the active phytochemical constituents on the metal surface.

On the basis of surface morphology it can be concluded that the inhibitor covers the metal surface forming a layer through adsorption which protects it in acidic environment. **(Prakash *et al,* 2012).**

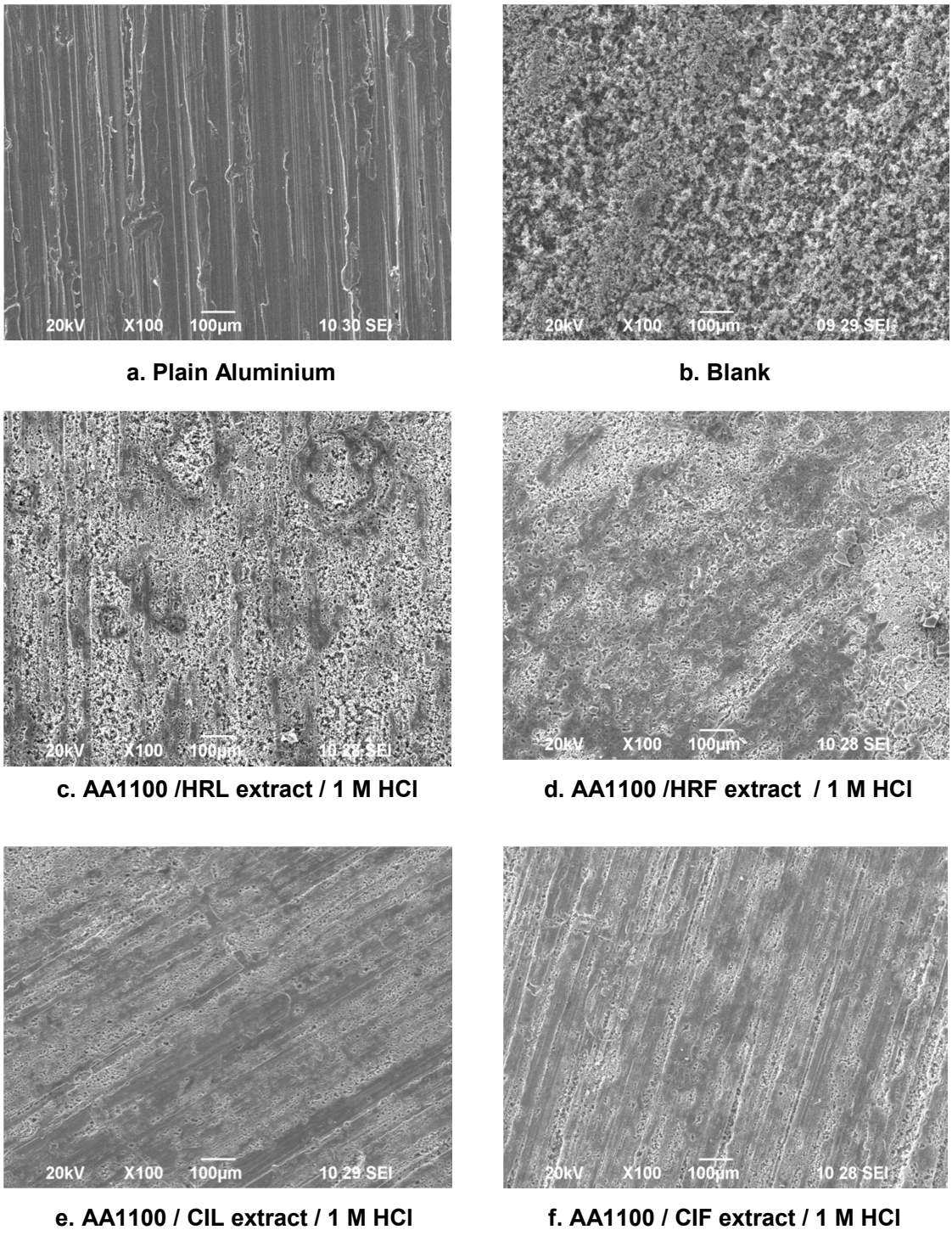

Figure 4.37: SEM images of AA1100 corrosion in absence and presence of (c) HRL (d) HRF (e) CIL (f) CIF extract in 1 M HCl

4.4.4 Energy dispersive X-ray analysis (EDX)

Energy dispersive X-ray analysis (EDX) technique has been employed to obtain information about the nature of the protective film formed on the metal surface.

4.4.4.1 EDX of extracts of HRL/HRF/CIL/CIF/ MS/1 M HCl

The EDX profile analysis and percentage of atomic content in MS samples in 1 M HCl solution in the absence and presence of 0.7% optimum concentration of HRL/HRF/CIL/CIF extracts are displayed in Tables along with the EDX Figures (4.38 a-f)

The analysis infers the characteristic peaks of elements constituting polished mild steel samples comprising of major Fe peaks with Mn, Si & P as minor constituents. The presence of Si may be attributed to the mechanical abrasion of the mild steel surface prior to the experiment.

For Mild steel in the presence of 1 M HCl the EDX analysis reports 80% Fe & 20% Oxygen (in weight %). The detection of small peak characterizing oxygen is detected due to the formation of iron oxide layer due to the immersion of mild steel in 1 M HCl medium. The low content of Fe when compared to the iron content in plain mild steel (97.17%) surface and the absence of Mn and the presence of high oxygen concentration indicates that the mild steel surface is completely covered with a thick layer of corrosion product**.(Sherif *et al,* 2011***)***. After Mild steel is immersed in 1 M HCl containing 0.7% concentration of HRL/HRF/CIL/CIF extracts the spectra shows that the Fe peaks are considerably increased relative to the samples immersed in 1 M HCl (blank) and the oxygen peak is also suppressed. This increase in Fe content corroborates the formation of iron – inhibitor complex on the mild steel surface (**Bobina *et al,* 2013).**

4.4.4.2 EDX of extracts of HRL/HRF/CIL/CIF/ AA1100/1 M HCl

The analysis of EDX spectra of AA1100/1 M HCl in the absence and presence of 0.7% of HRL/HRF/CIL/CIF extracts are shown in Figures (4.39 a-f). When AA1100 is immersed in uninhibited solution (blank) peaks for aluminium and oxygen detected which shows formation of aluminium oxide on the surface. For inhibited solution the spectra shows that the Al peaks are considerably increased relative to the samples immersed in 1 M HCl (blank).

a.Plain MS

Element	Wt %	At %
Si	0.35	0.69
P	0.10	0.18
Mn	2.38	2.41
Fe	97.17	96.72

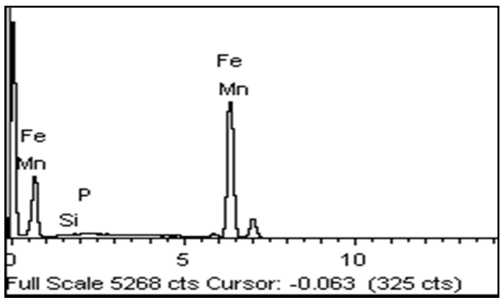

b.Blank HCl

Element	Wt %	At %
O	20.00	46.59
Fe	80.00	53.41

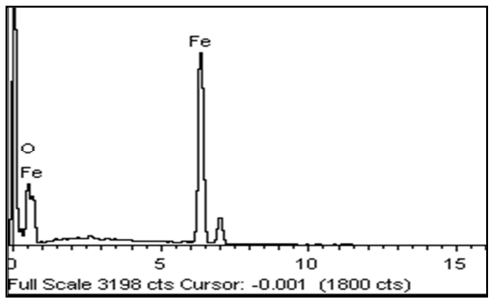

c. Mild Steel /HRL extract / 1 M HCl

Element	Wt %	At %
O	3.55	11.32
Si	0.46	0.85
Cl	0.04	0.05
Fe	95.95	87.77

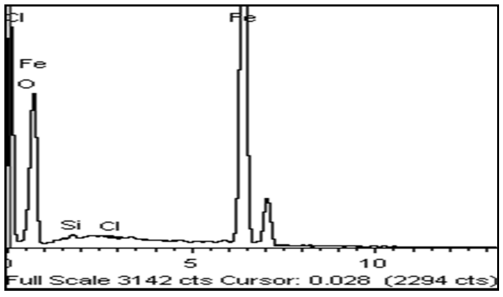

d. Mild Steel /HRF extract / 1 M HCl

Element	Wt %	At %
O	5.86	17.74
Si	0.73	1.26
Fe	93.40	80.99

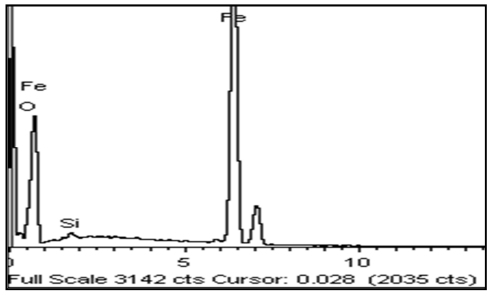

e. Mild Steel /CIL extract / 1 M HCl

Element	Wt %	At %
O	4.44	13.86
Si	0.81	1.45
Fe	94.74	84.69

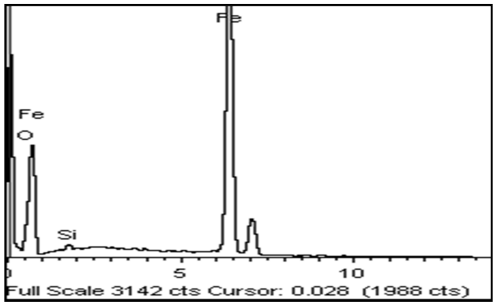

f. Mild Steel /CIF extract / 1 M HCl

Element	Wt %	At %
O	12.10	32.35
Si	0.48	0.73
Fe	87.42	66.93

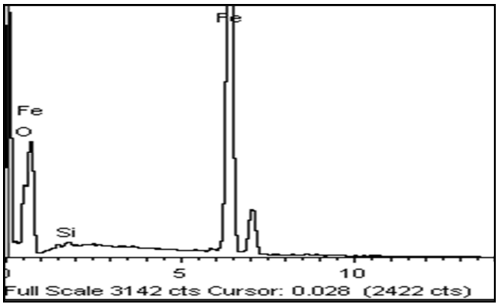

Figure 4.38: EDX images of Mild steel corrosion in the absence and presence of (a) HRL (b) HRF (c) CIL (d) CIF extract in 1 M HCl

a. Plain AA1100

Element	Wt %	At %
O	0.87	1.46
Al	97.87	97.34
Si	1.26	1.20

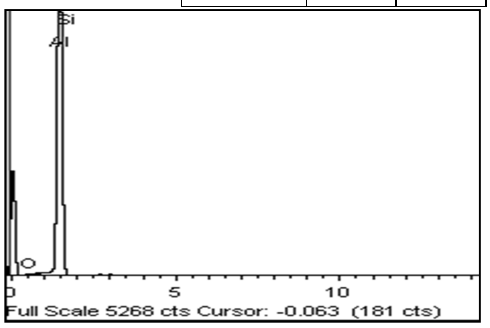

b.Blank HCl

Element	Wt %	At %
O	18.21	27.30
Al	81.68	72.62
S	0.11	0.09

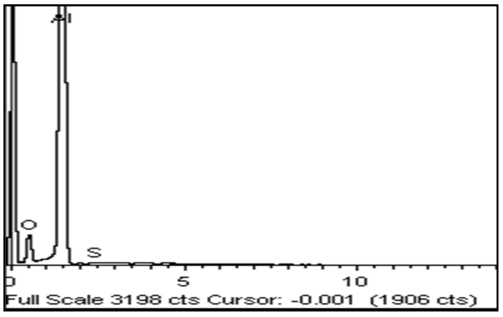

c. AA1100 /HRL extract / 1 M HCl

Element	Wt %	At %
O	14.66	22.47
Al	85.29	77.50
Cl	0.04	0.03

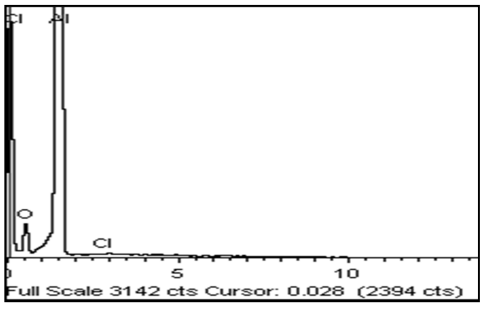

d. AA1100 /HRF extract / 1 M HCl

Element	Wt %	At %
O	25.42	36.50
Al	74.58	63.50

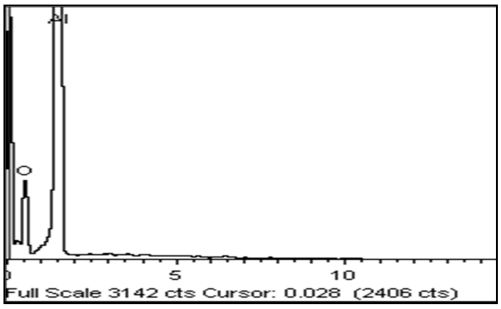

e. AA1100 /CIL extract / 1 M HCl

Element	Wt %	At %
O	7.74	12.39
Al	92.26	87.61

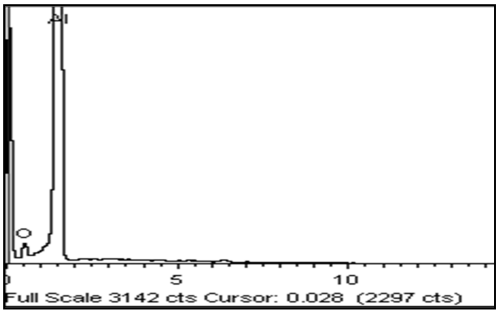

f. AA1100 /CIF extract / 1 M HCl

Element	Wt %	At %
O	11.33	17.73
Al	88.67	82.27

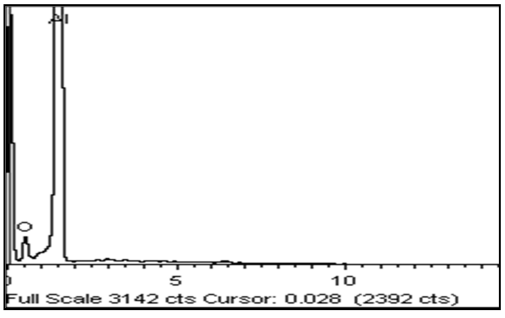

Figure 4.39: EDX images of AA1100 corrosion in the absence and presence of (a) HRL (b) HRF (c) CIL (d) CIF extract in 1 M HCl

4.4.5 X-ray diffraction Analysis (XRD)

XRD is the method of choice for the analysis of corrosion products as it is only analysis that readily provides information about quantitative phase analysis (**Kamimura *et al*, 2002**) based on measuring the intensity of diffraction units in the pattern. In the case of mild steel corrosion, XRD will reveal the composition of iron oxides (magnetite, goethite and ferrihychite) while other methods will only reveal that corrosion product is iron based. The set of 'd' spacing that represent the finger print of the substance can be calculate by 2θ values.

i) XRD of MS/1 M HCl/HRL/HRF/CIL/CIF extract

The XRD spectrum of Mild steel in absence and presence of investigated inhibitors is depicted in the Figure 4.40. XRD pattern of mild steel immersed in corroding solution (1 M HCl) shows peaks at 45.2, 65.4 suggesting the presence of iron. The peak at 65.4 can be assigned to oxides of iron. Thus it may be observed that the surface of metal immersed in 1 M HCl solution contains of Fe_3O_4 and FeOOH. (**Ramesh *et al,* 2003**). It is quite evident that peak at 45.2 is the most important product as indicated by the peak at 2θ of 45.2. This line is finger print of Fe with a maximum relative intensity.

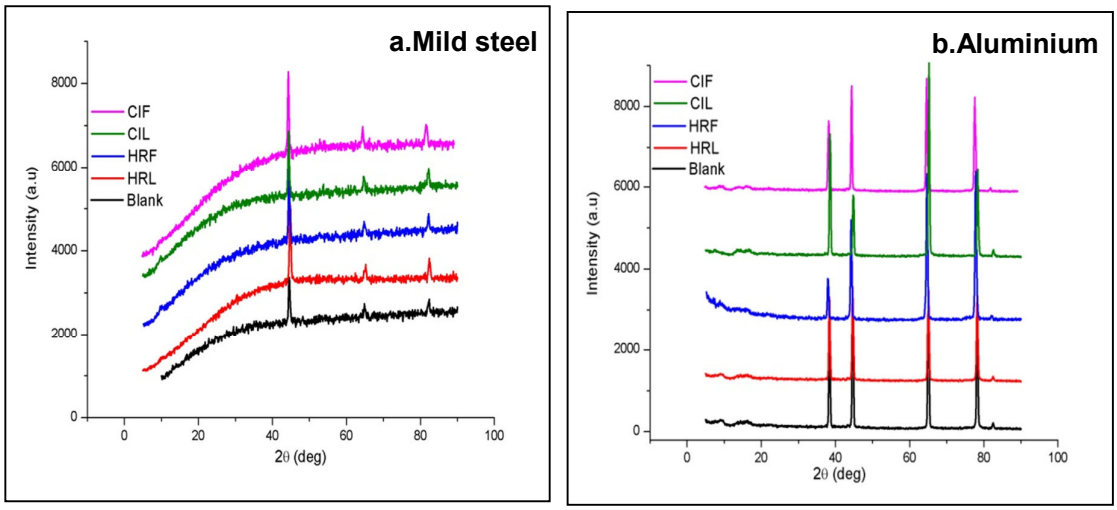

Figure 4.40: XRD spectrum of a) Mild steel b) AA1100 corrosion in presence and absence of investigated inhibitors in 1 M HCl

The grazing angles XRD of the specimens immersed in the tested HR/CI extracts are presented in Figure 4.40 (a). This indicates the amorphous layer of surface film which is expected to be the adsorption of Fe- HR/CI complex on to the surface of mild steel. The XRD patterns of inhibited surface shows a smooth pattern with very small peaks of iron oxide as compared with the spectral data of mild steel immersed in 1 M HCl solution.

ii) XRD of AA1100/1 M HCl/HRL/HRF/CIL/CIF

The XRD spectrum of AA1100 in the absence and presence of investigated inhibitors is depicted in the Figure 4.40 (b). XRD pattern of AA1100 immersed in 1 M HCl exhibit several peaks associated with Al and Al_2O_3. Khan et al,2013 reported the XRD patterns of alumina and stated that emergence of two diffraction peaks at 2θ values of 38.82° and 45.2° respectively can be correlated to Al_2O_3 $H_2O(111)$ and $Al(OH)_3$ (214) phases. The XRD patterns of inhibited surface shows a smooth pattern with very small peaks of aluminium oxide as compared with the spectral data of AA1100 immersed in 1 M HCl solution.The XRD patterns obtained in the present investigation are on par with literature reports **(Khan *et al*, 2013).**

4.4.6 3D optical profilometry:

It is a powerful tool to investigate the surface morphology of various samples at nano-micro scale that is currently used to study the influence of corrosion inhibitors on metal/solution interface. From the analysis, insight can be gained regarding the roughness & uniformity of the surface. **The roughness profile values play an important role in identifying / deciding the efficiency of the inhibitors under study.** Among the various parameters R_a takes a pivotal role in providing explanation about the nature of the adsorbed film on the metal surface.

4.4.6.1 Laser profilometry of MS/AA1100/1 M HCl/HRL/HRF/CIL/CIF

Figure 4.41(b) and Figure 4.42(b) show the 3D images as well as elevation profiles of polished Mild steel and AA1100 in 1 M HCl respectively. Figure 4.41 (c),(d),(e), (f) & Figure 4.42 (c),(d),(e),(f) shows the 3D images as well as elevation profiles of Mild steel /Aluminium/ 1 M HCl in the presence of investigated biomass extracts.

As observed in Figure 4.41 (b) and Figure 4.42 (b) the surface of Mild steel/Aluminium electrode exposed to corrodent solution has a considerably porous structure with large and deep pores. Figure 4.41 (c), (d),(e),(f) and 4.42 (c),(d),(e),(f) reveal that there is wrapping zonal film adsorbed on mild steel surface. In accordance, it can be concluded that the adsorption film can efficiently protect the mild steel from corrosion. It should be noted that laser profiler has examined only the microstructure; we focus on only the comparison of the mild steel surface corrosion before and after addition of the inhibitor. Some limitations of this study are that it could not provide the chemical composition of adsorption film (**Li *et al,* 2012**).

a. Plain MS

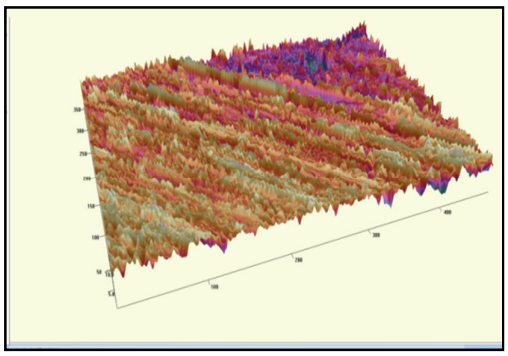

Ra=0.6

b. Blank HCl

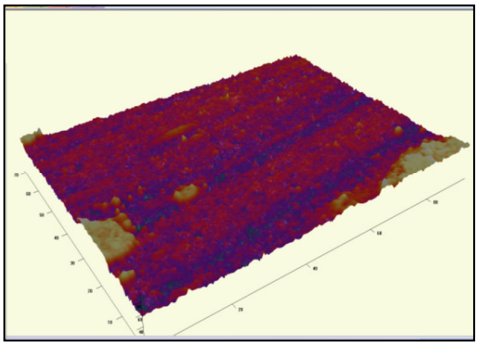

Ra=27.1

c. Mild Steel /HRL extract / 1 M HCl

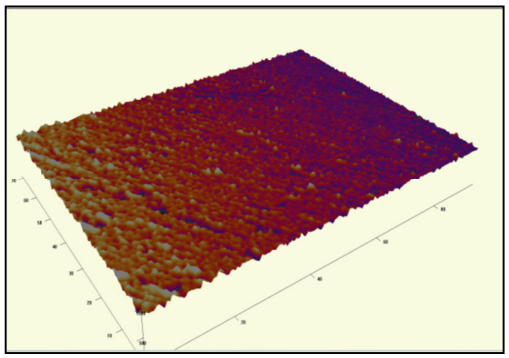

Ra=17.28

d.Mild Steel /HRF extract / 1 M HCl

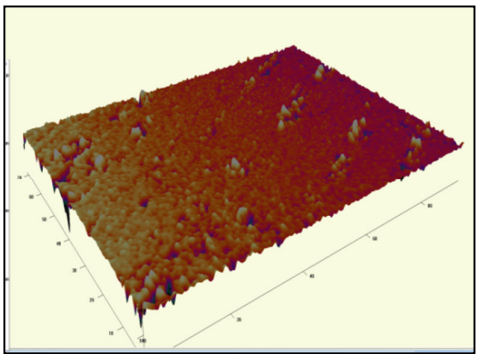

Ra=18.1

e. Mild Steel /CIL extract / 1 M HCl

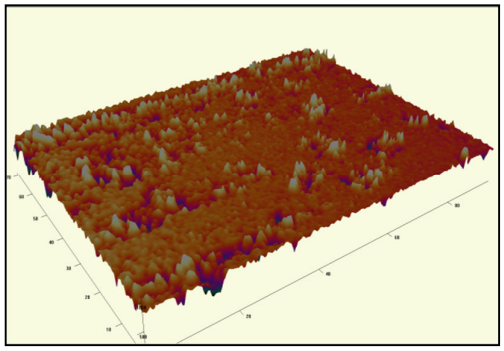

Ra=11.63

f. Mild Steel /CIF extract / 1 M HCl

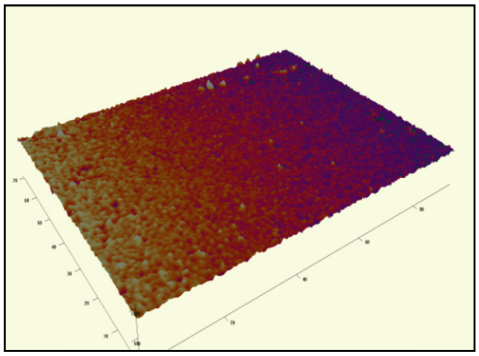

Ra=9.53

Figure 4.41: 3D profilometry images of MS corrosion in the absence and presence of (c) HRL (d) HRF (e) CIL (f) CIF extract in 1 M HCl

a.Plain AA1100

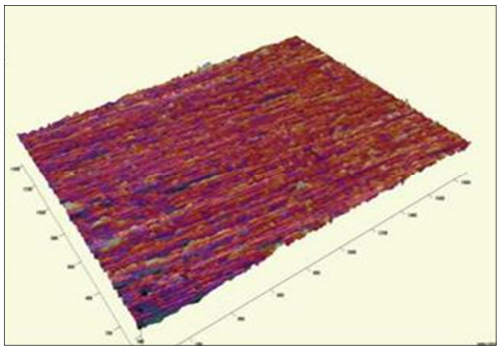

Ra=1.29

b.Blank HCl

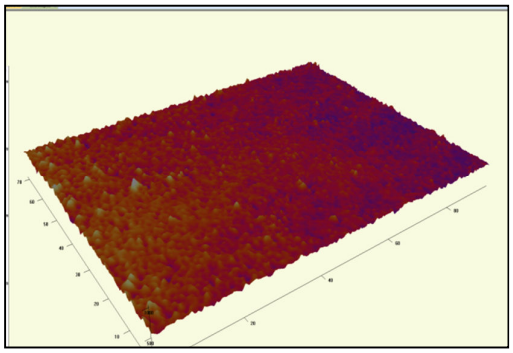

Ra=15.21

c. AA1100/HRL extract/ 1 M HCl

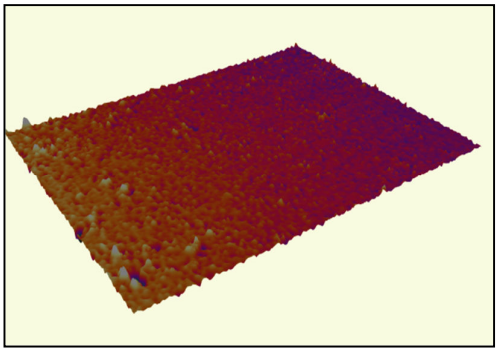

Ra=11.79

d. AA1100/HRF extract / 1 M HCl

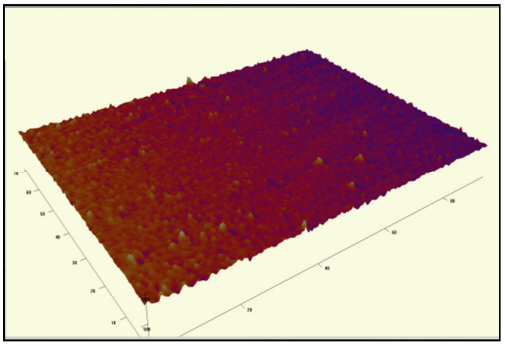

Ra=11.91

e. AA1100/CIL extract / 1 M HCl

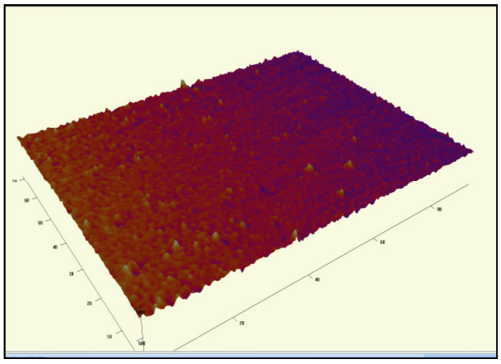

Ra=11.60

f. AA1100/CIF extract / 1 M HCl

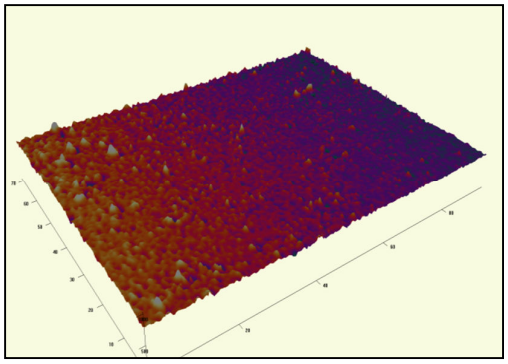

Ra=10.93

Figure 4.42: 3D profilometry images of AA1100 corrosion in the absence and presence of (c) HRL (d) HRF (e) CIL (f) CIF extract in 1 M HCl

Analysis of the value indicates that, higher the distance, higher the values of roughness parameter reached. The mean roughness R_a is found to be 27.1 for the blank acid solution. Visualizing the Figure 4.41 c-f, it can be observed that the R_a of Mild steel immersed in 1 M HCl in the presence of 0.7% of inhibitors (HRL/HRF/CIL/CIF extracts) varied from 9.53 to 18.1 as compared to blank solution. Similarly in the case of AA1100, from Figure 4.42 c-f, R_a value is found to be 15.21 in 1 M HCl but in presence of the inhibitors the value is lower than that of blank .The decrease in the R_a value reflects the adsorption of inhibitor molecules on Mild steel/AA1100 surface thereby reducing the corrosion rate.

In the case of MS and AA1100 in 1 M HCl the inhibitor CIF exhibit excellent behaviour in corrosion inhibition process and this CIF is found to inhibit corrosion of Mild steel as well as AA1100 more effectively than the rest of the investigated inhibitors. This efficient behaviour is remarkably noticed from the R_a values (9.53 for MS & 10.93 for AA1100). This proves that CIF extract has highest efficiency among the investigated inhibitors.

4.5 QUANTUM CHEMICAL CALCULATION

Theoretical investigations based on quantum chemical calculations are proposed as a powerful tool for predicting a number of molecular parameters directly related to the corrosion inhibiting property of any chemical compound **(Khaled and Hackerman, 2003; Bouayed *et al,* 1999; Kutej *et al,* 1995)**. Among several theoretical methods available, the classical semiempirical parameterisation is used to obtain the geometry optimisation of the phytoconstituents (**Rahim *et al,* 2007**). Quantum chemical methods and molecular dynamic simulation are effective in studying the correlation between molecular structure and inhibition properties. Quantum chemical calculations prove to be a very powerful tool for studying corrosion inhibition mechanism and help to design the novel high efficiency inhibitors by the Quantitative Structure-Activity Relationship (QSAR) method.

Our experimental results indicate that CI/HR extract functions as an adsorption-type corrosion inhibitor. The complex processes associated with metal-inhibitor interactions can be theoretically investigated at the molecular level using computer simulations of suitable models in the framework.

The reactive ability of the inhibitor is considered to be closely related to their frontier molecular orbitals, the HOMO and LUMO. Higher HOMO energy (E_{HOMO}) of the molecule means a higher electron donating ability to appropriate acceptor molecules with low-energy

empty molecular orbital and thus explain the adsorption on metallic surfaces by way of delocalized pairs of π-electrons. E_{LUMO}, the energy of the lowest unoccupied molecular orbital signifies the electron receiving tendency of a molecule.

In general, significant differences can be appreciated referring to the inhibitory efficiency of phytochemical constituents. The understanding that the corrosion inhibition efficiency of organic compounds is related to their adsorption properties allows us to propose a possible mechanism. The inhibition efficiency depends strongly on the structures and chemical properties of the species formed under the experimental conditions studied. The extent of adsorption is dependent upon the electronic structure of the metal and the inhibitor.

In research on organic corrosion inhibitors, attention is paid to the mechanism of adsorption and also to the relationship between inhibitor structures and their adsorption properties. It has been observed that the adsorption depends mainly on the electronic and structural properties of the inhibitor molecule such as functional groups, steric factors, aromaticity, electron density on donor atoms and π orbital character of donating electrons **(Martinez*,* 2002)**.

In the present investigation, efforts are taken to characterize the CI / HR extract obtained by using FT-IR, UV and GC-MS studies. Based on these results and phytochemical screening, the major components present in CI/HR extracts are found to be flavonoids, diterpenoids, alkaloids, flavanones, isoflavanones, tannins, Imidazole derivatives, anthraquinones and polyphenols. Literature surveys, followed by characterization of CI/HR confirm the presence of flavonoids, anthraquinones, alkaloids, terpenoids, tannins, saponins, reducing sugar and polyphenols. Analyzing these aspects, to suggest a suitable mechanism for inhibitive action of HRL/HRF/CIL/CIF biomass extracts on Mild steel surface /AA1100, efforts are undertaken to perform theoretical calculations for few phytochemicals **Oleonolic acid, Betunilic acid, Traraxer-14-en-3-one** from **CI** and these have been fully optimized using Mopac software using the PM3 semiempirical parameterization.

Oguzie *et al,* 2010 analysed the corrosion-inhibiting efficacy of *Dacryodis edulis* extract which results from adsorption of the extract organic matter on the corroding metal surface. This normally results from Lewis acid–base interactions in which the metal and inhibitor molecules act as a Lewis acid and Lewis base, respectively, and their interaction is accomplished by favourable overlap of frontier orbitals and sharing of electrons between

the inhibitor and the partially filled d-orbitals of the metal. We have performed such calculations to model the adsorption structures of the major chemical constituents of CI extract chosen for the computations.

The following quantum chemical parameters which indicate the structural characteristics of these common phytochemical constituents are considered: $E_{HOMO,}$ $E_{LUMO,}$ ΔE and μ. The optimized geometry of the corresponding Frontier Molecular Orbital density distribution of Oleonolic acid, Betunilic acid, Traraxer-14-en-3-one from CI are depicted in Figure 4.43 . Table 4.45 lists some quantum chemical parameters which are thought important, due to their direct influence on electronic interaction between the inhibitor molecules and the mild steel surface. The values of some quantum chemical parameters, namely the energy of the highest occupied molecular orbital (E_{HOMO}), energy of the lowest unoccupied molecular orbital (E_{LUMO}), the energy gap (E_{LUMO}-E_{HOMO}) and dipole moment (μ) for selected major components in the investigated CI extract is listed in Table 4.45 and calculated quantum chemical parameters such as number of electrons, Ionisation potential, Electron affinity, Hardness, Softness, Electronegativity and Electrophilic index are included in Table 4.46.

In the current investigation, efforts have been taken to characterize the phytochemicals present in the investigated extracts qualitatively and using FT-IR, UV and GC-MS and coupled with elucidation of their molecular structures. Analyzing the optimized geometry and frontier molecular orbital density distribution of main phytochemical constituents, it is clear that the phenyl ring, methoxy group, C=O and –OH being plane helps in the interaction of phytoconstituents with the metal surface. The ground state geometry of the inhibitor as well as the nature of its molecular orbitals, namely the HOMO and LUMO is involved in the activity properties of the inhibitors.

When the frontier molecules are analyzed, the HOMO are localized over the oxygen, -OCH_3, -OH and the phenyl ring, consequently this is the preferred zone of the molecular interaction with the metal surface. Both the -OCH_3 and -OH can coordinate with mild steel. The effectiveness of a corrosion inhibitor can be related to its molecular spatial structure, molecular electronic structure as well as to its hydrophobicity, solubility and dispersibility **(Sastri and Paerumareddi, 1991)**.

4.5.1 Dipole Moment

The dipole moment (μ) is an index that can also be used for the prediction of the direction of a corrosion inhibition process. Dipole moment is the measure of polarity in a

bond and is related to the distribution of electrons in a molecule. Although literature is inconsistent on the use of 'μ' as a predictor for the direction of a corrosion inhibition reaction, it is generally agreed that the adsorption of polar compounds possessing high dipole moments on the metal surface should lead to better inhibition efficiency.

The dipole moment is the first derivative of the energy with respect to an applied electric field and is a measure of the asymmetry in the molecular charge distribution. A low value of the dipole moment favours accumulation of inhibitor molecules on the metal surface and is also an indication of the hydrophobic character of the molecule. Values of μ ranging from 3 to 5 have been reported in the literature (**Khaled *and* Hackerman, 2003**).

4.5.2 E_{HOMO} & E_{LUMO}

The HOMO energy (E_{HOMO}) is a quantum chemical descriptor often associated with the electron donating ability of the molecule, whereas the (E_{LUMO}) indicates the ability of the molecule to accept electron. The regions of highest electron density (HOMO) are the sites at which electrophiles attack and represent the active centers, with the utmost ability tobond to the metal surface, whereas the LUMO orbital can accept the electrons in the orbital of the metal using antibonding orbitals to form feedback bonds **(Martinez and stagljar, 2003)**. Therefore, high values of the E_{HOMO} indicate an increased tendency of the inhibitor to donate electron to the vacant d orbital of Fe in mild steel. Similarly, E_{LUMO} represents the ability of the molecule to accept electrons

Table – 4.45 Quantum chemical parameters for the selected phytoconstituents

Selected phytoconstituents	Total energy (eV)	E_{HOMO} (eV)	E_{LUMO} (eV)	Change in energy - ΔE (eV)	Dipole Moment- μ (Debye)
***Canna indica* (CI)**					
Oleonolic acid	-4629.70	-8.873	1.025	9.898	-3.924
Betunilic acid	-4629.70	-9.438	0.926	10.364	-4.256
Traraxer-14-en-3-one	-4413.05	-9.52	0.926	10.446	-4.297

The lower the values of E_{LUMO}, the more probable it is that the molecule would accept electrons. Increasing values of E_{HOMO} and decreasing value of E_{LUMO} suggest efficient adsorption process. Generally, the lower the energy gap, the better the electron transfer process. According to **Mihit *et al.,* (2010)** high values of the E_{HOMO} facilitate adsorption and enhance inhibition efficiency by influencing the transport process through

the adsorbed layer. Large values of energy gap ($E_{L-H} = E_{LUMO} - E_{HOMO}$) implies increased electronic stability and low reactivity, while low values render good inhibiting efficiency because the energy to remove an electron from the last occupied orbital will be low.

The values of ΔE are shown in the Table 4.45. The value of HOMO pertaining to the main phytochemical constituents indicates the greater tendency of these phytochemical constituents to donate the electron to the vacant d-orbital of the iron atom. Therefore CI extract has the tendency to bind with the metal surface.

4.5.3 ΔN (number of electrons)

Inorder to calculate ΔN, a theoretical value for the electronegativity of bulk iron has been used $\chi_{Fe} \approx 7$ eV and global hardness of $\eta_{Fe} \approx 0$,and for Aluminium $\chi_{Al} \approx 3.23$ eV and global hardness of $\eta_{Al} \approx 0$ by assuming that for a metallic bulk IP = EA, because they are softer than the neutral metallic atoms. The values of ΔN for the phytochemicals present in CI plant are represented in Table- 4.46. If $\Delta N < 3.6$, the inhibition efficiency increases with increasing electron donors ability at the metal surface. It can be inferred from the results, that, phytochemicals investigated in this current study are donating electrons and the iron surface the acceptor.

4.5.4 Global Softness and Hardness

As expected, there are some similarities in the trends between the quantum chemical parameters and frontier orbital molecular energies. The global softness σ for the phytochemicals is the same, suggesting that softer molecules are stronger inhibitors. Calculated values of σ and η are also presented in Table 4.46. This frontier orbital may also be used to predict the adsorption centers of the inhibitor molecule. For the easiest transfer of electrons, adsorption should occur at the part of the molecule where the softnessσ, which is a local property, has the highest value **(Martinez, 2002)**.

4.5.5 Ionization Potential and Electron Affinity

Values of IP and EA calculated are presented in Table 4.46. From the table it can be noticed that IP is directly related with the E_{HOMO}, while EA is related to the $E_{LUMO.}$ High volume of IP and low volume of EA, (Table 4.45) favour the inhibiting potential of selected phytoconstituents which in turn highlight the efficiency of the investigated plant extracts.

Figure 4.43 represents the optimized structures and the HOMO and LUMO diagrams of phytochemicals of CI. The spatial distribution of the HOMO and the LUMO are important for understanding the adsorption preferences of the inhibitors. Considering that the inhibitors would be electron donors with respect to the steel surface, the HOMO

distribution would be of particular importance. The HOMO distribution maps presented in Figure 4.43 are very similar and the HOMO is localized on the phenyl ring suggesting strong docking to the phenyl ring and lone pair of electrons.

Quantum chemical studies are carried out only with few selected phytochemicals present commonly in the investigated plant extracts. Literature survey helped us to collect the details about the adsorption centers of some phyotchemicals reported in various journals. Based on the details extracted from the literature, the following conclusions are drawn.

Martinez *et al,* 2002 rationalizes the inhibitory action of the mimosa tannin by using quantum chemical calculation. The highest density values of HOMO are found at the vicinity of the functional groups of aromatic rings in flavonoid molecules. They concluded that adsorption of flavonoid molecule could proceed via oxygen lone pair electrons (or) aromatic ring π electrons, between the inhibitor molecule and partly filled 'd' orbitals of iron.

Rahim *et al,* 2007 investigated the adsorptive behaviour of flavonoids on the mild steel surface using the quantum chemical calculations and their molecular modeling of flavonoid monomers and furnished the information about the electron density of the frontier orbital which was found in the vicinity of aromatic rings The authors also report that the adsorption could therefore proceed via sharing of the donor group (-OH) electrons or aromatic π electrons, between the flavonoid molecule and the partially filled d- orbitals of iron. According to Pearson's hard and soft acid and base (HSAB) principle, hard acids prefer to bind to hard bases and soft acids prefer to bind to soft bases. When the HOMO-LUMO energy gap is small, this results in electron transfer from donor base atom to acceptor atom in the acid molecule and the resulting compound is covalent in nature. Thus soft-soft interactions are frontier controlled (**Rahim *et al,* 2007**).

Oguzie *et al* (2010) performed quantum chemical calculation to model the adsorption and the structures of the major chemical constituents of *Dacryodis edulis* extract – caryophyllene, ascorbic acid and alkaloids. It is observed that the HOMO orbital for caryophyllene is saturated around the C=C double bond while that of ascorbic acid is mainly around the lactone nucleus. The highest polarizability α value of flavonoids further confirms the strong adsorption ability of flavonoids. The planar structure of flavonoid molecule favours the largest contact area between flavonoid molecule and C-steel surface as the flavonoids molecule adsorbing at nearly 0° contact angle, which is helpful to form firm and uniform adsorption layer on C-steel surface. The steric hindrance of their structure will affect their adsorption onto C-steel surface.

Akalezi *et al,* 2012 investigated *Coffee senna* extract and reported the molecular dynamic simulation of the phytochemicls - anthraquinone (ATQ), emodine (EMD), chrysophanol (CRP), aloe emodine (ALE), and rhein (RH). The quantum chemical parameters HOMO, LUMO, ΔE for the above mentioned phytochemicals are obtained from molecular dynamic simulation point of view the author reported that these phytochemicals can be seen to maintain a flat-lying adsorption orientation on the Fe surface, in order to maximize contact and enhance the degree of surface coverage. This parallel adsorption orientation also facilitates interaction of π − electrons of the anthraquinone nucleus and the hetero-atoms with the metal surface.

Li *et al,* 2012a identified ascorbic acid, gallic acid, flavonoids and β-caryophyllene as the major effective components of *Osmanthus fragran* leaves extract. The quantum chemical calculations are performed for the these phytochemicals and the authors reports that, HOMO orbital for ascorbic acid is located on the lactone nucleus while the HOMO of β-caryophyllene is mainly around the nine membered ring. Gallic acid and flavonoids have similar HOMO distributions, which all distribute on the entire inhibitor moiety. Flavonoids has the lowest E_{LUMO} (-2.22 eV) and ΔE (4.48 eV), which implies the high ability to accept electrons from the d-orbital of Fe and the high stability of the [Fe– Flavonoids] complexes.

Based on our theoretical calculation & literature results, the adsorption centers for the phytochemcials present in the investigated plant extracts, could be understood. The planar structures of phytochemicals favour the largest contact area, forming a firm and uniform adsorption layer on mild steel.

Analyzing the quantum chemical parameters obtained the inhibition process can be explained as follows:

In a corrosion system containing inhibitor, the inhibitor and the metal act as a lewis base and a lewis acid, respectively, therefore the frontier orbital theory may be used to determine possible modes of interaction between the inhibitor and metal **(Sastri, 1998)**. If bulk iron metal and the inhibitor molecule are brought together, the flow of electrons will occur from the molecule of lower electronegativity to the iron that has higher electronegativity until the value of the chemical potential becomes equal.

The stability of the adsorption bond may further be related to the Pearson's HSAB principle **(Pearson, 1989)**. Bulk metals are soft acids, thus soft base inhibitors are most effective for metals corroding in acid solutions. **Klopman, (1968)** relates the hard-

hard at soft-soft bond character, respectively, to electrostatic (charge controlled) and covalent (Frontier controlled) reactions. In case of the soft-soft inhibitor-metal interaction, the bond is largely covalent in character and is accomplished by a favourable overlap of the frontier orbitals, i.e., HOMO and LUMO. The results obtained by the above analysis (Table – 4.46) imply the possibility of soft-soft interaction between metal acting as a soft acid and inhibitor acting as a soft base in the investigated system as described by **Martinez and Stagljar, (2003)**.

Frontier orbital theory may also be used to predict the adsorption centers of the inhibitor molecules. For the easiest transfer of electron, adsorption should occur at the part of the molecule where the softness σ, which is a local property, has the highest value. Characterization of CI reveals the presence of many phytochemical constituents (Table 4.45). The adsorption centers in the present system are found to be C=O, $-OCH_3$, -OH and phenyl ring of the phytochemical constituents.

Quantum chemical studies are conducted for the main constituents present in all the investigated extracts. Hence it is reasonable to assume that the higher mass fraction of CI extracts, not included in the present analyses would contain even more polar compounds and more complicated geometric structures. Thus the suggested adsorption mechanism would also apply to this fraction of extract **(Martinez and Stagljar, 2003)**.

It is also illustrated by the results of this work that analysis of the action of metal corrosion inhibition by the quantum chemical values, may to great extent, eliminate to the research work in this sphere. It may also facilitate a rational selection and design of new inhibitors.

Table 4.46 Derived Quantum chemical parameters for the selected hytoconstituents

Selected Phytoconstituents	IP (eV)	EA (eV)	η (eV)	σ (eV)	χ (eV)	ω	ΔN (Fe)	ΔN (AA1100)
***Canna indica* (CI)**								
Oleonolic acid	8.873	-1.025	4.949	0.2021	3.924	1.5556	0.3092	-0.0702
Betunilic acid	9.438	-0.926	5.181	0.1930	4.255	1.7477	0.2648	-0.0990
Traraxer-14-en-3-one	9.520	-0.926	5.223	0.1915	4.297	1.7676	0.2587	-0.1022

Figure No	Optimised Structure CI	Frontier Molecular Orbital distribution - HOMO	Frontier Molecular Orbital distribution - LUMO
4.43 a	Betulinic acid 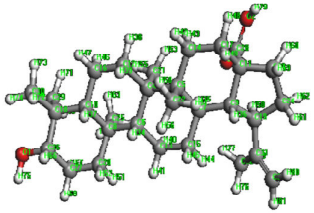	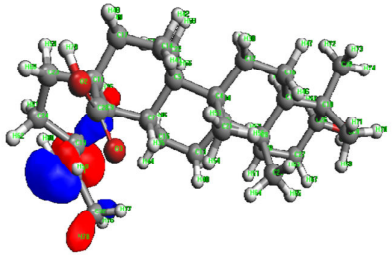	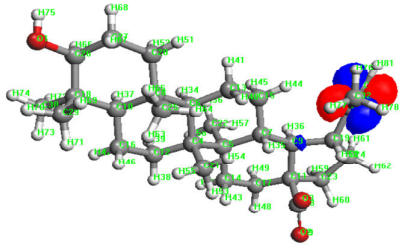
4.43 b	Oleonolic acid 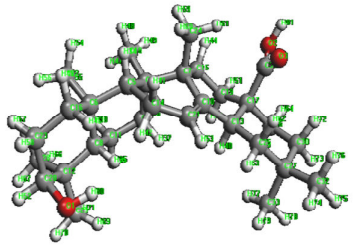	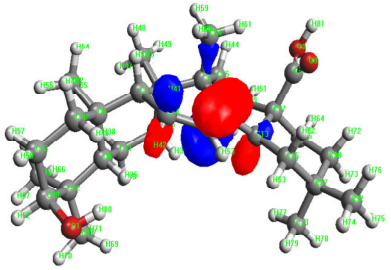	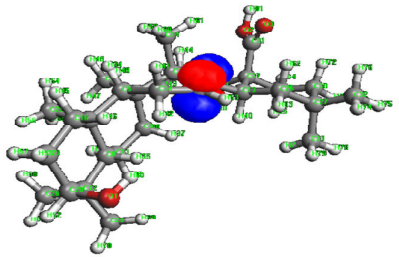
4.43 c	Traraxer-14-en-3-one 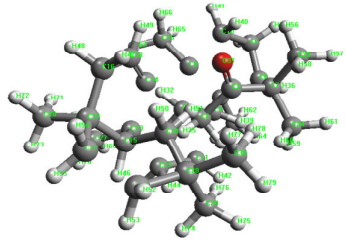	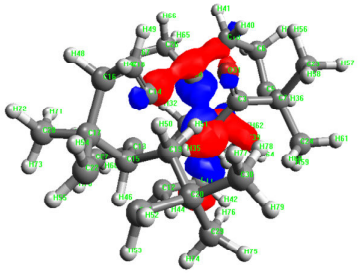	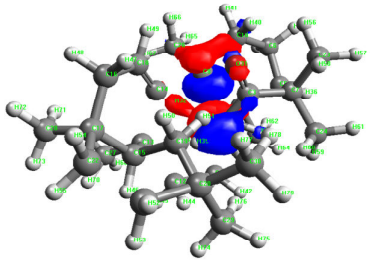

4.6 Mechanism of inhibition process

Mechanism of the inhibition process for studied inhibitors can be discussed on the basis of the experimental findings from mass loss, electrochemical measurements and surface analytical techniques. Theoretical studies on quantum chemical calculation using MOPAC confirmed the active centers of adsorption.

In the present investigation corrosion inhibition of Mild steel / AA 1100 in 1 M HCl using CI/HR extracts could furnish the following results:

- ✶ All the investigated extracts obey Langmuir adsorption isotherm indicating that the CI/ HR extracts are of adsorptive type.
- ✶ Electrochemical studies confirm that the investigated extracts under study act as mixed type of inhibitors.
- ✶ UV-visible spectroscopic studies and FT-IR studies highlights the formation of phytoconstituents-metal complex in the investigated systems.
- ✶ SEM - EDX spectra images prove that extracts could adsorb onto the metal surface to form a dense and tighter protective film.
- ✶ 3D laser profiler images also prove the formation of Fe/AA 1100-inhibitor complex. The parameter R_a of the images confirms the complex formation.
- ✶ The quantum chemical computations of parameters associated with the electronic structures of specific components of the extract confirm their inhibiting potentials.

4.6.1 PROPOSED MECHANISM FOR MILD STEEL /1 M HCl / INHIBITORS

The mechanism of inhibitive action can be different, depending on metal, the medium and the structure of the inhibitor. Generally, two modes of adsorption are considered on the metal surface in acid media. In one mode, the neutral molecules may be adsorbed on the surface of mild steel through the chemisorption mechanism, involving the displacement of water molecules from the mild steel surface and the sharing of electrons between the hetero atoms and iron. The inhibitor molecules can also adsorb on the mild steel surface on the basis of donor-acceptor interactions between π-electrons of the aromatic ring and vacant d-orbitals of surface iron atoms.

In second mode, since it is well known that the steel surface bears positive charge in acid solution **(Mu *et al,* 1996)**, it is difficult for the protonated molecules to approach the positively charged mild steel surface (H_3O^+/metal interface) due to the electrostatic repulsion. Since chloride ions have a smaller degree of hydration, they could bring excess negative charges in the vicinity of the interface and favour more adsorption of the positively charged inhibitor molecules, the protonated inhibitors adsorb through electrostatic interactions between the positively charged molecules and the negatively charged metal surface. Thus, there is a synergism between adsorbed Cl^- ions and protonated inhibitors.

The high performance of HR/CI extracts could also be due to synergistic effect of all constituents which covers wide areas on the metal surface and thus retarding the corrosion **(Trabenelli and Mansfeld, 1987).** It is not possible to consider a single adsorption mode between inhibitor and metal surface because of the complex nature of adsorption and inhibition of a given inhibitor. The adsorption of main constituents of HR/CI extracts can be attributed to the presence of O-atom, π-electrons and aromatic rings. Presence of methoxy group also enhances the inhibition efficiency. Therefore, the possible reaction centers are unshared electron pair of hetero-atoms and π-electrons of aromatic ring which was also confirmed from quantum chemical studies.

In aqueous acidic solutions, main constituents exist either as neutral molecules or as protonated molecules (cations). The inhibitors may adsorb on the metal/acid solution interface by one and/or more of the following ways:

- Electrostatic interaction of protonated molecules with already adsorbed chloride ions,
- Donor-acceptor interactions between the π-electrons of aromatic ring and vacant d orbital of surface iron atoms,
- Interaction between unshared electron pairs of hetero atoms and vacant d-orbital of iron surface atoms.

The corrosion of mild steel in aqueous acidic solutions can be inhibited by the extract of leaves and flowers of HR/CI. It is often not possible to assign a single general mechanism of action to an inhibitor, because the mechanism may change with experimental conditions. Thus, the predominant mechanism of action of an inhibitor in acidic solutions may vary with factors such as concentration of the extracts, the nature of

the anion of the acid, the presence of other species in the solution, the extent of reaction to form secondary inhibitors and the nature of the metal **(Shreir *et al,* 1994)**.

In the present situation two modes of adsorption could be considered:

i. The neutral may adsorb onto the metal surface via the chemisorption mechanism, involving the displacement of water molecules from the metal surface and sharing electrons between the O atoms and Fe. The phytochemical constituents of the selected inhibitor can also adsorb on the metal surface on the basis of donor-acceptor interactions between π-electrons of aromatic ring and vacant d-orbitals of Fe.

$$Fe \longrightarrow Fe^{2+} + 2e^{-} \quad \textbf{(4.23)}$$

$$[\ HR/Cl\ ] + Fe^{2+} \leftrightarrow [HR/Cl\ -Fe]^{2+} \quad \textbf{(4.24)}$$

ii. The protonated extracts may adsorb through electrostatic interactions between the positively charged molecules and the negatively charged metal surface. In other words, there may be a synergism between Cl^- and extract, which improves the inhibitive capability of the inhibitor.

$$[HR/Cl\ Hx]^{x+} + Fe^{2+} \leftrightarrow [HR/Cl\ -Fe]^{(2+x)+} \quad \textbf{(4.25)}$$

$$[HR/Cl\ ] + Fe^{2+} \leftrightarrow [HR/Cl\ -Fe]^{2+} \quad \textbf{(4.26)}$$

When protonated HR/Cl extract is adsorbed on metal surface, a coordinate bond may be formed by partial transference of electrons from polar atoms (O atoms) to the metal surface. In addition, owing to lone-pair electrons of O atom in HR/Cl extract or protonated extracts may combine with freshly generated Fe^{2+} ions on steel surface forming metal-inhibitor complexes.

The inhibition efficiency afforded by selected phytoconstituents may be attributed to the presence of electron rich phenol groups and aromatic rings. The possible reaction centers are unshared electron pair of hetero-atoms and/or p -electrons of aromatic ring. Generally, phytoconstituents can absorb on the mild steel surface on the basis of donor – acceptor interactions between π (pi) electrons of the O and aromatic ring and vacant d orbitals of surface iron.

Similar type of mechanism has also been proposed by Xiang-Hong **Li *et al,* (2010)**. These complexes might be adsorbed onto steel surface by vander Waals force to form a protective film to prevent mild steel from corrosion.

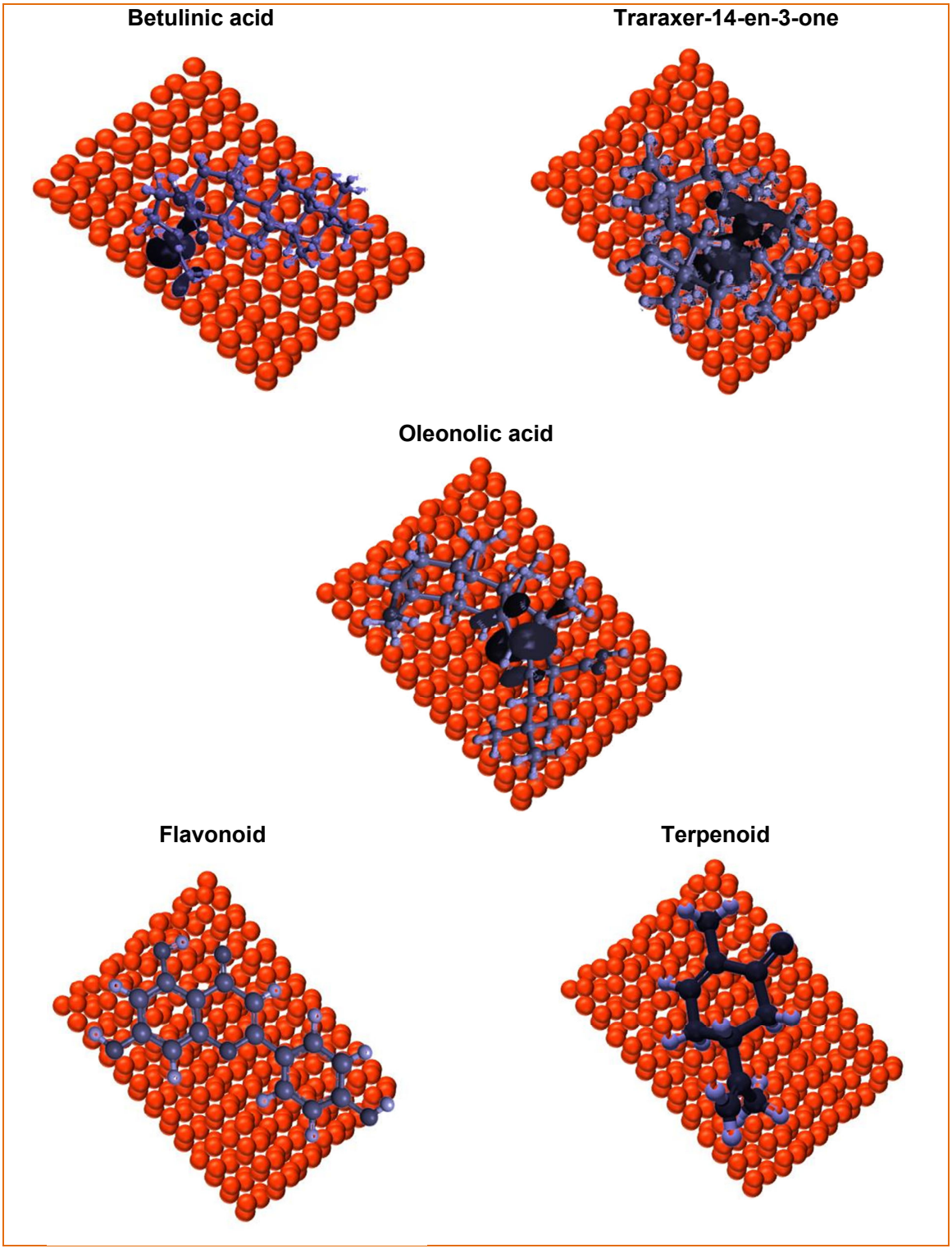

Figure 4.44 Schematic Illustration of Selected Phyto Constituents of *Canna indica* on MS Surface and General Illustration of Flavonoid and Terpenoid on MS Surface.

The main constituents of CI extract are Oleonolic acid, Betunilic acid, Traraxer-14-en-3-one and the adsorption models are schematically illustrated (Figure 4.44)

The specific phyto constituents of HR are yet to be identified. Hence HPTLC analysis has been performed. HPTLC analysis confirmed the presence of terpenoids, coumarins and flavonoids. Phytochemical screening and GC-MS have also been performed in addition to HPTLC to corroborate the results. Therefore the general skeletal representation has been chosen to depict the adsorption model and it has been schematically illustrated (Figure 4.44).

Adsorption is the primary step in achieving inhibition in acid solutions. This is a consequence of the fact that the corroding metal surface to be inhibited is usually oxide-free allowing the inhibitor ready access to retard the cathodic and/or the anodic electrochemical processes of corrosion. Once the inhibitor has adsorbed on the metal surface it can then affect the corrosion reactions in a number of ways: by offering a physical barrier to the diffusion of ions or molecules to or from the metal surface; direct blocking of anodic and/or cathodic reaction sites; interaction with corrosion reaction intermediates; change the make-up of the electrical double layer which develops at the metal/solution interface and so affect the rate of electrochemical reactions **(Graeme Wright, 1998).**

While considering electrostatic interaction of the inhibitors with the metal surface the question arises whether the inhibitor molecule exits, in a solution, in a molecular or a protonated form. Analyzing the values of ΔG_{ads} and E_a it may be concluded that mixed adsorption involving physical as well as chemical adsorption takes place in the present case. The phytochemical constituents in HR/CI extracts interact with metal surface both in a molecular form as well as protonated form **(Martinez and Stagljar, 2003)**. Similar type of mechanism is also proposed by **Ehteram A. Noor, 2007 and Emeka E. Oguzie, 2008b.**

4.6.2 PROPOSED MECHANISM FOR AA1100 /1 M HCl / INHIBITORS

As discussed in standard adsorption free energy (ΔG^0), the adsorption is mainly the physical adsorption. In accordance, the following adsorption mechanisms are presented.

i) In acid solution, HR/CI could be protonated in the acid media due to the interaction between O atom and H^+. AA1100 surface is positively charged due to accumulation of Al-OH_2^+ species in acidic solution **(Brett *et al*, 1990)**. In HCl solution, Cl^- ions could accumulate gradually closely to the aluminum/solution interface, being specifically

adsorbed; they create an excess negative charge toward the solution and favour more adsorption of the cations. Thus, the protonated HR/CI may adsorb through electrostatic interactions between the positively charged molecules and the negatively charged metal surface. In other words, there is a synergism between Cl^- and protonated inhibitor. **(Li *et al*, 2012)**

$$Al_{(s)} + H_2O \longleftrightarrow AlOH_{ads} + H^+ + e^- \quad \textbf{(4.27)}$$

$$AlOH_{ads} + 5\ H_2O + H^+ \longleftrightarrow Al^{3+}.6\ H_2O + 2\ e^- \quad \textbf{(4.28)}$$

$$Al^{3+} + H_2O \longleftrightarrow [AlOH]^{2+} + H^+ \quad \textbf{(4.29)}$$

$$[AlOH]^{2+} + X^- \longleftrightarrow [AlOHX]^+ \quad \textbf{(4.30)}$$

The controlling step in the metal dissolution is the complexation reaction between the hydrated cation and the anion present (Equation 4.29). In the presence of chloride ions the reaction will correspond to

$$[AlOH]^{2+} + Cl^- \longleftrightarrow [AlOHCl]^+ \quad \textbf{(4.31)}$$

ii) The soluble complex ion formed increases the metal dissolution rate which depends on the chloride concentration. In order to predict the adsorption mechanism of protonated HR/CI to positive charged AA1100 surface, corrosion mechanism of AA1100 in HCl must be known. According to this mechanism, anodic dissolution of Al follows the steps:

$$Al + Cl^- \longleftrightarrow AlCl^-_{ads} \quad \textbf{(4.32)}$$

$$AlCl^-_{ads} + Cl^- \longleftrightarrow AlCl^-_2 + 3e^- \quad \textbf{(4.33)}$$

The cathodic hydrogen evolution follows the steps:

$$H^+ + e^- \longrightarrow H_{ads} \quad \textbf{(4.34)}$$

$$H^+ + H_{ads} \longrightarrow H_2 \quad \textbf{(4.35)}$$

The protonated inhibitors electrostatically adsorb onto the anion covered AA1100 surface, through their protonated form. Thus the oxidation reaction in Equation 4.32 can be prevented. This phenomenon is attributable to the stabilisation of the adsorbed halides by the electrostatic interaction with the inhibitor molecules resulting in greater surface coverage. The protonated molecules also adsorb on the cathodic sites in competition with H^+ ions. Also the inhibitors can adsorb from the negatively charged O atoms and the pi bonds of the aromatic systems to positively charged AA1100 surface.

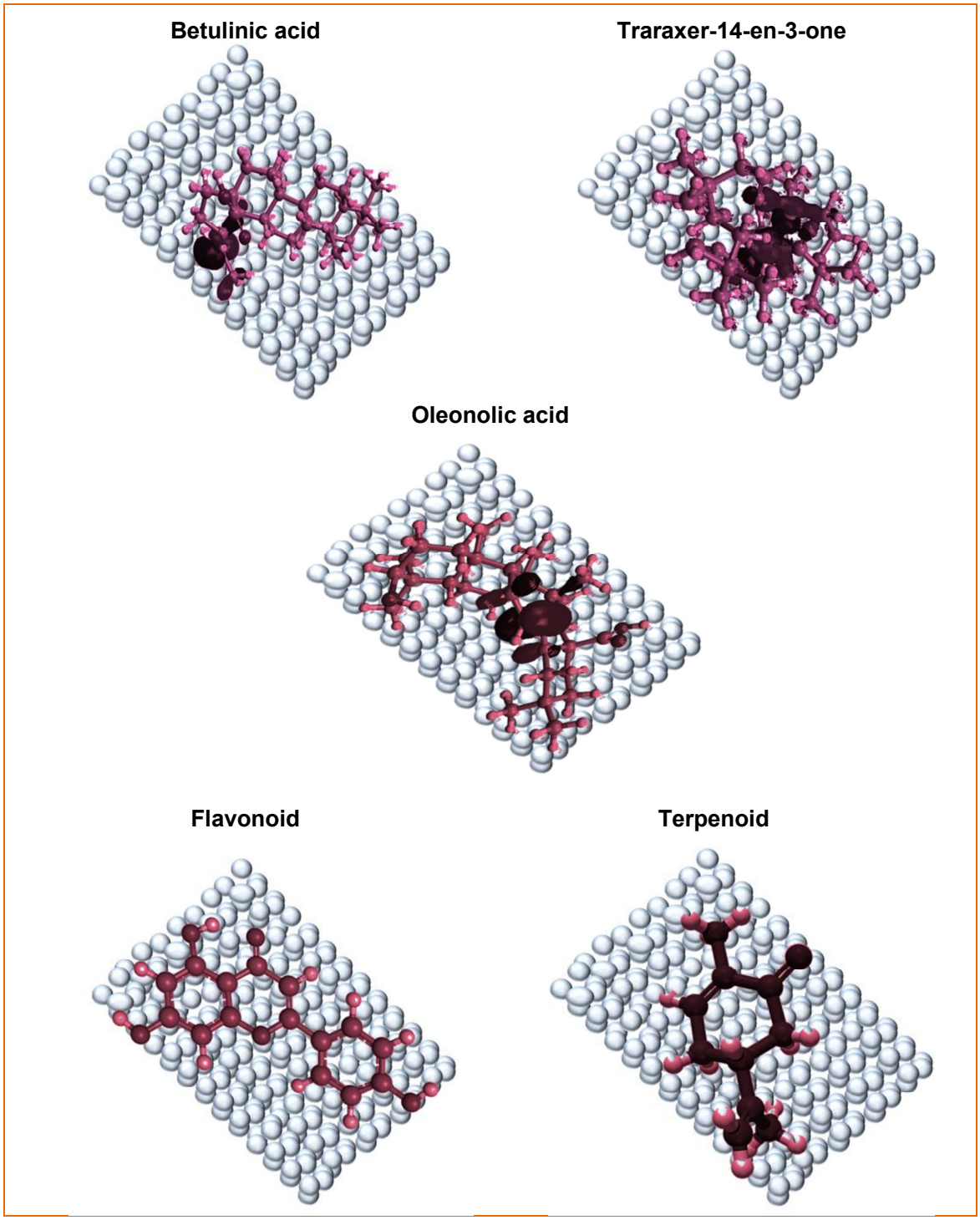

Figure 4.45 Schematic Illustration of Selected Phyto Constituents on AA1100 surface General Illustration of Flavonoid and Terpenoid on AA1100 surface